



universität
wien

MASTERARBEIT

Titel der Masterarbeit

„Semi-classical and Numerical Aspects of Fuzzy Brane
Solutions in Yang-Mills Theories“

verfasst von

Lukas Schneiderbauer, BSc

angestrebter akademischer Grad

Master of Science (MSc)

Wien, 2015

Studienkennzahl lt. Studienblatt:

A 066 876

Studienrichtung lt. Studienblatt:

Masterstudium Physik

Betreut von:

Mag. Harold Steinacker, Privatdoz. PhD

I would like to extend my sincere gratitude to my supervisor Priv.-Doz. Dr. Harold C. Steinacker who sacrificed countless hours to patiently guide me through this compelling field of work.

Further I would like to thank my parents, Margarete and Helmut, for their unconditional support of my studies without whose financial backing this work could not exist. I am grateful, too, to my siblings, David, Teresa and Magdalena, as well as my friends for proofreading and providing viable feedback.

ABSTRACT. This work describes an algorithm which aims to numerically find an approximation to the semi-classical limit of a given NC-Brane configuration embedded in \mathbb{R}^m defined by a finite set of finite-dimensional matrices. This approximation is numerically given by a point cloud within \mathbb{R}^m which represents the semi-classical limit as manifold.

To this end an introduction to non-commutative geometry is given and various examples thereof are discussed. The focus lies on *coherent states* in the context of non-commutative geometry which constitute the main ingredient for the theoretical background of the algorithm.

After establishing the algorithm it is applied (amongst other examples) to an interesting solution of a supersymmetric $\mathcal{N} = 4$ Yang-Mills theory deformed by a cubic potential. This solution is studied in detail and various results are presented.

ZUSAMMENFASSUNG. Die vorliegende Arbeit beschreibt einen Algorithmus, um numerisch eine Näherung des semi-klassischen Limes einer durch eine endliche Menge an endlich-dimensionalen Matrizen gegebenen NC-Brane Konfiguration zu finden. Diese Näherung ist numerisch beschrieben durch eine Sammlung von Punkten in \mathbb{R}^m , die wiederum eine Mannigfaltigkeit eingebettet in \mathbb{R}^m darstellen sollen.

Zu diesem Zweck wird eine kurze Einführung in die Theorie der sogenannten “nicht-kommutativen Geometrie” gegeben, die von wichtigen Beispielen begleitet wird. Einen Schwerpunkt dabei bilden die *kohärenten Zustände*, die einen Grundstein für den theoretischen Hintergrund dieses Algorithmus bilden.

Nachdem der Ablauf des Algorithmus begründet und beschrieben wurde, wird dieser unter anderem auf eine interessante Lösung einer deformierten supersymmetrischen $\mathcal{N} = 4$ Yang-Mills Theorie angewendet. Diese Lösung wird im Detail diskutiert und diverse sowohl numerische als auch analytische Resultate werden präsentiert.

Contents

Chapter 1. Introduction	7
Chapter 2. Non-Commutative Geometry	9
2.1. Quantization Procedure	9
2.2. Embedded Non-commutative Brane (NC-Brane)	10
2.3. Fuzzy Sphere	11
2.4. Fuzzy \mathbb{CP}^2	12
2.5. Fuzzy Torus	16
Chapter 3. Coherent States	19
3.1. Localization and Dispersion	19
3.2. Coherent States on the fuzzy sphere S_n^2	20
3.3. Coherent States on fuzzy \mathbb{CP}_n^2	21
Chapter 4. Squashed \mathbb{CP}^2	23
4.1. Supersymmetric Yang-Mills Theory	23
4.2. Squashed Fuzzy \mathbb{CP}^2 As Solution	24
4.3. Coherent States on Squashed \mathbb{CP}_n^2	26
Chapter 5. Numerical Analysis of Coherent States	31
5.1. Definition of Coherent States	31
5.2. Intersecting Point Probe	34
5.3. Numerically finding coherent states	37
5.4. Fuzzy Sphere revisited	40
5.5. Fuzzy Torus revisited	42
5.6. Squashed \mathbb{CP}_n^2 revisited	44
Chapter 6. Conclusion	49
Bibliography	51
Appendix A. The Lie group $SU(3)$	53
A.1. Definition	53
A.2. Representations	54
A.3. Constructing matrices for arbitrary representations (n, m)	55
Appendix B. Calculations for coherent states of Squashed \mathbb{CP}^2	59
B.1. Expectation values	59
B.2. Dispersion	60

CHAPTER 1

Introduction

Historical remarks. Until now the vast success of the *Standard Model* in modern particle physics are indisputable. However, the early formulators of realistic quantum field theories (as for example QED) were not always satisfied with the situation since the theories contained divergences like the infamous and well-known UV-divergences. To quote Dirac from 1975:

“Most physicists are very satisfied with the situation. They say: ‘Quantum electrodynamics is a good theory and we do not have to worry about it any more.’ I must say that I am very dissatisfied with the situation, because this so-called ‘good theory’ does involve neglecting infinities which appear in its equations, neglecting them in an arbitrary way. This is just not sensible mathematics. Sensible mathematics involves neglecting a quantity when it is small – not neglecting it just because it is infinitely great and you do not want it!” – Dirac [17], 1975

The negative feelings about renormalization began to vanish in the community when they realized that the theory should be understood as an *effective* theory, i.e. the extent of validity of the theory is limited and breaks down at low distances/high energies. This view was also supported by Heisenberg, who brought up the concept of an universal length-scale where new physics is to be expected.

„Wenn man an die umfassenden Änderungen denkt, welche die formale Darstellung der Naturgesetze beim Verständnis der Konstanten c und \hbar erfahren hat, so wird man damit rechnen, dass auch die Länge r_0 zu völlig neuen Begriffsbildungen zwingt, die weder in der Quantentheorie noch in der Relativitätstheorie ein Analogon besitzen.“ – Heisenberg [13], 1938

Own translation:

“If one thinks about the extensive modifications of the formal description of the laws of nature with respect to the understanding of the constants c and \hbar , one would anticipate the necessity of new formulations for the understanding of the length r_0 , which do not possess an analogon neither in quantum theory nor in the theory of relativity.”

This problem also leads to the question whether our current mathematical description of spacetime — as Einstein created it — as pseudo-Riemannian manifold is correct from a fundamental point of view. The answer to this question might also lead to hints for a satisfying unification of gravity with the other three fundamental forces of nature, which to this day was not successful.

The following popular (simplified¹) argument suggests that the classical description of spacetime is inappropriate at very short distances, i.e. distances below the Planck scale: In Quantum Mechanics localizing an object at a length scale Δx requires wave-numbers $k \sim 1/\Delta x$.² This corresponds to an energy $E = \hbar k \sim \hbar/\Delta x$. The theory of General Relativity predicts that an energy distribution localized within its Schwarzschild radius $R \sim GE$ (G being the gravitational constant) forms a black hole, i.e. one cannot measure what’s inside. Therefore only a length Δx makes sense which satisfies $\Delta x \gtrsim R \sim G\hbar/\Delta x$ or equivalently $(\Delta x)^2 \gtrsim \hbar G = l_P^2$ where $l_P \approx 1.6 \times 10^{-35}$ m is the Planck length.

¹A more refined version of this argument is given in [9].

²In this context (and only in this context) the symbol \sim means: “same order of magnitude”.

About this thesis. One possible way to achieve such minimal lengths/areas/volumes is to quantize spacetime itself, which — in contrast to what Heisenberg said — is analogous to the quantization procedure in Quantum Mechanics. The mathematical framework is called *non-commutative geometry*. This framework will be the basis of the work for this thesis, therefore a short introduction with examples is given in chapter 2.

In analogy to Quantum Mechanics one can discuss so-called *coherent states* on quantized manifolds to deepen the understanding of the behavior of quantized spaces. Since in this thesis coherent states are exhaustively used tools, chapter 3 is dedicated to them.

In chapter 4 a deformed Yang-Mills theory is discussed, which admits the *squashed fuzzy \mathbb{CP}^2* — a variant of quantized \mathbb{CP}^2 — as solution. Since this solution is of main interest for this thesis, it is treated in great detail. Further, some results with respect to coherent states for this specific example are presented. More involved calculations are delayed to appendix B to hopefully provide a more compact and clearer picture of the relevant results.

One of the main goals of this thesis is to establish a numerical algorithm using the notion of coherent states to extract an approximation of the semi-classical limit from non-commutative geometries defined by a set of finite dimensional matrices. The semi-classical limit is then given by a manifold in the usual mathematical sense which is numerically represented by a point cloud as subset of \mathbb{R}^m . This algorithm is further tested on well known examples such as *Fuzzy Sphere S_n^2* or *Fuzzy Torus T_n^2* . In addition, this algorithm is applied to *Squashed Fuzzy \mathbb{CP}^2* which in general lacks closed expressions for coherent states. As a result some interesting findings can be reported. This and more is captured in chapter 5.

Since the calculations heavily depend on group theory, especially in the case of \mathbb{CP}^2 the group $SU(3)$, appendix A provides an overview of $SU(3)$ and fixes conventions which are consistently used throughout the whole thesis.

A word on notation. The author’s aim was to make this thesis readable by master students of physics with sufficient interest in a reasonable amount of time. To be more concrete the reader should bring a rudimentary understanding of the mathematical theory of manifolds, s/he should be familiar with the theory of Lie groups, especially the theory of the groups $SU(2)$ and $SU(3)$, and of course the ability to use Linear algebra tools without effort is highly recommended.

Therefore, it was attempted to keep “non-standard”³ notation at a minimum. In the case that “non-standard” notations occur, the relevant expressions are defined on the way, while “standard” notation is used without further explanation.

³“Standard” refers to notations an average master student of physics is expected to be familiar with at the time of writing this thesis.

CHAPTER 2

Non-Commutative Geometry

As we have seen there are some good arguments that spacetime should be “quantized” in some sense. One approach to tackle this problem is to perform a “quantization” — as one knows it from ordinary Quantum Mechanics — of spacetime itself.

2.1. Quantization Procedure

Loosely speaking this means we replace the commutative algebra of functions $\mathcal{C}(\mathcal{M})^1$ on a manifold \mathcal{M} with a non-commutative one, usually $End(\mathcal{H})$ where \mathcal{H} is a Hilbert space. For reference see e.g. a book by Waldmann [27]. It turns out to define a useful notion of a *quantization map* one has to bestow more structure on the manifold \mathcal{M} . To make the previous statements more precise we introduce the following concepts:

DEFINITION 2.1. A map $\{.,.\} : \mathcal{C}(\mathcal{M}) \times \mathcal{C}(\mathcal{M}) \rightarrow \mathcal{C}(\mathcal{M})$ which satisfies

- *linearity in one argument*
- *antisymmetry* $\{f, g\} = -\{g, f\} \quad \forall f, g \in \mathcal{C}(\mathcal{M}),$
- the *Leibniz rule* $\{f \cdot g, h\} = f \cdot \{g, h\} + \{f, h\} \cdot g,$
- and the *Jacobi identity* $\{f, \{g, h\}\} + \{g, \{h, f\}\} + \{h, \{f, g\}\} = 0$

is called *Poisson structure* or *Poisson bracket*.

DEFINITION 2.2. A manifold \mathcal{M} equipped with a Poisson structure $\{.,.\}$ is called a *Poisson manifold* $(\mathcal{M}, \{.,.\})$.

Since for a fixed $f \in \mathcal{C}(\mathcal{M})$ the map $\{f, .\} : \mathcal{C}(\mathcal{M}) \rightarrow \mathcal{C}(\mathcal{M})$ satisfies the Leibniz rule and is linear, $\{f, .\}$ is a derivation on $\mathcal{C}(\mathcal{M})$ and thus for a point $p \in \mathcal{M}$ it holds $\{f, .\}(p) \in T_p\mathcal{M}$ or alternatively stated the map $p \mapsto \{f, .\}(p)$ is a vector field on \mathcal{M} . Since the same arguments hold for the first slot in the Poisson bracket we can write it in the following form using local coordinates

$$\{f, g\} = \Theta^{ab}(\partial_a f)(\partial_b g), \quad (2.1.1)$$

with summation over indices appearing twice understood. Because of the antisymmetry property of the Poisson bracket, Θ^{ab} is antisymmetric in its indices and obeys the relation

$$\Theta^{ak} \partial_k \Theta^{bc} + \Theta^{bk} \partial_k \Theta^{ca} + \Theta^{ck} \partial_k \Theta^{ab} = 0 \quad (2.1.2)$$

due to the Jacobi identity. We see that the Poisson structure is completely determined by Θ^{ab} .

In the context of geometric quantization the Poisson structure on the manifold is in some sense controlling the non-commutativity of the target algebra $End(\mathcal{H})$ as we will see in the following definition of the quantization map \mathcal{Q} .

DEFINITION 2.3. Let \mathcal{M} be a Poisson manifold. A map

$$\mathcal{Q} : \mathcal{C}(\mathcal{M}) \rightarrow End(\mathcal{H}) \quad (2.1.3)$$

satisfying the axioms

- (1) *linearity*,
- (2) $\mathcal{Q}(\mathbf{1}) = \mathbb{1},$

¹which is equipped with point-wise addition $+$ and multiplication \cdot .

- (3) $Q(f)^\dagger = Q(f^*) \quad \forall f \in \mathcal{C}(\mathcal{M})$,
 (4) *correspondence principle*:

$$\lim_{\theta \rightarrow 0} \frac{1}{\theta} (Q^{-1}([Q(f), Q(g)]) - i\{f, g\}) = 0 \quad \forall f, g \in \mathcal{C}(\mathcal{M}), \quad (2.1.4)$$

$$\lim_{\theta \rightarrow 0} Q(fg) - Q(f)Q(g) = 0 \quad \forall f, g \in \mathcal{C}(\mathcal{M}), \quad (2.1.5)$$

(5) *irreducibility*: If $\{f_i, g\} = 0 \quad \forall i \in I$ implies $g \propto \mathbf{1}$ then $[Q(f_i), A] = 0 \quad \forall i \in I$ implies $A \propto \mathbf{1}$ where $[\cdot, \cdot]$ is the commutator and θ some scale parameter is called a *quantization map*.

In practice these requirements are often tightened or softened as the physical situation requires it and the definition varies from author to author. Note that we assume here that the limit $\theta \rightarrow 0$ exists in some appropriate sense. Also note that although we used the symbol Q^{-1} , in general we do not require Q to be invertible; invertibility on a subspace will suffice.

Property (4) makes it clear that the quantization map cannot be unique since higher order corrections in θ can be chosen arbitrarily. However, one often fixes this freedom by demanding the quantization map to respect certain symmetries.

The *semi-classical* limit is then given by the pre-image of Q in the limit $\theta \rightarrow 0$ and is below denoted by the symbol \sim .

2.2. Embedded Non-commutative Brane (NC-Brane)

Having completed a quantization procedure leaves us with a non-commutative algebra consisting of matrices. The sole algebra contains certainly not enough structure since we would not be able to retrieve any geometry of our manifold \mathcal{M} . But since the quantized space ought to be considered more fundamental this is a required feature.

Now the key to obtain the required structure is to consider \mathcal{M} as an embedded manifold in \mathbb{R}^D [23] which is encoded in the embedding map

$$x : \mathcal{M} \hookrightarrow \mathbb{R}^D \quad (2.2.1)$$

or equivalently in D coordinate functions denoted by $x^a \in \mathcal{C}(\mathcal{M})$, $a = 1, \dots, D$.

Given a manifold \mathcal{M} and a quantization Q thereof as in definition 2.3 we gain quantized embedding functions

$$X^a := Q(x^a) \in \text{End}(\mathcal{H}) \quad (2.2.2)$$

given by D specific matrices/operators. The crucial point here is that this also works the other way around: By stating D matrices X^a , the embedded functions are determined by $x^a = Q^{-1}(X^a)$ and so is the geometry of \mathcal{M} .

Of course that does not mean that for any set of matrices $\{X^a | a = 1, \dots, D\}$ the embedded functions make sense as such. The actual question is: Given some $n \times n$ matrices X^a which generate a matrix algebra $\mathcal{A} \subset \text{Mat}_n(\mathbb{C})$ and interpreting them as quantized embedding functions $X^a \sim x^a$, can we make sense of the semi-classical limit, i.e. can we find a manifold \mathcal{M} where $Q(\mathcal{C}(\mathcal{M})) = \mathcal{A}$ for some quantization map Q ? This is in general a hard question for which we try to present at least partial answers in the following work.

Examples of Fuzzy Geometries. We will now discuss some examples of such matrix (or fuzzy) geometries. In practice, it seems that quantizing a given manifold is actually much easier than finding the semi-classical limit of an algebra generated by a set of quantized embedding functions $X^a \sim x^a$. Due to this we will present the following well known examples in this “wrong” way.

2.3. Fuzzy Sphere

One of the simplest and well understood example is the so called *fuzzy sphere* and goes back to Madore and Hoppe [18, 14].

Let’s begin with the usual two-sphere

$$\mathcal{M} = S^2 = \{x \in \mathbb{R}^3 \mid \sum_{i=1}^3 x_i^2 = 1\}. \quad (2.3.1)$$

Of interest is the sphere’s $SO(3)$ symmetry which acts on $S^2 \subset \mathbb{R}^3$ via matrix multiplication of the usual $SO(3)$ matrices:

$$\begin{aligned} SO(3) \times S^2 &\rightarrow S^2 \\ (G, \vec{x}) &\mapsto G \cdot \vec{x} \end{aligned} \quad (2.3.2)$$

This action induces an action on its algebra of functions $\mathcal{C}(S^2)$ which is — as we have seen — of main interest in the quantization procedure. We have

$$\begin{aligned} SO(3) \times \mathcal{C}(S^2) &\rightarrow \mathcal{C}(S^2) \\ (G, f) &\mapsto G \triangleright f \\ (G \triangleright f)(\vec{x}) &:= f(G^{-1} \cdot \vec{x}) \end{aligned} \quad (2.3.3)$$

which enables us to decompose the algebra $\mathcal{C}(S^2)$ into irreducible representations of $SO(3)$. A basis that respects this decomposition is exactly the set of the well known spherical harmonics Y_m^l . Therefore

$$\mathcal{C}(S^2) \doteq \bigoplus_{l=0}^{\infty} \langle \{Y_m^l \mid m = -l, \dots, l\} \rangle. \quad (2.3.4)$$

Quantization map. At this point it has to be recalled that the quantization map \mathcal{Q} with the axioms defined in 2.3 is not at all unique. Correspondingly, we want to use this freedom now and demand that the map $\mathcal{Q} : \mathcal{C}(S^2) \rightarrow \text{End}(\mathcal{H})$ preserves the $SO(3)$ symmetry, i.e.

$$\mathcal{Q}(G \triangleright f) = G \triangleright \mathcal{Q}(f) \quad \forall G \in SO(3) \quad \forall f \in \mathcal{C}(S^2). \quad (2.3.5)$$

To accomplish this the algebra of $n \times n$ matrices $\text{Mat}_n(\mathbb{C})$ equipped with the adjoint $SU(2)$ action

$$\begin{aligned} SU(2) \times \text{Mat}_n(\mathbb{C}) &\rightarrow \text{Mat}_n(\mathbb{C}) \\ (G, M) &\mapsto \Pi_G \cdot M \cdot \Pi_G^{-1} \end{aligned} \quad (2.3.6)$$

has to be considered, where Π is the (unique up to equivalences) n -dimensional representation of $SU(2)$. This is in general a reducible representation. To decompose it, we can use that $\text{End}(\mathcal{H})$ is not only isomorphic to $\mathcal{H} \otimes \mathcal{H}^*$ as vector space, but also as representation² with \mathcal{H} carrying the representation Π . After applying the usual Clebsch-Gordon decomposition we get

$$\text{Mat}_n(\mathbb{C}) \doteq \mathbb{C}^n \otimes \mathbb{C}^{n*} \doteq (1) \oplus (3) \oplus \dots \oplus (2n-1) \quad (2.3.7)$$

²We use the extra symbol \doteq to emphasize that the isomorphism between spaces is also compatible with the action. For a usual isomorphism the symbol \cong is used.

with (d) denoting the d -dimensional representation of $SU(2)$. We choose a basis that is compatible with this decomposition and call the basis vectors \hat{Y}_m^l (the reason becomes clear in a moment) so that $(2l+1) = \langle \{\hat{Y}_m^l | m = -l, \dots, l\} \rangle$.

Now we are in a position to define a quantization map \mathcal{Q} which obviously preserves the $SO(3)$ symmetry:

$$\begin{aligned} \mathcal{Q} : \mathcal{C}(S^2) &\rightarrow \text{Mat}_n(\mathbb{C}) \\ Y_m^l &\mapsto \begin{cases} \hat{Y}_m^l & 2l+1 < 2n-1 \\ 0 & 2l+1 \geq 2n-1 \end{cases} \end{aligned} \quad (2.3.8)$$

For this reason, we call the matrices \hat{Y}_m^l spherical harmonics of the fuzzy sphere S_n^2 . It is clear that this map is surjective. Hence by restricting ourselves to finite dimensional matrices, we were led to introduce a natural angular momentum cutoff (at $l = n-1$).

Embedding functions. As mentioned in section §2.2 we are especially interested in the quantized embedding functions $X^a \sim x^a$. To identify them we can consider $Y_{\pm 1}^1 = x^1 \pm ix^2$ and $Y_0^1 = x^3$ where the x^i 's are viewed as coordinate functions $S^2 \hookrightarrow \mathbb{R}^3$, and their quantized versions $\hat{Y}_{\pm 1}^1 = X^1 \pm iX^2$ and $\hat{Y}_0^1 = X^3$. We already know that $\{\hat{Y}_0^1, \hat{Y}_{\pm 1}^1\}$ is a basis of a 3-dimensional $SU(2)$ representation³, hence the X^a have to be the generators of the n -dimensional $SU(2)$ representation and thus satisfy

$$[X^a, X^b] = iC \varepsilon_{abc} X^c \quad (2.3.9)$$

for some constant C ; ε_{abc} being the Levi-Civita symbol.

In the semi-classical limit we want to have a sphere with radius 1, therefore we choose C so that $\sum_{i=1}^3 (X^i)^2 = \mathbb{1}$, which implies that $C = 2/\sqrt{n^2 - 1}$. It also becomes apparent what the scale parameter θ in the case of the fuzzy sphere should be. Since we want the commutator to vanish in semi-classical limit we choose $\theta = 1/n$.

Poisson structure. We have seen in section §2.1 that for a proper quantization map one also needs a Poisson structure on the manifold S^2 . Having established equation (2.3.9) and looking at the correspondence principle in definition 2.3 one can read off (up to leading order in $\theta = 1/n$) the required Poisson structure

$$\{x^a, x^b\}_{S^2} = \frac{2}{n} \varepsilon_{abc} x^c \quad (2.3.10)$$

which happens to be the unique (up to a constant factor) $SU(2)$ -invariant Poisson structure on S^2 .

Remaining quantization map axioms. It can be rigorously shown that the remaining quantization map axioms defined in (2.3) are also true for the Fuzzy Sphere. [8]

We, therefore, conclude that the fuzzy sphere S_n^2 is indeed a quantization of $(S^2, \{.,.\}_{S^2})$.

2.4. Fuzzy \mathbb{CP}^2

The sphere S^2 can also be seen as co-adjoint orbit of the Lie group $SU(2)$. The complex projective space \mathbb{CP}^2 is a generalization of the fuzzy sphere in the sense that we go from $SU(2)$ to $SU(3)$. The following construction of fuzzy \mathbb{CP}^2 could also be directly generalized to $SU(n)$ and is based on [3, 12].

Fuzzy \mathbb{CP}^2 is not only an interesting example for itself, but is also of importance to us since in chapter 4 it turns out that a variant thereof is a solution of a deformed Yang-Mills theory, which is studied later.

³also often called a “Vector operator”

Co-adjoint orbits. First, consider the adjoint orbit of the Lie group G in general. Let \mathfrak{g} be its Lie algebra. Then G has a natural action on \mathfrak{g}^* called the co-adjoint action given by $g \triangleright \mu = \mu(g \cdot \cdot g^{-1})$ for a $g \in G$ and $\mu \in \mathfrak{g}^*$.

DEFINITION 2.4. The co-adjoint orbit \mathcal{O}_μ^* of a Lie group G at $\mu \in \mathfrak{g}^*$ is defined as

$$\mathcal{O}_\mu^* := \{\mu(g \cdot \cdot g^{-1}) \mid g \in G\}. \quad (2.4.1)$$

By definition, the co-adjoint orbit \mathcal{O}_μ^* is invariant under the co-adjoint action. It is an interesting fact that every orbit of G goes through an element of the dual space of the Cartan algebra \mathfrak{g}_0^* .

One of the reasons why co-adjoint orbits are of relevance to us is because they carry a natural symplectic form (which implies they also carry a Poisson structure): The tangent space of this orbit $T_\mu \mathcal{O}_\mu$ can be identified with $\mathfrak{g}/\mathfrak{K}_\mu$ where \mathfrak{K}_μ is the Lie algebra of the stabilizer group K_μ of μ . We are now able to define the G -invariant symplectic form as

$$\omega_\mu(X, Y) := \mu([X, Y]) \quad (2.4.2)$$

which is obviously antisymmetric and since $\mu([X, Y]) = 0 \iff X \in \mathfrak{K}_\mu$ it is also non-degenerate.

Let us now consider the special case $G = SU(3)$ ⁴. Since the Cartan algebra of $\mathfrak{su}(3)$ is generated by two elements t_3 and t_8 we have two possibilities to get different orbits. For our purpose we choose $\mu = t_8^*$ where $t_8 \in \mathfrak{su}(3)$ reads

$$t_8 = \frac{1}{2\sqrt{3}} \begin{pmatrix} 1 & 0 & 0 \\ 0 & 1 & 0 \\ 0 & 0 & -2 \end{pmatrix}.$$

We recognize a two-dimensional and a one-dimensional subspace where t_8 acts as a multiple of unity. Therefore the stabilizer group amounts to $K_{t_8^*} = SU(2) \times U(1)$ and we have found a characterization of the orbit $\mathcal{O}_{t_8^*}^*$ as

$$\mathcal{O}_{t_8^*}^* \cong SU(3)/(SU(2) \times U(1)). \quad (2.4.3)$$

The connection to \mathbb{CP}^2 . Let us consider S^5 embedded in \mathbb{C}^3 . The natural action of $SU(3)$ on $S^5 \subset \mathbb{C}^3$ is then given by matrix multiplication. This action is transitive according to the definition of $SU(3)$. Now it is easy to see that a subgroup $SU(2)$ (acting as $\begin{pmatrix} 1 & 0 \\ 0 & SU(2) \end{pmatrix}$) stabilizes the point $(1, 0, 0) \in \mathbb{C}^3$. Therefore,

$$S^5 \cong \frac{SU(3)}{SU(2)}. \quad (2.4.4)$$

The complex projective space \mathbb{CP}^2 is defined as

$$\mathbb{CP}^2 := \frac{\mathbb{C}^3 \setminus \{0\}}{\sim} \quad (2.4.5)$$

with $\xi_1 \sim \xi_2 : \iff \xi_1 = \lambda \xi_2, \lambda \in \mathbb{C} \setminus \{0\}$. The map ψ

$$\begin{aligned} \psi : S^5 \subset \mathbb{C}^3 &\rightarrow \mathbb{CP}^2 \\ (\xi_1, \xi_2, \xi_3) &\mapsto [\xi_1, \xi_2, \xi_3] \end{aligned} \quad (2.4.6)$$

is surjective but not injective because $\psi(e^{i\theta}\xi) = \psi(\xi)$. Hence we get an isomorphism

$$S^5/U(1) \cong \mathbb{CP}^2 \quad (2.4.7)$$

from which we conclude that the co-adjoint orbit $\mathcal{O}_{t_8^*}^*$ and \mathbb{CP}^2 are isomorphic.

⁴For more information on $SU(3)$ see appendix A.

Characteristic equation. We are now able to show that the elements of $\mathcal{O}_{t_8}^*$ satisfy a characteristic equation. Let $T \in \mathfrak{su}(3)$, then

$$T^* \in \mathcal{O}_{H_8}^* \iff T \cdot T + \frac{1}{2\sqrt{3}}T - \frac{1}{6} = 0 \quad (2.4.8)$$

PROOF. Let $T^* \in \mathcal{O}_{t_8}^*$, then $T = g \cdot t_8 \cdot g^{-1}$ for some $g \in SU(3)$ and $T \cdot T + \frac{1}{2\sqrt{3}}T - \frac{1}{6} = g \cdot (t_8 \cdot t_8 + \frac{1}{2\sqrt{3}}t_8 - \frac{1}{6}) \cdot g^{-1} = 0$ by explicit calculation.

On the other hand, let $T \in \mathfrak{su}(3)$ and the characteristic equation be true, then the eigenvalues of T have to satisfy $\lambda^2 + \frac{1}{2\sqrt{3}}\lambda - \frac{1}{6} = 0$. This quadratic equation has two solutions $\lambda \in \{-\frac{1}{\sqrt{3}}, \frac{1}{2\sqrt{3}}\}$. Since T is traceless, its diagonal form is $D = \text{diag}(\frac{1}{2\sqrt{3}}, \frac{1}{2\sqrt{3}}, -\frac{1}{\sqrt{3}})$. Therefore, $T = U \cdot D \cdot U^{-1}$ for some $U \in SU(3)$ and $T^* \in \mathcal{O}_{t_8}^*$. \square

We can expand equation (2.4.8) in some basis of $\mathfrak{su}(3) \cong \mathbb{R}^8$, i.e. $T = \sum_{a=1}^8 x^a t_a$ and obtain equations for the coordinates x^a

$$\begin{aligned} x^a x^b d^{abc} &= -\frac{1}{\sqrt{3}} x^c \\ x^a x^b \delta^{ab} &= 1 \end{aligned} \quad (2.4.9)$$

where d^{abc} are the symmetric structure constants of $\mathfrak{su}(3)$ (see section §A.1). These equations define the embedding of \mathbb{CP}^2 as 4-dimensional manifold in \mathbb{R}^8 .

The following procedure is performed in close analogy to the fuzzy sphere case.

Decomposition of its algebra of functions. Because of equation (2.4.3) we have — as in the case of the fuzzy sphere — a natural action on the algebra of functions $\mathcal{C}(\mathbb{CP}^2)$ which enables us to decompose it as

$$\mathcal{C}(\mathbb{CP}^2) \doteq \bigoplus_{p=0}^{\infty} \mathcal{H}_{(p,p)}, \quad (2.4.10)$$

herein $\mathcal{H}_{(p,p)}$ carries the (p, p) representation of $SU(3)$.

Quantization map. In contrast to the fuzzy sphere case we now demand our quantization map \mathcal{Q} to be compatible with the $SU(3)$ symmetry, i.e.

$$\mathcal{Q}(g \triangleright f) = g \triangleright \mathcal{Q}(f) \quad \forall g \in SU(3) \quad \forall f \in \mathcal{C}(\mathbb{CP}^2). \quad (2.4.11)$$

In analogy to the fuzzy sphere we consider the algebra of $m \times m$ matrices $Mat_m(\mathbb{C}) \cong End(\mathcal{H}_{(0,n)})^5$ equipped with the adjoint action of $SU(3)$

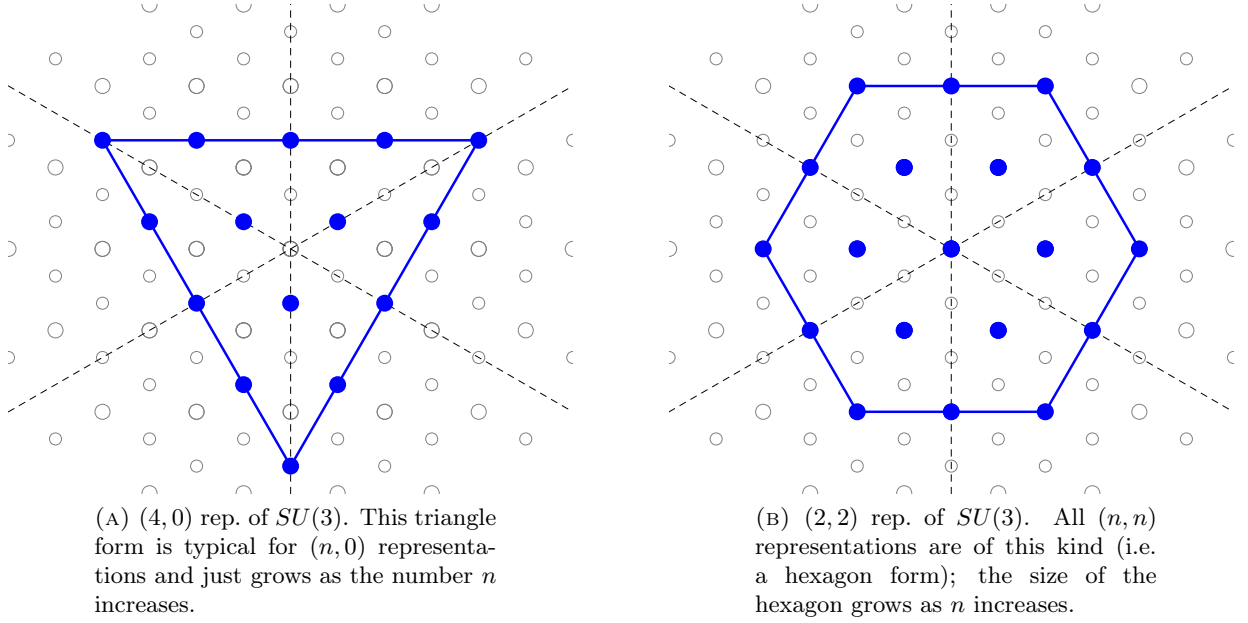
$$\begin{aligned} SU(3) \times Mat_m(\mathbb{C}) &\rightarrow Mat_m(\mathbb{C}) \\ (g, M) &\mapsto \Pi_g^{(0,n)} \cdot M \cdot (\Pi_g^{(0,n)})^{-1} \end{aligned} \quad (2.4.12)$$

where $\Pi^{(0,n)}$ is the $(0, n)$ representation of $SU(3)$ (see figure 2.4.1a for a graphical portrayal). Under this action $Mat_m(\mathbb{C})$ decomposes as⁶

$$Mat_m(\mathbb{C}) \doteq \mathcal{H}_{(0,n)} \otimes \mathcal{H}_{(0,n)}^* \doteq \bigoplus_{p=0}^n \mathcal{H}_{(p,p)} \quad (2.4.13)$$

⁵In accordance with the general formula (A.2.3) $m = \dim(\mathcal{H}_{(n,0)}) = \frac{1}{2}(n+1)(n+2)$.

⁶The dual of the $(0, n)$ representation is just $(n, 0)$ (figure 2.4.1a) and its weight space diagram is a reflection of the $(0, n)$ -diagram at the horizontal axes.

FIGURE 2.4.1. Weight space diagrams of $(n, 0)$ and (n, n) -type representations of $SU(3)$

and we define the $SU(3)$ -action preserving quantization map \mathcal{Q} to be

$$\begin{aligned} \mathcal{Q} : \mathcal{C}(\mathbb{CP}^2) &\rightarrow \text{Mat}_m(\mathbb{C}) \\ Y_{(p,p)}^\Lambda &\mapsto \begin{cases} \hat{Y}_{(p,p)}^\Lambda & p \leq n \\ 0 & p > n \end{cases} \end{aligned} \quad (2.4.14)$$

where $Y_{(p,p)}^\Lambda$ respectively $\hat{Y}_{(p,p)}^\Lambda$ is an appropriate basis of the particular $\mathcal{H}_{(p,p)}$ (see figure 2.4.1b).

Quantized embedding functions. Let X^a be the quantized embedding functions, i.e. $X^a = \mathcal{Q}(x^a)$ where the coordinate functions x^a are defined by equation (2.4.9). Since equation (2.4.11) holds in particular for the quantized embedding functions X^a we see by applying an infinitesimal $SU(3)$ transformation that

$$[d\Pi_{t^a}^{(0,n)}, X^b] = i c_{abc} X^c \quad (2.4.15)$$

with c_{abc} being the asymmetric structure constants of $SU(3)$ (see section §A.1). Equation (2.4.15) shows that the 8-dimensional vector space spanned by the matrices X^a , $a = 1, \dots, 8$ is invariant and irreducible under the adjoint action of $\mathfrak{su}(3)$. Therefore, by (2.4.13) it must hold that $X^a \in \mathcal{H}_{(1,1)}$ and hence

$$[X^a, X^b] = i C c_{abc} X^c \quad (2.4.16)$$

for some constant C . In the end the latter just determines the scale of the \mathbb{CP}^2 reached in the semi-classical limit. Using the quadratic Casimir operator of $SU(3)$ one sees that setting the constant to $C = 1/\sqrt{n(1+n/3)}$ yields a \mathbb{CP}^2 with radius 1 in the semi-classical limit.

Let us emphasize again that these relations are the defining equations of \mathbb{CP}_n^2 . They contain enough information to reconstruct the manifold \mathcal{M} reached in the semi-classical limit providing that the matrices X^a are interpreted as quantized embedding functions x^a .

The commutation relations (2.4.16) for the quantized embedding functions $X^a \sim x^a$ are compatible with the $SU(3)$ -invariant Poisson structure on \mathbb{CP}^2 in the sense that the correspondence principle (see definition 2.3) holds.

This concludes our discussion about Fuzzy \mathbb{CP}^2 for now. We will revisit it again in chapter 4.

2.5. Fuzzy Torus

An example which does not belong to the class of co-adjoint orbits is the torus $T^2 = S^1 \times S^1$. It can be embedded in \mathbb{R}^4 via the relations

$$\begin{aligned} x^1 + ix^2 &= e^{i\varphi} \\ x^3 + ix^4 &= e^{i\psi} \end{aligned} \quad (2.5.1)$$

where $\varphi, \psi \in [0, 2\pi)$ or more explicitly

$$\begin{aligned} x : T^2 &\hookrightarrow \mathbb{R}^4 \\ (\varphi, \psi) &\mapsto \begin{pmatrix} (e^{i\varphi} + e^{-i\varphi})/2 \\ -i(e^{i\varphi} - e^{-i\varphi})/2 \\ (e^{i\psi} + e^{-i\psi})/2 \\ -i(e^{i\psi} - e^{-i\psi})/2 \end{pmatrix} = \begin{pmatrix} \cos(\varphi) \\ \sin(\varphi) \\ \cos(\psi) \\ \sin(\psi) \end{pmatrix}. \end{aligned} \quad (2.5.2)$$

It becomes apparent by equation (2.5.1) that $T^2 \subset S^3$. Applying a generalized stereographic projection $S^3 \rightarrow \mathbb{R}^3$ yields a torus embedded in \mathbb{R}^3 which resembles the usual doughnut form (see figure 2.5.1).

We are again interested in symmetry properties of T^2 . It can easily be seen that the torus carries a $U(1) \times U(1)$ symmetry which acts simply by a multiplication of a phase factor

$$\begin{aligned} (U(1) \times U(1)) \times T^2 &\rightarrow T^2 \\ ((\Phi, \Psi), (\varphi, \psi)) &\mapsto (\varphi + \Phi, \psi + \Psi) \end{aligned} \quad (2.5.3)$$

which again induces an action on the algebra of functions on the torus $\mathcal{C}(T^2)$. A basis of $\mathcal{C}(T^2)$ which respects the symmetry is given by the functions $\phi_{l,k}$:

$$\phi_{l,k}(\varphi, \psi) := e^{il\varphi} e^{ik\psi}. \quad (2.5.4)$$

A function $f \in \mathcal{C}(T^2)$ expanded in this basis, i.e. $f(\varphi, \psi) = \sum_{l,k=-\infty}^{\infty} f_{l,k} \phi_{l,k}(\varphi, \psi)$, is nothing but the Fourier series of f .

Construction of matrix algebra⁷. To construct the appropriate form of the matrix algebra $Mat_n(\mathbb{C})$ we introduce the *shift matrix* U and the *clock matrix* V

$$U = \begin{pmatrix} 0 & 1 & & & \\ & 0 & 1 & & \\ & & \ddots & \ddots & \\ & & & 0 & 1 \\ 1 & & & & 0 \end{pmatrix}, \quad V = \begin{pmatrix} 1 & & & & \\ & q & & & \\ & & q^2 & & \\ & & & \ddots & \\ & & & & q^{n-1} \end{pmatrix} \quad (2.5.5)$$

⁷For reference see e.g. [22]

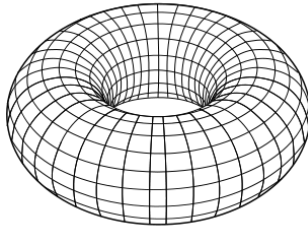


FIGURE 2.5.1. Torus

with $q := e^{2\pi i/n}$. These are unitary matrices with the property $U^n = V^n = \mathbb{1}$ obeying the commutation relations

$$[U, V] = (q - 1) V \cdot U. \quad (2.5.6)$$

It is clear that the set of matrices $\{\mathbb{1}, U, U^2, \dots, U^n\}$ respectively $\{\mathbb{1}, V, V^2, \dots, V^n\}$ forms a representation of the cyclic group $\mathbb{Z}_n = \langle w \rangle$.

Let us define the matrices $\Phi_{l,k}$

$$\Phi_{l,k} := U^l \cdot V^k \quad (2.5.7)$$

for $l, k \in \{-\frac{n-1}{2}, \dots, 0, \dots, \frac{n-1}{2}\}^8$ which are n^2 linear independent matrices and, therefore, a basis of $Mat_n(\mathbb{C})$. Let us consider now the adjoint action of $\mathbb{Z}_n \times \mathbb{Z}_n \subset U(1) \times U(1)$ on $Mat_n(\mathbb{C})$ given by

$$\begin{aligned} (\mathbb{Z}_n \times \mathbb{Z}_n) \times Mat_n(\mathbb{C}) &\rightarrow Mat_n(\mathbb{C}) \\ ((w^r, w^s), M) &\mapsto V^s \cdot (U^r \cdot M \cdot U^{-r}) \cdot V^{-s}. \end{aligned} \quad (2.5.8)$$

We can calculate the action on the basis $\Phi_{l,k}$ using equation (2.5.6) and get

$$(w^r, w^s) \triangleright \Phi_{l,k} = q^{\min\{s,l\}} q^{\min\{k,r\}} \Phi_{l,k}. \quad (2.5.9)$$

Therefore the one-dimensional subspaces spanned by the basis vectors are invariant under the $\mathbb{Z}_n \times \mathbb{Z}_n$ action.

Quantization map. Now it is easy to construct a quantization map \mathcal{Q} which respects the $\mathbb{Z}_n \times \mathbb{Z}_n \subset U(1) \times U(1)$ symmetry on our algebras.

$$\mathcal{Q} : \mathcal{C}(T^2) \rightarrow Mat_n(\mathbb{C}) \quad (2.5.10)$$

$$\phi_{l,k} \mapsto \begin{cases} q^{-\min\{l,k\}/2} \Phi_{l,k} & |l|, |k| \leq (n-1)/2 \\ 0 & \text{otherwise} \end{cases}.$$

The factor $q^{-\min\{l,k\}/2}$ is necessary for the quantization map \mathcal{Q} to fulfill $\mathcal{Q}(f^*) = \mathcal{Q}(f)^\dagger$ (property (3) of the quantization map axioms 2.3).

Poisson structure. From equation (2.5.6) we also can guess a suitable Poisson structure on $\mathcal{C}(T^2)$. Since $[\mathcal{Q}(e^{i\varphi}), \mathcal{Q}(e^{i\psi})] = [U, V] = (q - 1) U \cdot V = (q - 1) \mathcal{Q}(e^{i\psi}) \cdot \mathcal{Q}(e^{i\varphi})$ and $q = e^{2\pi i/n} = 1 + \frac{2\pi i}{n} + \mathcal{O}((\frac{1}{n})^2)$ it must hold by the correspondence principle in definition 2.3 that

$$2\pi i \mathcal{Q}(e^{i\psi}) \cdot \mathcal{Q}(e^{i\varphi}) = i \lim_{n \rightarrow \infty} n \mathcal{Q}(\{e^{i\varphi}, e^{i\psi}\}) \quad (2.5.11)$$

which can be achieved by requesting $\{e^{i\varphi}, e^{i\psi}\} = \frac{2\pi}{n} e^{i\varphi} e^{i\psi}$ assuming that $\mathcal{Q}(f \cdot g) \rightarrow \mathcal{Q}(f) \cdot \mathcal{Q}(g)$ as $n \rightarrow \infty$ ⁹. This allows us to conclude that

$$\{\varphi, \psi\}_{T^2} = -\frac{2\pi}{n} \quad (2.5.12)$$

which obviously is $U(1) \times U(1)$ invariant since it is constant. Furthermore, it can be proven by induction that this Poisson structure obeys the correspondence principle for all quantized functions in $Mat_n(\mathbb{C})$.

⁸We assume here and in the following text that n is odd. If n is not odd, we can just shift the indices $l, k \in \{-\frac{n}{2}, \dots, 0, \dots, \frac{n}{2} - 1\}$.

⁹This can be seen by using $\phi_{l,k} \phi_{n,m} = \phi_{l+n, k+m}$.

Quantized embedding functions. From equation (2.5.2) we can directly read off the quantized embedding functions $X^a = \mathcal{Q}(x^a)$:

$$\begin{aligned} X^1 &= (U + U^\dagger)/2 \\ X^2 &= -i(U - U^\dagger)/2 \\ X^3 &= (V + V^\dagger)/2 \\ X^4 &= -i(V - V^\dagger)/2 \end{aligned} \tag{2.5.13}$$

CHAPTER 3

Coherent States

Having discussed some examples of quantized spaces in chapter 2 by means of a bottom-up approach, we now want to turn around and address the problem within a top-down course of action. A powerful tool which provides a lot of insight is the so called *coherent state*.

Coherent states loosely speaking are localized states which are in some sense closest to the corresponding classical states; “closest” often means having minimum uncertainty. They correspond so to speak to points in classical space, i.e. states of the classical system. Extensive and differing treatments of coherent states were presented amongst others in [20, 29, 21, 19, 5, 11]. Nevertheless we follow a group theoretical approach of Perelomov [20] which fits quite well into the framework of non-commutative geometry - especially for those spaces that arise from co-adjoint orbits of Lie groups — and seems quite suitable for our needs.

Furthermore, coherent states provide the theoretical basis for the numerical algorithm which will be developed to retrieve the classical limit of a given brane configuration.

3.1. Localization and Dispersion

Given some matrices $\{X^a, a = 1, \dots, d\}$ and interpreting them as quantized embedding functions $X^a \sim x^a$ of a classical manifold embedded in \mathbb{R}^d which generate a matrix algebra $\mathcal{A} \subset \text{Mat}_n(\mathbb{C})$ acting on a Hilbert space \mathcal{H}_n we can interpret a normalized vector $|\Psi\rangle \in \mathcal{H}_n$ as quantized function on the fuzzy brane, i.e. $|\Psi\rangle\langle\Psi| \in \mathcal{A}$. Hence we can calculate the expectation value of X^a given by

$$\bar{p}(\Psi)_a := \langle X^a \rangle_\Psi = \text{tr}(X^a |\Psi\rangle\langle\Psi|) = \langle\Psi| X^a |\Psi\rangle, \quad (3.1.1)$$

similar to ordinary quantum mechanics. In analogy we can calculate the square of its standard deviation $(\Delta_\Psi X^a)^2$ as

$$(\Delta_\Psi X^a)^2 := \langle\Psi| (X^a)^2 |\Psi\rangle - \langle\Psi| X^a |\Psi\rangle^2. \quad (3.1.2)$$

A good measure for its localization is the *dispersion* $\delta(\Psi)$

$$0 \leq \delta(\Psi) := \sum_{a=1}^d (\Delta_\Psi X^a)^2. \quad (3.1.3)$$

The dispersion δ will be a guidepost for our definition of a coherent state. We would like the dispersion of states classified as coherent to be minimal. However, this requirement seems only to be realizable in very symmetric fuzzy spaces.¹ Consequently, in general we will weaken this criterion to allow states which are “near”² the minimum of δ .

¹We will see that the fuzzy branes obtained by co-adjoint orbits of Lie groups are candidates thereof.

²What is meant by “near” should become clearer in chapter 5.

3.2. Coherent States on the fuzzy sphere S_n^2

Recall that the fuzzy sphere S_n^2 is defined by three $n \times n$ matrices $X^a \sim x^a$ which satisfy the commutation relations

$$[X^a, X^b] = i \frac{2}{\sqrt{n^2 - 1}} \varepsilon_{abc} X^c \quad (3.2.1)$$

and generate the whole matrix algebra $Mat_n(\mathbb{C})$ which acts on the carrier space $\mathcal{H}_n \cong \mathbb{C}^n$.

Dispersion in the fuzzy sphere case. In the fuzzy sphere case we can simplify the dispersion (3.1.3) to

$$0 \leq \delta(\Psi) = \sum_{a=1}^3 (\Delta_\Psi X^a)^2 = \langle \Psi | \sum_{i=1}^3 (X^i)^2 | \Psi \rangle - \vec{p}(\Psi)^2 = 1 - |\vec{p}(\Psi)|^2, \quad (3.2.2)$$

noticing that $\sum_{i=1}^3 (X^i)^2 = \mathbb{1}$ is the quadratic Casimir of $SU(2)$. Since $0 \leq \delta(\Psi)$ this relation also shows that $|\vec{p}(\Psi)| \leq 1$. Since the expectation value square $|\vec{p}(\Psi)|^2$ is maximal for Ψ being an extremal weight vector Ψ_0 , $\delta(\Psi_0)$ is minimal.

In equation (3.2.2) we explicitly see that in the case of the fuzzy sphere S_n^2 the dispersion is minimized for states which are localized at (or near) the unit sphere S^2 . The fact that the dispersion is determined only by the localization of a state seems to be a little counter intuitive, but it only means that states localized near the unit sphere are forced to possess little dispersion in each direction because of the high symmetry.

Construction of coherent states. Since $(X^a)_{a=1,2,3}$ is a vector operator, \vec{p} also transforms as a vector, i.e. for $R \in SO(3)$ and $U_n(R)$ the n -dimensional representation of R we have

$$p^a(U_n(R) \cdot \Psi) = \sum_{b=1}^3 R^a_b p^b(\Psi) \quad (3.2.3)$$

and since $|\vec{p}(\Psi)|^2$ is an $SO(3)$ -invariant expression it follows that δ is invariant under the $SU(2)$ action. Because of the $SU(2)$ -invariance of the dispersion δ we can rotate the state Ψ_0 and obtain a class of states

$$\mathcal{O}_{\Psi_0} := \{U(g) \cdot \Psi_0 \mid g \in SU(2)\} \quad (3.2.4)$$

which are all optimally localized. One can also show that this is the only class that offers optimal locality (quantified by δ in equation (3.1.3)). Since the stabilizer group K_{Ψ_0} is $U(1)$ (acting with $e^{iX_3 t}$ yields a phase shift), we have $\mathcal{O}_{\Psi_0} \cong \frac{SU(2)}{U(1)} \cong S^2$, which at first sight looks promising.

Let us now explicitly calculate the dispersion and the expectation value for this orbit. For this purpose we consider the highest weight vector

$$\Psi_0 = \left| \frac{n-1}{2}, \frac{n-1}{2} \right\rangle \in \mathcal{H}_n,$$

written in standard QM notation. One can calculate the expected location of this state and the dispersion using standard knowledge of $SU(2)$ representations and we get

$$\vec{p}(\Psi_0) = \begin{pmatrix} 0 \\ 0 \\ \sqrt{\frac{n-1}{n+1}} \end{pmatrix} = \begin{pmatrix} 0 \\ 0 \\ 1 \end{pmatrix} + \mathcal{O}\left(\frac{1}{n}\right), \quad (3.2.5)$$

$$\delta(\Psi_0) = 1 - \frac{n-1}{n+1} = \frac{2}{n+1} = \mathcal{O}\left(\frac{1}{n}\right). \quad (3.2.6)$$

Furthermore, because of property (3.2.3) and equation (3.2.5) we get that the image of the orbit \mathcal{O}_{Ψ_0} under \vec{p} is

$$\vec{p}(\mathcal{O}_{\Psi_0}) = S^2 + \mathcal{O}\left(\frac{1}{n}\right), \quad (3.2.7)$$

which implies that in the limit $n \rightarrow \infty$ the coherent states are localized at the unit sphere S^2 . Additionally, their dispersion $\delta(\mathcal{O}_{\Psi_0})$ goes to zero as n tends to infinity. So in the limit the coherent states — which we can think of as quantized functions — become Dirac- δ -functions localized at the unit sphere; this leads us to the conclusion that we really retrieved S^2 from fuzzy S_n^2 in the limit $n \rightarrow \infty$!

3.3. Coherent States on fuzzy \mathbb{CP}_n^2

Fuzzy \mathbb{CP}_n^2 was defined by 8 matrices X^a which obey the commutation relation

$$[X^a, X^b] = i \frac{1}{\sqrt{n(1+n/3)}} c_{abc} X^c, \quad (3.3.1)$$

c_{abc} being the antisymmetric structure constants of $SU(3)$ given in section §A.1 which generate the matrix algebra $Mat_n(\mathbb{C})$ that acts on $\mathcal{H}_{(0,n)}$.

The construction of coherent states on \mathbb{CP}_n^2 is conducted in complete analogy with the fuzzy sphere S_n^2 . In fact, for all quantized spaces which arise from co-adjoint orbits this construction is valid as shown in [20].

The recipe works as follows: Take the highest weight vector $\Psi_0 \in \mathcal{H}$ of the given representation. Consider the orbit \mathcal{O}_{Ψ_0} generated by the group action. One easily recognizes that the orbit \mathcal{O}_{Ψ_0} is isomorphic to the co-adjoint orbit of G . Furthermore, Ψ_0 minimizes the dispersion δ defined in equation (3.1.3) when considering $G = SU(n)$. Since δ is group invariant, the whole orbit \mathcal{O}_{Ψ_0} minimizes the dispersion δ .

Explicit calculation for \mathbb{CP}_n^2 . Let us evaluate the expectation value and the dispersion of the highest weight vector $\Psi_0 \in \mathcal{H}_{(0,n)}$ explicitly for \mathbb{CP}_n^2 . Having a look at equation (3.2.2) we see that the relation is still valid when we replace the $SU(2)$ generators with $SU(3)$ ones:

$$0 \leq \delta(\Psi) = \sum_{a=1}^8 (\Delta_{\Psi} X^a)^2 = 1 - |\vec{p}(\Psi)|^2. \quad (3.3.2)$$

For the expectation value we get

$$\vec{p}(\Psi_0) = \begin{pmatrix} 0 \\ 0 \\ 0 \\ 0 \\ 0 \\ 0 \\ 0 \\ \sqrt{\frac{n}{3+n}} \end{pmatrix} = \begin{pmatrix} 0 \\ 0 \\ 0 \\ 0 \\ 0 \\ 0 \\ 0 \\ 1 \end{pmatrix} + \mathcal{O}\left(\frac{1}{n}\right), \quad (3.3.3)$$

and therefore,

$$p^a(\Psi_0) p^b(\Psi_0) \delta^{ab} = \frac{n}{3+n} = 1 + \mathcal{O}\left(\frac{1}{n}\right), \quad (3.3.4)$$

$$p^a(\Psi_0) p^b(\Psi_0) d^{abc} = \begin{pmatrix} 0 \\ 0 \\ 0 \\ 0 \\ 0 \\ 0 \\ -\frac{1}{\sqrt{3}} \frac{n}{3+n} \end{pmatrix}_c = -p^c(\Psi_0) + \mathcal{O}\left(\frac{1}{n}\right),$$

which reproduces the characteristic equations of \mathbb{CP}^2 (2.4.9) in the limit $n \rightarrow \infty$.³ The dispersion δ is then easily calculated:

$$\delta(\Psi_0) = 1 - \frac{n}{n+3} = \frac{3}{n+3} = \mathcal{O}\left(\frac{1}{n}\right) \quad (3.3.5)$$

and goes to zero as n tends to infinity as expected.

And since these equations transform correctly under the $SU(3)$ -action they are valid for the whole orbit $\mathcal{O}_{\Psi_0} \cong \mathbb{CP}^2$.

Note that $\mathcal{H}_{(0,n)}$ has three extremal weight vectors (see figure 2.4.1a) and we could also have evaluated the other two since they lie on the same orbit generated by the $SU(3)$ -action.

³The reason for choosing $\mathcal{H}_{(0,n)}$ and not $\mathcal{H}_{(n,0)}$ for \mathbb{CP}^2 in the first place is that we would only reproduce equation (2.4.9) up to a sign and therefore get a different embedding in \mathbb{R}^8 which would not match the embedding arisen from the co-adjoint orbit.

CHAPTER 4

Squashed \mathbb{CP}^2

Having discussed some examples of non-commutative geometry and methods to find their semi-classical limit we will now look into the applications to physics. For this reason we will study the $\mathcal{N} = 1$ supersymmetric $U(N)$ Yang-Mills (SYM) theory reduced to 4 dimensions modified by a cubic potential [24]. We will then determine the equation of motions for static scalar fields.

After establishing the setup, a modification of \mathbb{CP}_n^2 , namely *Squashed \mathbb{CP}_n^2* [24] will be introduced in section §4.2 which — as we will see — is a solution to the model introduced below.

4.1. Supersymmetric Yang-Mills Theory

10-dimensional SYM. The action of the $\mathcal{N} = 1$ supersymmetric $U(N)$ Yang-Mills theory in 10 dimensions can be written as

$$\mathcal{S}_{\text{YM}} = \int d^{10}x \left(\frac{1}{g^2} \mathcal{F}_{IJ} \mathcal{F}^{IJ} - i \bar{\Psi} \Gamma^I D_I \Psi \right), \quad (4.1.1)$$

which after a dimensional reduction [4] to 4 dimensions reads

$$\begin{aligned} S_{\text{YM}} = \int d^4x \operatorname{tr}_N \left(-\frac{1}{g^2} F^{\mu\nu} F_{\mu\nu} - \frac{1}{2} D^\mu \Phi^a D_\mu \Phi_a + \frac{1}{4} g^2 [\Phi^a, \Phi^b][\Phi_a, \Phi_b] + \right. \\ \left. + \bar{\Psi} \gamma^\mu D_\mu \Psi + g \bar{\Psi} \Gamma^a [\Phi_a, \Psi] \right) \end{aligned} \quad (4.1.2)$$

with $F_{\mu\nu}$ being the antisymmetric field strength tensor, D_μ the covariant derivative,

$$\begin{aligned} F_{\mu\nu} &= \partial_\mu A_\nu - \partial_\nu A_\mu + g [A_\mu, A_\nu], \\ D_\mu &= \partial_\mu - i [A_\mu, \cdot], \end{aligned}$$

Φ_a , $a \in \{1, \dots, 6\}$ matrix valued scalar fields and Ψ a dimensionally reduced matrix valued Majorana-Weyl spinor of $SO(9, 1)$ (i.e. $\Psi \in \mathbb{C}^{2^{4/2}} \otimes \mathbb{C}^{2^{6/2}} \otimes \operatorname{Mat}_N(\mathbb{C})$). The symbol γ^μ denotes the usual 4 Dirac-Gamma matrices (i.e. a representation of the Clifford algebra $C\ell_{3,1}(\mathbb{R})$) while $\{\Gamma^a, a = 1, \dots, 6\}$ forms a representation of $C\ell_6(\mathbb{R})$.

The action (4.1.2) is interpreted as field theory on $\mathcal{M}_4 \times \mathcal{K}_6$ where \mathcal{M}_4 is a 4-dimensional manifold with Minkowski metric signature and $\mathcal{K}_6 \subset \mathbb{R}^6$ an internal 6-dimensional compact fuzzy space. Hence the scalar fields Φ^a are to be interpreted as quantized embedding functions on \mathcal{K}_6 .

Deformed model. For our purpose we consider the model deformed by a (soft supersymmetry breaking) cubic potential,

$$S_{\text{YM}} + \int d^4x \operatorname{tr}_N \left(\frac{i}{2} g^{3/2} f_{abc} \Phi^a \Phi^b \Phi^c \right) \quad (4.1.3)$$

where f_{abc} is a constant tensor antisymmetric in all indices.

At this point we are only interested in static solutions of the scalar fields Φ_a . After absorbing the coupling constant g by the substitution $X^a := \sqrt{g} \Phi^a$ we get the resulting 6-dimensional matrix

model

$$S[X] = \text{tr} \left(\frac{1}{4} [X^a, X^b] [X_a, X_b] + \frac{i}{2} f_{abc} X^a X^b X^c \right). \quad (4.1.4)$$

Symmetries. The action (4.1.4) is invariant under *gauge transformations*

$$X^a \mapsto U X^a U^{-1}, \quad U \in U(N), \quad (4.1.5)$$

which can be seen by noting that $[X^a, X^b] \mapsto U [X^a, X^b] U^{-1}$ and using cyclic permutations under the trace operation.

Additionally, it is symmetric under *translations*

$$X^a \mapsto X^a + c^a \mathbb{1} \quad (4.1.6)$$

which is obvious for the first term $[X^a, X^b] [X_a, X_b]$ while the second term transforms as

$$f_{abc} X^a X^b X^c \mapsto f_{abc} X^a X^b X^c + f_{abc} (X^a X^b c^c + X^a c^b X^c + c^a X^b X^c)$$

but since f_{abc} is antisymmetric in all indices we can use that $f_{abc} X^a X^b = f_{abc} \frac{1}{2} [X^a, X^b]$ and thus the trace of the extra terms yields zero.

Equations of motion. As usual the equations of motion can be obtained via the equations

$$\frac{dS[X]}{dX^a} = 0 \quad (4.1.7)$$

where usual matrix calculus can be applied.

Evaluating the derivative of the first term making heavy use of the Leibniz rule and cyclic permutations under the trace yields¹

$$\begin{aligned} 0 &= d \left(\text{tr} \frac{1}{4} [X^a, X^b] [X_a, X_b] \right) \\ &= -\text{tr} \left([X^b, [X_b, X_a]] dX^a \right) \end{aligned}$$

while the second term reads

$$\begin{aligned} 0 &= d \left(\text{tr} \frac{i}{2} f_{abc} X^a X^b X^c \right) \\ &= \text{tr} \left(\frac{3}{2} i f_{abc} X^b X^c dX^a \right). \end{aligned}$$

Therefore after introducing the matrix Laplace operator $\square := \delta_{ab} [X^a, [X^b, \cdot]]$ the equations of motion for the quantized embedding functions X^a can be written as:

$$\boxed{\square X^a = \frac{3}{2} i f_{abc} X^b X^c} \quad (4.1.8)$$

4.2. Squashed Fuzzy \mathbb{CP}^2 As Solution

To begin with we consider again \mathbb{CP}_n^2 described by eight $\frac{1}{2}(n+1)(n+2) \times \frac{1}{2}(n+1)(n+2)$ matrices X^a interpreted as quantized embedding functions $X^a \sim x^a$ which satisfy

$$[X^a, X^b] = i \frac{1}{\sqrt{n(1+n/3)}} c_{abc} X^c. \quad (4.2.1)$$

¹Note that throughout this paper $X^a = X_a$.

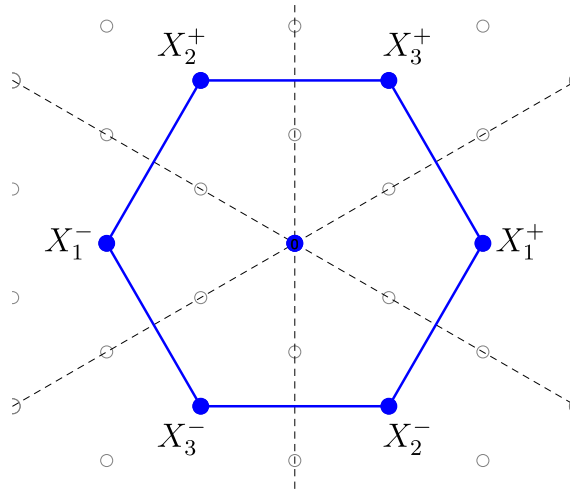


FIGURE 4.2.1. The $(1,1)$ representation of $SU(3)$. One sees that $|1,0\rangle_1 \cong X_1^+$, $|\frac{-1}{2}, \frac{\sqrt{3}}{2}\rangle_1 \cong X_2^+$, $|\frac{1}{2}, \frac{\sqrt{3}}{2}\rangle_1 \cong X_3^+$ and so on.

Squashed fuzzy \mathbb{CP}^2 is then defined by six of the eight matrices $\{X^a, a \in \mathcal{I} = \{1, 2, 4, 5, 6, 7\}\}$ which corresponds² to a squashed \mathbb{CP}^2 in the semiclassical limit defined by the projection

$$\begin{aligned} \Pi : \mathbb{R}^8 &\rightarrow \mathbb{R}^6 \\ (x^a)_{a=1,\dots,8} &\mapsto (x^a)_{a \in \mathcal{I}} \end{aligned} \quad (4.2.2)$$

as squashed 4-dimensional manifold embedded in \mathbb{R}^6 , $\Pi(\mathbb{CP}^2) \hookrightarrow \mathbb{R}^6$. Since the Cartan generators X^3 and X^8 can be generated by $X^a, a \in \mathcal{I}$ due to the commutator relations, the algebra generated by them is as in the non-squashed case the full matrix algebra $Mat_m(\mathbb{C})$.

Squashed \mathbb{CP}_n^2 as solution of the matrix model. We want to show that these matrices are a solution of the matrix model (4.1.4) discussed above. To this end we consider now the natural Laplace operator \square on squashed \mathbb{CP}_n^2

$$\square := \sum_{a \in \mathcal{I}} [X^a, [X^a, \cdot]] \quad (4.2.3)$$

which can be written as $\square = \sum_{i=1}^8 ad_{X^i}^2 - ad_{X^3}^2 - ad_{X^8}^2$ where ad denotes the adjoint representation of $\mathfrak{su}(3)$. The first term can be identified with the quadratic Casimir operator of $SU(3)$. Choosing a basis

$$|\lambda, y\rangle_p \in Mat_m(\mathbb{C}) \doteq \bigoplus_{p=0}^n V_{(p,p)}$$

so that $|\lambda, y\rangle_p \in V_{(p,p)}$ and $ad_{\pi_{(p,p)}(t_3)} |\lambda, y\rangle_p = \lambda |\lambda, y\rangle_p$ respectively $ad_{\pi_{(p,p)}(t_8)} |\lambda, y\rangle_p = y |\lambda, y\rangle_p$ one can immediately read off the eigenvectors respectively eigenvalues as

$$\square |\lambda, y\rangle_p = c_n^2 (p(2+p) - (\lambda^2 + y^2)) |\lambda, y\rangle_p \quad (4.2.4)$$

with $1/c_n^2 = n(1 + n/3)$.

In particular since the vectors $|\lambda, y\rangle_1$ correspond to the roots of $SU(3)$ (see figure 4.2.1) we find that $\square X_i^\pm = 2c_n^2 X_i^\pm$ and hence

$$\square X^a = 2c_n^2 X^a \quad \forall a \in \mathcal{I}. \quad (4.2.5)$$

²This claim will be justified in section §4.3 and later supported by numerical calculations.

Let us now define the *reduced structure constants* g_{abc} where the indices are confined to \mathcal{I} and $g_{abc} = c_{abc} \forall a, b, c \in \mathcal{I}$. Then

$$\sum_{c \in \mathcal{I}} i g_{abc} X^c = \underbrace{\sum_{c=1}^8 i c_{abc} X^c}_{1/c_n [X^a, X^b]} - \sum_{c=3,8} i c_{abc} X^c$$

and hence

$$\begin{aligned} \sum_{b \in \mathcal{I}} \sum_{c \in \mathcal{I}} i g_{abc} [X^b, X^c] &= \frac{1}{c_n} \underbrace{\sum_{b \in \mathcal{I}} [X^b, [X^a, X^b]]}_{-\square X^a} - \sum_{b \in \mathcal{I}} \sum_{c=3,8} i c_{abc} \underbrace{[X^b, X^c]}_{\sum_{d=1}^8 i c_n c_{bcd} X^d} \\ &= -\frac{1}{c_n} \square X^a + c_n \sum_{d=1}^8 \underbrace{\left(\sum_{c=3,8} \sum_{b \in \mathcal{I}} c_{abc} c_{bcd} \right)}_{\delta_{ad}} X^d \\ &= -\frac{1}{c_n} \square X^a + c_n X^a \end{aligned}$$

and using equation (4.2.5) we get

$$i g_{abc} [X^b, X^c] = -c_n X^a$$

or equivalently

$$\square X^a = -i 4 c_n g_{abc} X^b X^c \quad (4.2.6)$$

which is in agreement with [24] apart from discrepancies due to different conventions.

Recalling the equations of motion (4.1.8) of the matrix model in consideration, we see that for

$$f_{abc} = -\frac{8}{3} c_n g_{abc} \quad (4.2.7)$$

the squashed fuzzy \mathbb{CP}^2 is a solution of this model!

4.3. Coherent States on Squashed \mathbb{CP}_n^2

For the squashed co-adjoint orbit the situation is not as easy as in section §3.3 since we lost the $SU(3)$ symmetry. Nevertheless, it turns out that explicit calculations even for squashed \mathbb{CP}^2 are possible.

Essential is, of course, again the dispersion δ which serves as measure for localization and is defined as in the general case (3.1.3)

$$\delta(\Psi) := \sum_{a \in \mathcal{I}} (\Delta_\Psi X^a)^2. \quad (4.3.1)$$

A $U(1) \times U(1)$ symmetry as remnant of $SU(3)$. We can rewrite the dispersion δ in terms of the roots of $SU(3)$ (see section §A.1) given by

$$\begin{aligned} X_1^\pm &= X_4 \pm i X_5, \\ X_2^\pm &= X_6 \pm i X_7, \\ X_3^\pm &= X_1 \pm i X_2 = \pm [X_1^\pm, X_2^\mp]. \end{aligned} \quad (4.3.2)$$

After the substitution the dispersion reads

$$\delta(\Psi) = \frac{1}{2} \sum_{i=1}^3 (\langle X_i^+ X_i^- \rangle_\Psi + \langle X_i^- X_i^+ \rangle_\Psi - 2 \langle X_i^+ \rangle_\Psi \langle X_i^- \rangle_\Psi). \quad (4.3.3)$$

Rewriting the dispersion δ into the form (4.3.3) makes it clear that it is invariant under a $U(1) \times U(1)$ group acting as

$$X_i^\pm \mapsto Ad_{\varphi T_3 + \vartheta T_8} (X_i^\pm) = e^{\pm i\varphi_i} e^{\pm i\vartheta_i} X_i^\pm, \quad (4.3.4)$$

since expressions like $X_i^+ X_i^-$ transform as

$$X_i^+ X_i^- \mapsto \left(e^{+i\varphi_i} e^{+i\vartheta_i} X_i^+ \right) \left(e^{-i\varphi_i} e^{-i\vartheta_i} X_i^- \right) = X_i^+ X_i^-, \quad (4.3.5)$$

i.e. they are invariant.

Note that also the norm of the expectation values $|\vec{p}(\Psi)|$ is invariant under $U(1) \times U(1)$ transformations since $|\vec{p}(\Psi)|^2$ can be written as

$$|\vec{p}(\Psi)|^2 = \sum_{i=1}^3 (\langle X_i^+ \rangle_\Psi \langle X_i^- \rangle_\Psi). \quad (4.3.6)$$

Explicit calculations. For explicit calculations it seems, nevertheless, more convenient to write the dispersion in the form

$$\delta(\Psi) = \langle \Psi | \underbrace{\sum_{a=1}^8 (X^a)^2}_{\mathbb{1}} | \Psi \rangle - \sum_{i=3,8} \langle \Psi | (X^i)^2 | \Psi \rangle - |\vec{p}(\Psi)|^2. \quad (4.3.7)$$

Evaluating the expectation value $\vec{p}(\Psi)$ and the dispersion $\delta(\Psi)$ explicitly for the extremal weight state $|\Psi_0\rangle$ is possible and yields

$$\vec{p}(\Psi_0) = 0 \quad (4.3.8)$$

and

$$\delta(\Psi_0) = 1 - \frac{n}{3+n} - 0 = \frac{3}{n+3} = \mathcal{O}\left(\frac{1}{n}\right). \quad (4.3.9)$$

We see that in the squashed case the extremal weight states are now located at the origin while the dispersion is the same as in the non-squashed case (cf. equation (3.3.5)). Since in addition $\delta(\Psi_0)$ also tends to zero as n goes to infinity the highest weight state $|\Psi_0\rangle$ is a good candidate for a coherent state. The same is true for the other two extremal states because of the remaining $SU(3)$ -Weyl symmetry.

Rotations of the highest weight state. Let us investigate how $SU(3)$ rotations of the highest weight state affect the location and the dispersion. First of all, since $T_3^\pm = T^1 \pm iT^2$ annihilate $|\Psi_0\rangle$ and T^3, T^8 are only acting via a phase shift³, we are left with 4 non-trivial directions⁴ which correspond to rotation generators T^4, T^5, T^6, T^7 . Calculating the expectation values \vec{p} of the rotated vectors

$$|\varphi\rangle := \exp(i\varphi_1 T^4 + i\varphi_2 T^5 + i\varphi_3 T^6 + i\varphi_4 T^7) |\Psi_0\rangle \quad (4.3.10)$$

with $\varphi = (\varphi_1, \varphi_2, \varphi_3, \varphi_4)$ yields (see appendix B for details)

$$\vec{p}(\varphi) = c_n \frac{n}{2} \frac{1}{|\varphi|} \begin{pmatrix} \frac{(\varphi_1 \varphi_3 + \varphi_2 \varphi_4)}{|\varphi|} (\cos |\varphi| - 1) \\ 2 \frac{(\varphi_1 \varphi_4 - \varphi_2 \varphi_3)}{|\varphi|} \sin^2 \frac{|\varphi|}{2} \\ \varphi_2 \sin |\varphi| \\ -\varphi_1 \sin |\varphi| \\ \varphi_4 \sin |\varphi| \\ -\varphi_3 \sin |\varphi| \end{pmatrix}, \quad (4.3.11)$$

³This corresponds to the stabilizer of $|\Psi_0\rangle$, $\mathcal{K}_{\Psi_0} = SU(2) \times U(1)$.

⁴The same consideration is true for the non-squashed \mathbb{CP}^2 which is one way of reasoning that it must be a 4-dimensional manifold.

and since $c_n \frac{n}{2} = \frac{1}{2} \sqrt{\frac{n}{1+n/3}}$, the norm $|\vec{p}(\varphi)|$ fulfills

$$|\vec{p}(\varphi)|^2 = \underbrace{\left(c_n \frac{n}{2}\right)^2}_{\frac{3}{4} + \mathcal{O}(\frac{1}{n})} \left(\frac{(\varphi_1 \varphi_3 + \varphi_2 \varphi_4)^2}{|\varphi|^2} (\cos |\varphi| - 1)^2 + 4 \frac{(\varphi_1 \varphi_4 - \varphi_2 \varphi_3)^2}{|\varphi|^2} \sin^4 \frac{|\varphi|}{2} + \sin^2 |\varphi| \right). \quad (4.3.12)$$

Note that we could also have considered a different parametrization, that is

$$e^{i\vartheta_1 T^4} e^{i\vartheta_2 T^5} e^{i\vartheta_3 T^6} e^{i\vartheta_4 T^7} |\Psi_0\rangle, \quad (4.3.13)$$

but the obtained expressions get hopelessly long.

To calculate the dispersion δ we have to take care of the second term in equation (4.3.7). See appendix B for the calculation details and the full expression. Plugging the results into the dispersion (4.3.7) and simplifying provides the final result:

$$\begin{aligned} \delta(\varphi) = & \frac{3}{8(3+n)} \frac{1}{|\varphi|^4} \left\{ 4(\varphi_1^2 + \varphi_2^2)(\varphi_3^2 + \varphi_4^2) \cos |\varphi| \right. \\ & + (\varphi_1^4 + \varphi_2^4 + \varphi_1^2(2\varphi_2^2 + \varphi_3^2 + \varphi_4^2) + \varphi_2^2(\varphi_3^2 + \varphi_4^2) + (\varphi_3^2 + \varphi_4^2)^2) \cos 2|\varphi| \\ & \left. + (7(\varphi_1^4 + \varphi_2^4) + 7(\varphi_3^2 + \varphi_4^2)^2 + 11\varphi_2^2(\varphi_3^2 + \varphi_4^2)) \right\}. \end{aligned} \quad (4.3.14)$$

Here we see that the dispersion δ vanishes as n goes to infinity, which means that even after squashing the rotated states can be considered to be coherent as they become completely localized in the semi-classical limit! This strongly supports the claim that the semi-classical limit of squashed \mathbb{CP}_n^2 is in fact $\Pi(\mathbb{CP}^2)$.

Moreover, one can check that the dispersion (4.3.14) satisfies the sharp inequality

$$\frac{2}{3+n} \leq \delta(\varphi) \leq \frac{3}{3+n} \quad (4.3.15)$$

which surprisingly implies that the highest weight vector $|\Psi_0\rangle$ actually has the highest dispersion in this class of states (and not the lowest as one might have guessed).

Let us discuss some limits to check the plausibility of the formulas (4.3.14) and (4.3.11).

Limit $|\varphi| \rightarrow 0$. First it can easily be seen that in the limit $|\varphi| \rightarrow 0$ the expectation value $\vec{p}(\varphi)$ goes to zero as expected. Furthermore

$$\lim_{|\varphi| \rightarrow 0} \delta(\varphi) = \frac{3}{3+n} \quad (4.3.16)$$

which correctly reproduces the dispersion of the highest weight state in formula (4.3.9).

Limit $\varphi_1, \varphi_3 \rightarrow 0$. In the limit $\varphi_1 \rightarrow 0, \varphi_3 \rightarrow 0$ the expectation values read

$$\lim_{\varphi_1, \varphi_3 \rightarrow 0} \vec{p}(\varphi) = c_n \frac{n}{2} \frac{1}{|\varphi|} \begin{pmatrix} \frac{\varphi_2 \varphi_4}{|\varphi|} (\cos |\varphi| - 1) \\ 0 \\ \varphi_2 \sin |\varphi| \\ 0 \\ \varphi_4 \sin |\varphi| \\ 0 \end{pmatrix}, \quad (4.3.17)$$

so this corresponds to a section of squashed \mathbb{CP}^2 through the $x_2 = x_5 = x_7 = 0$ hyperplane.⁵ Plotting this 2-dimensional manifold reproduces figure 4.3.1 first published in [24].

⁵Remember: the numbering was chosen to be consistent with the non-squashed scheme. Since x_3 and x_8 were “projected away”, the third component in \vec{p} corresponds to x_4 and so on.

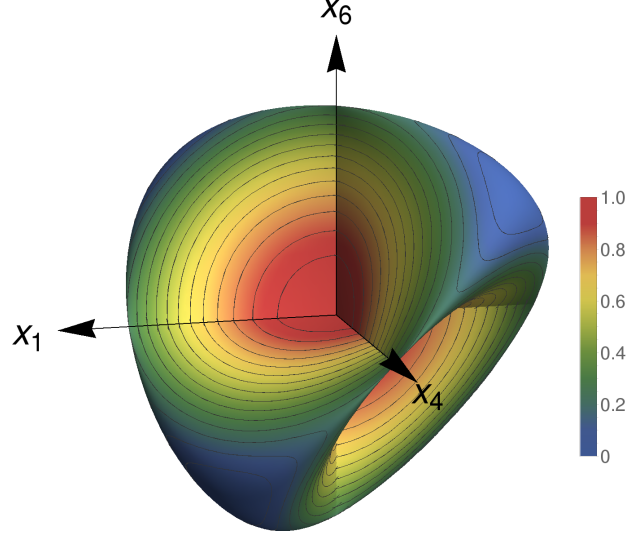


FIGURE 4.3.1. A 3-dimensional section of $\Pi(\mathbb{CP}^2)$ through $x_2 = x_5 = x_7 = 0$ plane, originally printed in [24]. The color indicates the corresponding scaled and shifted dispersion $\bar{\delta}$, which has its minimum at 0 ($\triangleq \frac{2}{3+n}$) and maximum at 1 ($\triangleq \frac{3}{3+n}$). The lines represent contour lines of $\bar{\delta}$.

The dispersion (4.3.14) reduces in the limit to

$$\begin{aligned} \lim_{\varphi_1, \varphi_3 \rightarrow 0} \delta(\varphi) = & \frac{3}{8(3+n)} \frac{1}{|\varphi|^4} \{ 4\varphi_2^2 \varphi_4^2 \cos |\varphi| \\ & + (\varphi_2^4 + \varphi_2^2 \varphi_4^2 + \varphi_4^4) \cos 2|\varphi| \\ & + 7(\varphi_2^4 + \varphi_4^4) + 11\varphi_2^2 \varphi_4^2 \} \end{aligned} \quad (4.3.18)$$

whose global minima lie at

$$|\varphi_2| = |\varphi_4| = \sqrt{2} \arctan(\sqrt{2}). \quad (4.3.19)$$

This corresponds to 4 points on $\Pi(\mathbb{CP}^2)$, namely

$$c_n \frac{n}{3} \begin{pmatrix} -1 \\ 0 \\ 1 \\ 0 \\ 1 \\ 0 \end{pmatrix}, \quad c_n \frac{n}{3} \begin{pmatrix} 1 \\ 0 \\ 1 \\ 0 \\ -1 \\ 0 \end{pmatrix}, \quad c_n \frac{n}{3} \begin{pmatrix} -1 \\ 0 \\ -1 \\ 0 \\ -1 \\ 0 \end{pmatrix}, \quad c_n \frac{n}{3} \begin{pmatrix} 1 \\ 0 \\ -1 \\ 0 \\ 1 \\ 0 \end{pmatrix},$$

which can be seen in figure 4.3.1 as centers of the blue zones.

Limit $\varphi_3, \varphi_4 \rightarrow 0$. Another interesting case is the limit $\varphi_3, \varphi_4 \rightarrow 0$. We are only allowing rotations by T^4 and T^5 and since $\{T^4, T^5, T^8\}$ form the $\mathfrak{su}(3)$ -subalgebra $\mathfrak{su}(2)$, this case essentially

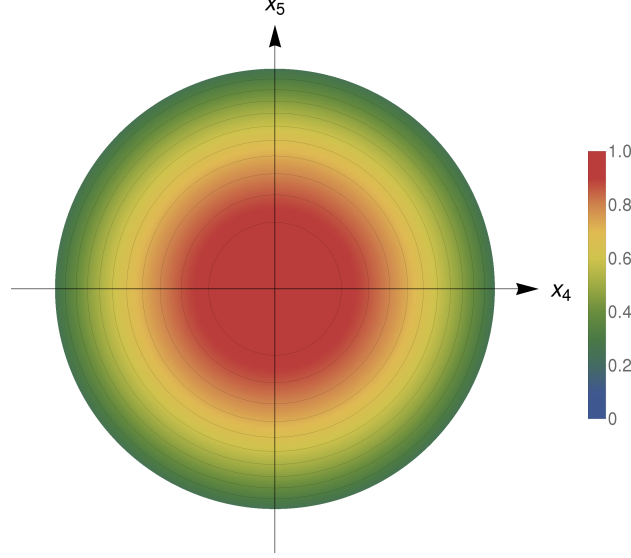


FIGURE 4.3.2. Semi-classical limit of the squashed fuzzy sphere. The color indicates the corresponding scaled dispersion $\bar{\delta}$ which has its minimum at 0 ($\triangleq \frac{2}{3+n}$) and maximum at 1 ($\triangleq \frac{3}{3+n}$). The lines represent contour lines of $\bar{\delta}$.

resembles the squashed fuzzy sphere⁶. Here we have

$$\lim_{\varphi_3, \varphi_4 \rightarrow 0} \vec{p}(\varphi) = c_n \frac{n}{2} \frac{1}{|\varphi|} \begin{pmatrix} 0 \\ 0 \\ \varphi_2 \sin |\varphi| \\ \varphi_1 \sin |\varphi| \\ 0 \\ 0 \end{pmatrix}, \quad (4.3.20)$$

which implies that the image of \vec{p} in this limit is the disk $\mathbb{D}_R = \{x, y \in \mathbb{R}, x^2 + y^2 \leq R^2 = c_n \frac{n}{2}\}$ which is of course nothing else but the ordinary squashed sphere.

The dispersion 4.3.14 reduces to

$$\lim_{\varphi_3, \varphi_4 \rightarrow 0} \delta(\varphi) = \frac{3}{8(3+n)} (7 + \cos(2|\varphi|)). \quad (4.3.21)$$

The minima are obviously given by $|\varphi| = \sqrt{\varphi_1^2 + \varphi_2^2} = \pi/2$, which corresponds to the boundary of the disk $\partial\mathbb{D}_R$. In figure 4.3.2 a picture of the 2-dimensional squashed fuzzy sphere with indicated dispersion is given.

Numerical considerations. To support the calculations above we will establish an algorithm in chapter 5 for numerical calculations of coherent states and in doing so (hopefully) find an adequate approximation to the semi-classical limit. This algorithm can then not only be used for the special case of squashed \mathbb{CP}_n^2 but for arbitrary matrix configurations which allow the existence of coherent states, i.e. arguably every matrix configuration with physical viability.

⁶The squashed fuzzy sphere is defined in analogy to squashed \mathbb{CP}^2 by omitting the Cartan generator X^3 .

CHAPTER 5

Numerical Analysis of Coherent States

So far we have studied coherent states by Perelomov for simple examples of non-commutative geometries and also for a more complicated space, the squashed fuzzy \mathbb{CP}^2 , as a solution of the Yang-Mills theory introduced in section §4.2. Our aim now is to extend the idea of coherent states to arbitrary matrix configurations, which should allow a more general numerical study of semi-classical limits of fuzzy spaces described by such matrices.

In the following chapter we will try to find an appropriate definition for a more general coherent state which fits our context. This definition will be chosen in such a way that it will be accessible by numerical means. In the already discussed examples this definition should of course essentially reduce to coherent states defined by Perelomov.

Subsequently, a numerical algorithm will be established, which should capture the coherent states defined below. This algorithm will be tested on various matrix configurations. As an important example will serve squashed \mathbb{CP}_n^2 .

5.1. Definition of Coherent States

Setup. For our purpose it is useful to consider the following concepts: Given is a sequence of matrix algebras $\mathcal{A}_n \subset \text{Mat}_{m(n)}(\mathbb{C})$ acting on Hilbert spaces \mathcal{H}_n and a sequence of quantized embedding functions $X_n^a \in \mathcal{A}_n$ for every $a \in \{1, \dots, d\}$. The expectation value $\vec{p}(\Psi)$ of X_n^a in a state $|\Psi_n\rangle \in \mathcal{H}_n$ is defined on $\bigoplus_{n=1}^{\infty} \mathcal{H}_n$ as

$$\vec{p}(\Psi_n) = \langle \Psi_n | X_n^a | \Psi_n \rangle \quad (5.1.1)$$

while the dispersion δ on $\bigoplus_{n=1}^{\infty} \mathcal{H}_n$ is defined as

$$\delta(\Psi_n) = \sum_a (\Delta_{\Psi_n} X_n^a)^2. \quad (5.1.2)$$

The semi-classical limit of the expectation value \vec{p} and the dispersion δ of a sequence of states $(|\Psi_n\rangle)_{n=1}^{\infty}$ are then simply given by

$$\vec{p}_{\infty} = \lim_{n \rightarrow \infty} \vec{p}(\Psi_n), \quad (5.1.3)$$

$$\delta_{\infty} = \lim_{n \rightarrow \infty} \delta(\Psi_n). \quad (5.1.4)$$

Coherent states. The question now is: How should we define a coherent state in \mathcal{H}_n ?

First, note that, since we want to use coherent states to describe the semi-classical limit of some fuzzy brane, we demand that the coherent state becomes completely localized in this limit; i.e. $\vec{p}_{\infty} < \infty$ and $\delta_{\infty} = 0$. Thus in our context a first naive attempt to define a coherent state is to define a sequence of states which obeys the following two conditions:

DEFINITION 5.1 (Weak Coherent State Sequence). A sequence $(|\Psi_n\rangle)_{n=1}^{\infty}$, $|\Psi_n\rangle \in \mathcal{H}_n$ is called a *weak coherent state sequence* if

- the semi-classical limit of the sequence of expectation values $\vec{p}(\Psi_n)_a = \langle X_n^a \rangle_{\Psi_n}$ exists:

$$\lim_{n \rightarrow \infty} \vec{p}(\Psi_n) = \vec{p}_{\infty} < \infty,$$

- and the dispersion δ vanishes in the semi-classical limit:

$$\lim_{n \rightarrow \infty} \delta(\Psi_n) = 0.$$

A closer examination of definition (5.1) reveals a lot of problems. For finite n practically any state could be an element of a weak coherent state sequence, and, of course, this would destroy the purpose of this definition.

One way to remedy this problem would be to require members of the sequence to minimize the dispersion δ on \mathcal{H}_n , but we have already seen that this only makes sense for very symmetric fuzzy branes and is too restrictive.

However, we can go a different route. Since we would like to have a good approximation of the semi-classical limit already for finite n , it seems appropriate to require that the expectation value $\vec{p}_n(\Psi_n)$ for finite n is optimal, in the sense that there is no $|\Psi\rangle \in \mathcal{H}_n$ so that $|\vec{p}_\infty - \vec{p}_n(\Psi_n)| > |\vec{p}_\infty - \vec{p}_n(\Psi)|$. This leads to the following definition of an “optimal localized state”:

DEFINITION 5.2 (Optimal Localized State). Let \vec{p} be a point in the target space \mathbb{R}^d . A state $|\Psi\rangle \in \mathcal{H}_n$ is called an *optimal localized state at $\vec{p} \in \mathbb{R}^d$* , if the following properties hold:

- (1) The expectation values $\vec{p}(\Psi)$ are optimal, i.e.

$$|\vec{p} - \vec{p}(\Psi)| = \min_{|\psi\rangle \in \mathcal{H}_n} |\vec{p} - \vec{p}(\psi)|. \quad (5.1.5)$$

- (2) Let $\mathcal{L} \subset \mathcal{H}_n$ be the set of states obeying property (1). We demand that the dispersion is optimal with respect to all states in \mathcal{L} , i.e.

$$\delta(\Psi) = \min_{|\lambda\rangle \in \mathcal{L}} \delta(\lambda). \quad (5.1.6)$$

This definition captures the notion of a state which can be thought of as “the best” approximation of a classical point $\vec{p} \in \mathbb{R}^d$. It is obvious that for each $\vec{p} \in \mathbb{R}^d$ there exists at least one optimal localized state.¹ So this can certainly not be the sole criterion on how to select coherent states (which in the end have to represent the semi-classical limit). In order to justify that optimal localized states “become” points in the semiclassical limit, the dispersion δ has to go to zero as n tends to infinity.

With the aim to make these vague statements more precise we firstly state the definition for a coherent state sequence as:

DEFINITION 5.3 (Coherent State Sequence). Let $\vec{p} \in \mathbb{R}^d$ be a fixed point in the target space \mathbb{R}^d . A sequence of *optimal localized states at $\vec{p} \in \mathbb{R}^d$* (in the sense of definition (5.2)) $(|\Psi_n\rangle)_{n=1}^\infty$, $|\Psi_n\rangle \in \mathcal{H}_n$ is called a *coherent state sequence* if it satisfies the conditions

- (1) The semi-classical limit of the sequence of expectation values $\vec{p}(\Psi_n)_a = \langle X_n^a \rangle_{\Psi_n}$ exists and is identical with $\vec{p} \in \mathbb{R}^d$:

$$\lim_{n \rightarrow \infty} \vec{p}(\Psi_n) = \vec{p} < \infty. \quad (5.1.7)$$

- (2) The sequence of dispersion $(\delta(\Psi_n))_{n=1}^\infty$ is monotonically decreasing and tends to zero in the semi-classical limit:

$$\delta(\Psi_n) \leq \delta(\Psi_{n+1}) \quad \forall n \in \mathbb{N}, \quad (5.1.8)$$

$$\lim_{n \rightarrow \infty} \delta(\Psi_n) = 0. \quad (5.1.9)$$

An element $|\Psi_n\rangle \in \mathcal{H}_n$ of a coherent state sequence $(|\Psi_n\rangle)_{n=1}^\infty$ is called a *coherent state*.

¹This is the reason why the “optimality condition” (1) in definition (5.2) is deliberately chosen very carefully. The naive approach would be to just demand that $\vec{p}(\Psi) = \vec{p}$. However, this cannot always be satisfied as the example in section §5.4 will show.

So if for a point $\vec{p} \in \mathbb{R}^d$ there exists a coherent state $|\Psi_n\rangle$, then $\vec{p} \in \mathbb{R}^d$ is an element of the manifold resembling the semi-classical limit. But since the numerical machinery is only served with the algebra \mathcal{A}_n for a fixed and finite n , the limit of the dispersion δ can, of course, not be determined in any exact way by numerical means. However, we will argue below that under reasonable assumptions, it is nevertheless possible to extract valuable information providing that n is “high enough”.

Considerations regarding finite n . First, one observes that because of property (2) in definition (5.3) there exists a finite n so that the dispersion of a coherent state is smaller than the dispersion of non-coherent (but nevertheless optimal localized) states. Therefore, one expects regions in state-space $\mathcal{CS} \subset \mathcal{H}_n$ where the dispersion is lower than in its “complement”. From now on we will assume that such a “gap” for high enough n in the dispersion of states exists. It is in the following referred to as the “hierarchy” of dispersion. The details on how such a hierarchy can be determined are discussed later in section §5.3.

It is not clear that states with low dispersion (with respect to this hierarchy) are *optimal located states* in general although we will see this to be true for all discussed examples below. Let us merely assume that for the moment. We would now have reduced the problem to finding a sub-manifold $\mathcal{CS} \subset \mathbb{CP}^m \cong S^{m-1}/U(1) \subset \mathcal{H}_m/U(1)$ equipped with the Fubini-Study metric [25] for which the dispersion

$$\delta(\Psi) = \sum_a (\Delta_\Psi X^a)^2 \quad (5.1.10)$$

is minimal or near the minimum with respect to a given hierarchy. Their expectation values $\vec{p}(\mathcal{CS})$ would then produce a manifold $\mathcal{M} = \vec{p}(\mathcal{CS})$ which would hopefully be a good approximation to the semi-classical limit.

It was attempted to implement this idea directly and it turned out to work for simple spaces where a good hierarchy exists even for low dimensional matrices. For more complicated spaces such as squashed \mathbb{CP}^2 the problem gets too high-dimensional and the corresponding computational effort is too large to produce results in a reasonable time frame.

For this reason, we investigate a different path in the next section, the *intersecting point probe*. Intersecting fuzzy branes and the idea of a point probe are for example studied in [7, 6].

Connection to Perelomov coherent states. Consider for example the fuzzy sphere. For each n we are given the n -dimensional $SU(2)$ representation acting on \mathcal{H}_n . Each such Hilbert space \mathcal{H}_n has a highest weight state $|\Psi_0^n\rangle \in \mathcal{H}_n$.

Let us have a look at the sequence $s_0 = (|\Psi_0^n\rangle)_{n=1}^\infty$. We know that the dispersion δ is minimized, hence equation (3.2.2) tells us that $|\vec{p}_n(\Psi_0^n)|^2$ is maximized and smaller than 1. Since $|\vec{p}_\infty| = \lim_{n \rightarrow \infty} |\vec{p}(\Psi_0^n)| = 1$ (see equation (3.2.5)), the distance $|\vec{p}_\infty - \vec{p}(\Psi_0^n)|$ is obviously minimized and hence every state in the sequence s_0 is an optimally localized state according to definition (5.2). Furthermore, as shown in section 3.2 on page 20 the properties (1) and (2) of definition (5.3) are certainly satisfied.

Therefore, the sequence s_0 is a coherent state sequence and $|\Psi_0^n\rangle$ is a coherent state in the sense of definition 5.3. The same considerations hold for the $SU(2)$ -rotated sequences.

According to this reasoning Perelomov coherent states agree with the coherent states in the sense above on the fuzzy sphere. The same reasoning is valid for \mathbb{CP}_n^2 and should also be valid for other co-adjoint orbits.

For the squashed orbit $\Pi(\mathbb{CP}_n^2)$ the situation again is not that clear. Considering the highest weight state sequence s_0 , it is evident that, since $\vec{p}(\Psi_0^n) = 0 = \vec{p}_\infty$ for all n , the sequence s_0 is a coherent state sequence indeed although the states’ dispersion is not minimized. This fact supports the above definition. There is also reason to believe (based on numerical evidence) that the expectation values are optimal at least with respect to the $SU(3)$ -orbit \mathcal{O}_{Ψ_0} .

5.2. Intersecting Point Probe

In the following section we develop yet another (only slightly different) definition of coherent states — which was also investigated in [16] by Ishiki, although differently motivated —, a definition based on the *intersecting point probe*. Heuristically speaking one measures the energies of strings connecting the probe with the fuzzy brane, c.f. Berenstein [6]. Coherent states can then be selected by probe locations where the energies are “low”.

Despite the different perspective, we will see in the detailed quantitative description in section §5.2 that this method has strong similarities with coherent states defined above.

Zero-dimensional brane. First let us consider the special case of a fuzzy brane defined by d real 1×1 matrices $\mathbf{p}^a \in \text{Mat}_1(\mathbb{C}) \cong \mathbb{C}$, $a = 1, \dots, d$ interpreted as quantized embedding functions. In any case they generate the algebra of complex numbers \mathbb{C} which acts on a one-dimensional Hilbert space $\mathcal{H}_1 \cong \mathbb{C}$. Since these embedding functions are all just constant numbers, they can only describe a single point

$$\vec{\mathbf{p}} = (\mathbf{p}^1, \dots, \mathbf{p}^d) \in \mathbb{R}^d \quad (5.2.1)$$

in the target space \mathbb{R}^d . This can also be seen in the context of coherent states: Every element in this algebra has expectation value $(\mathbf{p}^1, \dots, \mathbf{p}^d)$ and zero dispersion. Hence these numbers \mathbf{p}^a describe a zero-dimensional point-brane embedded in \mathbb{R}^d .

Stack of branes. We now go back to our original matrix configuration X^a which characterizes some fuzzy brane embedded in \mathbb{R}^d and generates a matrix algebra $\mathcal{A} \subset \text{Mat}_m(\mathbb{C})$. Given a second fuzzy brane defined by a set of matrices Y^a generating the algebra $\mathcal{B} \subset \text{Mat}_l(\mathbb{C})$, we can describe the two branes in one target space \mathbb{R}^d simultaneously simply by constructing the new quantized embedding functions \mathfrak{X}^a ,

$$\mathfrak{X}^a := X^a \oplus Y^a, \quad a = 1, \dots, d \quad (5.2.2)$$

or explicitly in matrix form

$$\mathfrak{X}^a = \begin{pmatrix} X^a & 0 \\ 0 & Y^a \end{pmatrix}, \quad a = 1, \dots, d \quad (5.2.3)$$

acting on $\mathcal{H}_m \oplus \mathcal{H}_l$ (see [7]). They generate the algebra $\mathcal{A} \oplus \mathcal{B} \subset \text{Mat}_m(\mathbb{C}) \oplus \text{Mat}_l(\mathbb{C})$.

So far we got nothing new physically. The issue becomes more interesting if we consider not only the algebra $\text{Mat}_m(\mathbb{C}) \oplus \text{Mat}_l(\mathbb{C})$ (i.e. matrices in block-diagonal form) but the whole matrix algebra $\text{Mat}_{m+l}(\mathbb{C})$, that is including the off-diagonal blocks which are elements of $\mathcal{H}_m \otimes \mathcal{H}_l^*$ respectively $\mathcal{H}_l \otimes \mathcal{H}_m^*$. Since these blocks connect the two branes (which means the branes “interact” in some way non-locally), they can be interpreted as oriented strings connecting the two branes described by the matrices X^a and Y^a .

Point probe. Now we combine the ideas of the point brane and brane interactions in the following way: Given a fuzzy brane embedded in some target space \mathbb{R}^d one can place a point brane as a probe at a definite location in this space. Then we are able to measure the energies of the strings connecting the brane and the probe. By varying the position of the probe the energies of the connecting strings will change. In particular, if the brane is not “too fuzzy”², there should be a region in space where the energies are relatively low compared to other regions which then can be regarded as an approximation of the semi-classical limit.

The quantized embedding functions are given by

$$\mathfrak{X}^a = \begin{pmatrix} X^a & 0 \\ 0 & \mathbf{p}^a \end{pmatrix}, \quad a = 1, \dots, d \quad (5.2.4)$$

with d real numbers \mathbf{p}^a .

²Not “too fuzzy” means that there exists a hierarchy of energies of the strings. We again refer to section §5.3 for a more precise treatment.

5.2.1. Laplace operator. The energy of scalar fields is measured by the Laplacian $\square_{\mathbf{p}} : \text{Mat}_{m+1}(\mathbb{C}) \rightarrow \text{Mat}_{m+1}(\mathbb{C})$,

$$\square_{\mathbf{p}} = \sum_{a=1}^d [\mathfrak{X}^a, [\mathfrak{X}^a, \cdot]]. \quad (5.2.5)$$

Since we are only interested in the energies of the string connecting the probe with the brane, we consider an element $\Phi \in \text{Mat}_{m+1}(\mathbb{C}) \cong \text{Mat}_m(\mathbb{C}) \oplus (\mathcal{H}_m \otimes \mathbb{C}) \oplus (\mathbb{C} \otimes \mathcal{H}_m)$ of the form

$$\Phi = \begin{pmatrix} 0 & \cdots & 0 & \\ \vdots & \ddots & \vdots & |\phi\rangle \\ 0 & \cdots & 0 & \\ & & \langle\phi| & 0 \end{pmatrix} \in \text{Mat}_m(\mathbb{C}) \oplus (\mathcal{H}_m \otimes \mathbb{C}) \oplus (\mathbb{C} \otimes \mathcal{H}_m) \quad (5.2.6)$$

with $|\phi\rangle \in \mathcal{H}_m$. Considering the action of the Laplacian $\square_{\mathbf{p}}$ on Φ yields

$$\begin{aligned} \square_{\mathbf{p}} \Phi &= \sum_a [\mathfrak{X}^a, [\mathfrak{X}^a, \Phi]] = \sum_a (\mathfrak{X}^a \mathfrak{X}^a \Phi + \Phi \mathfrak{X}^a \mathfrak{X}^a - 2\mathfrak{X}^a \Phi \mathfrak{X}^a) \\ &= \begin{pmatrix} 0 & \cdots & 0 & \sum_a (X^a - \mathbf{p}^a)^2 |\varphi\rangle \\ \vdots & \ddots & \vdots & \\ 0 & \cdots & 0 & \\ \langle\varphi| \sum_a (X^a - \mathbf{p}^a)^2 & & & 0 \end{pmatrix} \end{aligned} \quad (5.2.7)$$

and thus the Laplace operator $\square_{\mathbf{p}}$ can be written as

$$\square_{\mathbf{p}} = \sum_{a=1}^d (X^a - \mathbf{p}^a)^2 \quad (5.2.8)$$

when restricted to $\mathcal{H}_m \otimes \mathbb{C} \cong \mathcal{H}_m$, cf. (5.2.6).

Let us consider the corresponding quadratic form $\frac{1}{2} \text{tr}(\Phi^\dagger \square_{\mathbf{p}} \Phi)$. It can be written as

$$\begin{aligned} \frac{1}{2} \text{tr}(\Phi^\dagger \square_{\mathbf{p}} \Phi) &= \langle\phi| \square_{\mathbf{p}} |\phi\rangle = \sum_a (\Delta_\phi X^a)^2 + \sum_a (\langle\phi| X^a |\phi\rangle - \mathbf{p}^a)^2 \\ &= \delta(\phi) + |\vec{p}(\phi) - \vec{\mathbf{p}}|^2. \end{aligned} \quad (5.2.9)$$

This means that low energies are given by states which have low dispersion δ and are also localized near the point probe.

As we can see there is a strong similarity between the method of the point probe and the method of coherent states in section §5.1 since the eigenstate of $\square_{\mathbf{p}}$ with the lowest eigenvalue minimizes (5.2.9) and hence also the dispersion δ . In particular for co-adjoint orbits \mathcal{O} this method is even equivalent since we can just minimize the second term in (5.2.9) by choosing $\vec{\mathbf{p}} = \vec{p}(\phi)$. In doing so the second term vanishes and the states are selected by minimizing $\delta(\phi)$ which are exactly the coherent states on the quantized co-adjoint orbits.

Numerical consequences. The formulation of the problem in this particular way has two implications which are important for the numerical computation of coherent states.

First, the function which is to be minimized³ is now written as a quadratic form $\langle\phi| \square_{\mathbf{p}} |\phi\rangle$, where $\square_{\mathbf{p}}$ is *linear*. This is a blessing because we can easily find minima by numerically solving the eigenvalue problem, which can be done very efficiently computational-wise.

Second, having handled the eigenvalue issue, the problem is reduced to a d -dimensional one where d is the dimension of the target space \mathbb{R}^d which is independent of the size of the matrices.

³Minimizing in this context means not only finding exact minima, but also states “near” the minima with respect to some given hierarchy.

This is a huge progress since in many cases one has to increase the size of the matrices to get a better hierarchy of energies. For example a satisfying hierarchy for the squashed \mathbb{CP}^2 case is achieved for $SU(3)$ -representations $(0, 20)$ and upward which according to formula (A.2.3) corresponds to a 231- (and more) dimensional state space. In contrast, the dimension of the target space in this case is $d = 6$.

It is remarkable that a method motivated exclusively by physical means can help to reduce the complexity of a problem to such an extent.

5.2.2. Dirac operator. In analogy to the Laplace operator we shall also define the Dirac operator $\mathcal{D}_{\mathbf{p}} \in \text{End}(\mathbb{C}^q \otimes \text{Mat}_{m+1}(\mathbb{C}))$, $q = 2^{\lfloor \frac{d}{2} \rfloor}$ for fermionic modes as

$$\mathcal{D}_{\mathbf{p}} = \sum_{a=1}^d \gamma^a \otimes [\mathfrak{X}^a, \cdot] \quad (5.2.10)$$

with $\{\gamma^a, a = 1, \dots, d\}$ forming a representation of the Clifford algebra $\mathcal{Cl}_d(\mathbb{R})$.

Again we are only interested in the off-diagonal entries of an element $\Psi \in \mathbb{C}^q \otimes \text{Mat}_{m+1}(\mathbb{C})$:

$$\Psi = \begin{pmatrix} 0 & \cdots & 0 & \\ \vdots & \ddots & \vdots & |s, \psi\rangle \\ 0 & \cdots & 0 & \\ \langle s, \psi| & & & 0 \end{pmatrix}. \quad (5.2.11)$$

In this case $|s, \psi\rangle \in \mathbb{C}^q \otimes \mathcal{H}_m$. Thus the action of the Dirac operator $\mathcal{D}_{\mathbf{p}}$ on Ψ is given by

$$\begin{aligned} \mathcal{D}_{\mathbf{p}} \Psi &= \sum_a \gamma^a [\mathfrak{X}^a, \Psi] = \sum_a \gamma^a (\mathfrak{X}^a \Psi - \Psi \mathfrak{X}^a) \\ &= \begin{pmatrix} 0 & \cdots & 0 & \\ \vdots & \ddots & \vdots & \sum_a \gamma^a (X^a - \mathbf{p}^a) |s, \psi\rangle \\ 0 & \cdots & 0 & \\ \langle s, \psi| \sum_a \gamma^a (X^a - \mathbf{p}^a) & & & 0 \end{pmatrix} \end{aligned} \quad (5.2.12)$$

and hence the operator $\mathcal{D}_{\mathbf{p}}$ when restricted to $\mathbb{C}^q \otimes \mathcal{H}_m$ reads

$$\mathcal{D}_{\mathbf{p}} = \sum_{a=1}^d \gamma^a (X^a - \mathbf{p}^a). \quad (5.2.13)$$

Note that

$$\mathcal{D}_{\mathbf{p}}^2 = \square_{\mathbf{p}} + \Sigma^{ab} [X^a, X^b] \quad (5.2.14)$$

with $\Sigma^{ab} := \frac{1}{4}[\gamma^a, \gamma^b]$. Writing $|s, \psi\rangle \in \mathbb{C}^q \otimes \mathcal{H}_m$ as $|s, \psi\rangle = |s\rangle \otimes |\psi\rangle$ the corresponding quadratic form reads

$$\begin{aligned} \frac{1}{2} \text{tr}(\Psi^\dagger \mathcal{D}_{\mathbf{p}}^2 \Psi) &= \langle s, \psi | \mathcal{D}_{\mathbf{p}}^2 | s, \psi \rangle = \langle \psi | \square_{\mathbf{p}} | \psi \rangle + \sum_{a,b=1}^d \langle s | \Sigma^{ab} | s \rangle \langle \psi | [X^a, X^b] | \psi \rangle \\ &= \delta(\psi) + |\vec{p}(\psi) - \vec{\mathbf{p}}|^2 + \sum_{a,b=1}^d \langle s | \Sigma^{ab} | s \rangle \langle \psi | [X^a, X^b] | \psi \rangle. \end{aligned} \quad (5.2.15)$$

The third term in equation (5.2.15) can be physically interpreted recalling the mathematically equivalent form of Heisenberg's uncertainty relation $\Delta_\Psi X^a \Delta_\Psi X^b \geq \frac{1}{2} |\langle \Psi | [X^a, X^b] | \Psi \rangle|$, hence

$$\begin{aligned} \left| \sum_{a,b=1}^d \langle s | \Sigma^{ab} | s \rangle \langle \psi | [X^a, X^b] | \psi \rangle \right| &\leq 2 \sum_{a,b=1}^d \overbrace{\left| \langle s | \Sigma^{ab} | s \rangle \right|}^{\leq \frac{1}{2}} \Delta_\Psi X^a \Delta_\Psi X^b \\ &\leq \delta(\Psi) + \sum_{a \neq b}^d \Delta_\Psi X^a \Delta_\Psi X^b. \end{aligned} \quad (5.2.16)$$

Minimizing the absolute value of the energy given by the Dirac operator corresponds to minimizing the function (5.2.15). In particular, the Dirac operator \mathcal{D}_p has zero modes if and only if \mathcal{D}_p^2 has zero modes. This is the case when (5.2.15) has roots. Berenstein [6] showed that indeed in many cases \mathcal{D}_p has exact zero modes on the whole manifold which constitutes the semi-classical limit of a given fuzzy brane.

An interesting question is whether the states selected by the Dirac operator yield the same manifold \mathcal{M} as the Laplacian. We will come back to this in section §5.4, section §5.5 and section §5.6 where we revisit our examples and show our numerical as well as analytic results.

5.3. Numerically finding coherent states

Now we want to investigate ways how to numerically calculate coherent states defined by the Laplacian \square_p as well as the Dirac operator \mathcal{D}_p for fixed n . In contrast to the theoretical situation above, where a whole sequence of algebras is given, in practice we are only served with a set of matrices X^a , $a = 1, \dots, d$ which are to be interpreted as quantized embedding functions $X^a \sim x^a$. They generate an algebra $\mathcal{A} \subset \text{Mat}_m(\mathbb{C})$. Nevertheless, let us assume such a sequence “exists” although not explicitly known.

The f -function. So far we have seen that finding coherent states can be done by finding states which have low-energies (defined by the Laplacian \square_p respectively Dirac operator \mathcal{D}_p) compared to energy levels of the whole state space. We try to clarify this vague statement in this section. For the sake of brevity we call such states *quasi-minima* from now on. Typically, there are an infinite number of quasi-minimal states which form a sub-manifold \mathcal{CS} of $\mathbb{C}P^m \subset \mathcal{H}_m$. Their expectation values produce a manifold $\mathcal{M} = \vec{p}(\mathcal{CS})$ which is an approximation to the semi-classical limit. Thus the problem is to rasterize the manifold \mathcal{M} . To this end we consider the function f

$$\begin{aligned} f : \mathbb{R}^d &\rightarrow \mathbb{R} \\ \vec{p} &\mapsto \left| \lambda_{\min}^{\vec{p}} \right| \end{aligned} \quad (5.3.1)$$

where $\lambda_{\min}^{\vec{p}}$ is the smallest (with respect to the modulus) eigenvalue of \square_p respectively \mathcal{D}_p . Consequently, finding quasi-minimal energy regions in \mathbb{R}^d is equivalent to finding quasi-minima of f .

Obviously, the function f is continuous everywhere. Furthermore, f is differentiable everywhere except on

- a countable set where the two smallest eigenvalues become equal and cross each other,
- the set $\{x \in \mathbb{R}^d \mid f(x) = 0\}$ due to the modulus in (5.3.1).

However, for our numerical purpose we will completely ignore the non-differentiability since in any case we are working with finite differential quotients, where we assume that the function f nevertheless behaves in a way that is “smooth enough” with respect to the finite differential quotients.

Identify the “hierarchy” using the f -function. Consider a global minimum x_0 of f . In this case the point x_0 is an element of $\mathcal{M} = \vec{p}(\mathcal{C}\mathcal{S})$.

We can write the change of the function f in some direction ε up to second order in $|\varepsilon|$ as

$$|f(x_0) - f(x_0 + \varepsilon)| = \frac{1}{2}|\varepsilon^T H_{x_0} \varepsilon| + \mathcal{O}(|\varepsilon|^3) \quad (5.3.2)$$

where H_{x_0} is the Hesse matrix at the point x_0 . Thus, the amount of change in some direction is characterized by the eigenvalues of H . If the coherent states form a continuous subset of \mathbb{R}^d , one should observe a **hierarchy of “small” and “large” eigenvalues**. Consequently, the directions corresponding to the small eigenvalues constitute a basis of the tangent space $T_{x_0}\mathcal{M}$ of \mathcal{M} at x_0 . Hence $x_0 + \varepsilon$ is approximately an element of \mathcal{M} for ε being an eigenvector corresponding to a “small” eigenvalue and $|\varepsilon|$ being sufficiently small. One also observes that the number of small eigenvalues constitutes the dimension k of the manifold \mathcal{M} .

If x_0 is not a local minimum of f the change of $f(x_0)$ in a direction ε is given by

$$f(x_0) - f(x_0 + \varepsilon) = \nabla f_{x_0} \cdot \varepsilon + \frac{1}{2}\varepsilon^T H_{x_0} \varepsilon + \mathcal{O}(|\varepsilon|^3) \quad (5.3.3)$$

with $(\nabla f_{x_0})_i = (\partial_i f)(x_0)$ denoting the gradient of f at point x_0 . In the regime of quasi-minima of f the norm of the gradient $|\nabla f_{x_0}|$ is assumed to be small compared to “large” eigenvalues of H_{x_0} . Therefore, it is assumed that the change in directions corresponding to large eigenvalues can be approximated by

$$|f(x_0) - f(x_0 + \varepsilon)| = \frac{1}{2}|\varepsilon^T H_{x_0} \varepsilon| + \mathcal{O}(|\varepsilon|^3), \quad (5.3.4)$$

which selects a $(d - k)$ -dimensional subspace. Hence the orthogonal complement represents the k -dimensional subspace which corresponds to small changes $|f(x_0) - f(x_0 + \varepsilon)|$ and is spanned by the eigenvectors corresponding to “small” eigenvalues of H_{x_0} .

The previous considerations provide the basis for the algorithm to rasterize the manifold \mathcal{M} . Locally we can find the tangent space $T_{x_0}\mathcal{M}$ by using algorithm 1 which is written as so-called pseudo-code.

Algorithm 1 Select directions corresponding to a “small” change in f

```

1: function GETDIRECTIONS(function  $f$ , point  $x_0$ , dimension  $k$ )
2:    $H \leftarrow \text{HESSEMATRIX}(x_0)$  ▷ Calculate Hesse Matrix  $H_{x_0}$  at point  $x_0$ .
3:    $\{(\lambda, \varepsilon)\} \leftarrow \text{DIAG}(H)$  ▷ Diagonalize  $H_{x_0}$  with eigenvectors  $\varepsilon$  corresponding to eigenvalues  $\lambda$ .
4:   return SELECT( $\{(\lambda, \varepsilon)\}, k$ ) ▷ Return eigenvectors corresponding to  $k$  smallest eigenvalues.
5: end function

```

On each point obtained by $x = x_0 + \varepsilon$ we can subsequently apply algorithm 1 and gather points of \mathcal{M} . Then each point x represents an open neighborhood $U_{|\varepsilon|}(x) \in \mathcal{U}(\mathcal{M})$ of the manifold \mathcal{M} . Of course, if this is done blindly then a lot of points are gathered twice or more often. To exclude the redundant information one can for example attempt a *nearest neighborhood search* [30] with respect to the euclidean metric to prevent accepting points which are already assimilated.

One also has to introduce some kind of stopping mechanism which prevents points to be accepted when the given hierarchy is broken down. There is a number of possibilities:

A local stop is necessary if

- f exceeds a certain value f_{crit} ,
- the norm of the gradient $|\nabla f|$ exceeds a certain value $(\nabla f)_{\text{crit}}$,
- the hierarchy of eigenvalues of the Hessian matrix H_x does not exist any more, i.e. the ratio of the highest “small” eigenvalue λ and the lowest “large” eigenvalue Λ exceeds a certain value $(\lambda/\Lambda)_{\text{crit}}$.

Since the given hierarchy depends on the limiting process of a sequence which in general is not known, these values cannot be determined by theoretical considerations and must be adjusted for each example individually.

This procedure is strictly speaking arbitrary. However, the situation can be compared to taking a picture with an ordinary photo camera. When taking a picture the photographer has to adjust the focus of the lenses to get a sharp image. In principle this action is arbitrary too. However, the photographer can adjust the focus in such a way as for the image to capture a maximal amount of information.

A simple unoptimized form of an algorithm which provides a complete point cloud of \mathcal{M} is presented by algorithm 2 where standard programming structures are used.⁴

Algorithm 2 Successively apply alg. 1 to gather a complete point cloud of \mathcal{M} .

```

1: function RASTERIZE(function  $f$ , startpoint  $x_0$ , dimension  $k$ )
2:    $pc \leftarrow List$                                  $\triangleright$  List of points which constitute the point cloud.
3:    $q \leftarrow Queue$                                  $\triangleright$  FIFO Queue which holds new unchecked points.
4:
5:   add point  $x_0$  to  $pc$ 
6:   add point  $x_0$  to  $q$ 
7:
8:   while  $q$  not empty do
9:
10:     $x \leftarrow$  take next element from  $q$                  $\triangleright$  Current point to process.
11:     $dirs \leftarrow GETDIRECTIONS(f, x, k)$ 
12:
13:    for all directions  $\varepsilon$  in  $dirs$  do
14:      if ISLEGAL( $x + \varepsilon$ ) is true then                 $\triangleright$  This refers to the considerations above.
15:        add point  $x + \varepsilon$  to  $pc$ 
16:        add point  $x + \varepsilon$  to  $q$ 
17:      end if
18:    end for
19:
20:  end while
21:
22: return  $pc$ 
23: end function

```

Another issue to be considered is that we have to restrict the search to a compact subset of \mathbb{R}^d for the obvious reason that the procedure should be deterministic. For compact manifolds \mathcal{M} this is automatically satisfied. Otherwise, one has to choose more or less arbitrary compact regions and confine the rasterize procedure to those.

The result is a point cloud which is an approximation of $\mathcal{M} = \vec{p}(\mathcal{CS})$ (or a compact subset thereof if \mathcal{M} itself is not compact). The quality of the approximation depends on three aspects. Obviously it is determined by the step length $|\varepsilon|$. Furthermore, the separation of the hierarchy has an impact which is itself dependent on the dimension of the given $m \times m$ matrices. At last, the approximation is affected by one of the above mentioned cut-off parameters f_{crit} , $(\nabla f)_{\text{crit}}$ or $(\lambda/\Lambda)_{\text{crit}}$.

⁴See for reference [28].

5.4. Fuzzy Sphere revisited

With the discussion above in mind let us recall the example of the fuzzy sphere defined by the three matrices X^a , $a = 1, \dots, 3$ which satisfy the commutation relations

$$[X^a, X^b] = i \frac{2}{\sqrt{n^2 - 1}} \varepsilon_{abc} X^c. \quad (5.4.1)$$

5.4.1. The point probe Laplacian $\square_{\mathbf{p}}$. For the simple case of the fuzzy sphere we can explicitly evaluate the the function (5.3.1), i.e. the minimal eigenvalue of the point probe Laplacian⁵

$$\square_{\mathbf{p}} = \sum_{a=1}^3 (X^a - \mathbf{p}^a)^2 = \mathbb{1} - 2 \sum_{a=1}^3 \mathbf{p}^a X^a + \sum_{a=1}^3 \mathbf{p}^a \mathbf{p}^a. \quad (5.4.2)$$

Since this expression is invariant under $SO(3)$ -rotations, it suffices to consider the operator at the north pole $\vec{\mathbf{p}} = (0, 0, \mathbf{p}^3)$ which corresponds to

$$U^{-1} \square_{\mathbf{p}} U = \mathbb{1} + |\vec{\mathbf{p}}|^2 - 2|\vec{\mathbf{p}}| X^3 \quad (5.4.3)$$

for a suitable unitary matrix U . Obviously, eigenvectors of the operator $U^{-1} \square_{\mathbf{p}} U$ are eigenvectors of X^3 and vice versa. The form (5.4.3) makes it clear that the eigenvalues are minimized for the highest state vectors $|\frac{n-1}{2}, \frac{n-1}{2}\rangle$. Using $X^3 |\frac{n-1}{2}, \frac{n-1}{2}\rangle = \sqrt{\frac{n-1}{n+1}} |\frac{n-1}{2}, \frac{n-1}{2}\rangle$ the minimal eigenvalue of $U^{-1} \square_{\mathbf{p}} U$ as a function of \mathbf{p} is given by

$$f(\vec{\mathbf{p}}) = 1 + |\vec{\mathbf{p}}|^2 - 2|\vec{\mathbf{p}}| \sqrt{\frac{n-1}{n+1}} \quad (5.4.4)$$

whose minima are given by $|\vec{\mathbf{p}}_{\min}| = \sqrt{\frac{n-1}{n+1}} = 1 + \mathcal{O}(\frac{1}{n})$. By definition the approximation of the semi-classical limit is then given by

$$\mathcal{M} = \{x \in \mathbb{R}^3 : |x| = \sqrt{\frac{n-1}{n+1}} = 1 + \mathcal{O}(\frac{1}{n})\}. \quad (5.4.5)$$

This shows that in the fuzzy sphere context the coherent states defined by the point probe Laplacian are equivalent to coherent states defined by Perelomov coherent states in section §3.2. Also the manifold \mathcal{M} agrees with the expectation values of the coherent states $\vec{p}(\mathcal{CS}) = \mathcal{M}$ and minimizes the dispersion $\delta(\Psi) = \sum_{a=1}^3 (\Delta_{\Psi} X^a)^2$.

A test of the numerical procedure. Independent of the above computations we check the implementation of the numerical algorithm in this well understood case. As input are given three 10×10 matrices X^1, X^2, X^3 which resemble the generators of $SU(2)$ with the correct normalization factor to be consistent with equation (5.4.1). They are explicitly given by

$$\begin{aligned} X^1 &= \frac{2}{\sqrt{99}} \times \text{diag}_2 \left(\frac{3}{2}, 2, \frac{\sqrt{21}}{2}, \sqrt{6}, \frac{5}{2}, \sqrt{6}, \frac{\sqrt{21}}{2}, 2, \frac{3}{2} \right) + \text{h.c.}, \\ X^2 &= -\frac{2i}{\sqrt{99}} \times \text{diag}_2 \left(\frac{3}{2}, 2, \frac{\sqrt{21}}{2}, \sqrt{6}, \frac{5}{2}, \sqrt{6}, \frac{\sqrt{21}}{2}, 2, \frac{3}{2} \right) + \text{h.c.}, \\ X^3 &= \frac{2}{\sqrt{99}} \times \text{diag} \left(\frac{9}{2}, \frac{7}{2}, \frac{5}{2}, \frac{3}{2}, \frac{1}{2}, -\frac{1}{2}, -\frac{3}{2}, -\frac{5}{2}, -\frac{7}{2}, -\frac{9}{2} \right) \end{aligned} \quad (5.4.6)$$

where $\text{diag}_2(\dots)$ represents a matrix with entries in the second diagonal.

The numerical procedure then tries to find a global minimum of f which in this case was determined as

$$\vec{\mathbf{p}}_{\min} \approx (0.0801529, -0.585913, 0.684444)$$

⁵This is also calculated in [16]

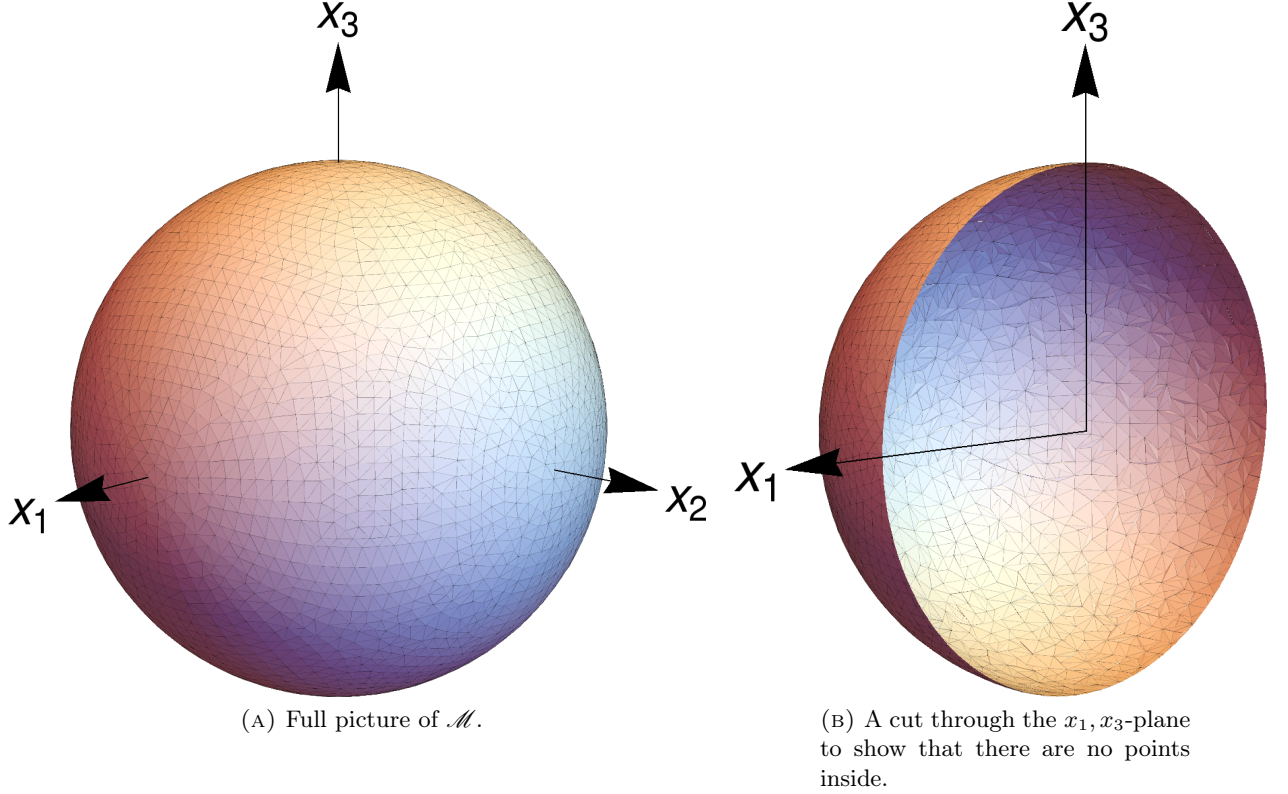


FIGURE 5.4.1. Visualization of the semi-classical limit of the fuzzy sphere S_n^2 constructed from S_{10}^2 .

with function value

$$f(\vec{\mathbf{p}}_{\min}) \approx 0.181818$$

which is in perfect agreement with the theoretical minimum $1 - \frac{n-1}{n+1} = 1 - \frac{9}{11} \approx 0.181818$ and the norm $|\vec{\mathbf{p}}_{\min}| = \sqrt{\frac{n-1}{n+1}} \approx 0.904534$.

The moduli of the eigenvalues of the Hesse matrix at this point $\vec{\mathbf{p}}_{\min}$ are given by $\approx (1.1 \times 10^{-6}, 2.4 \times 10^{-6}, 2.)$ where a hierarchy can be determined without problems. Obviously, two directions are in the category “small”.

After applying algorithm 2 the result is a point cloud representing the manifold \mathcal{M} . Under the assumption that the point cloud constitutes a two-dimensional manifold, one can build a mesh of polygons connecting these points to create a visualization of \mathcal{M} . A picture is shown in figure 5.4.1. As expected one gets the sphere S^2 with radius $R = \sqrt{\frac{n-1}{n+1}}$ reasonably approximated.

5.4.2. The point probe Dirac operator $\mathcal{D}_{\mathbf{p}}$. Similar considerations are possible for the Dirac operator

$$\mathcal{D}_{\mathbf{p}} = \sum_{a=1}^3 \sigma^a (X^a - \mathbf{p}^a) \quad (5.4.7)$$

with σ^a being the Pauli matrices

$$\sigma^1 = \begin{pmatrix} 0 & 1 \\ 1 & 0 \end{pmatrix}, \quad \sigma^2 = \begin{pmatrix} 0 & -i \\ i & 0 \end{pmatrix}, \quad \sigma^3 = \begin{pmatrix} 1 & 0 \\ 0 & 1 \end{pmatrix}. \quad (5.4.8)$$

Again due to the $SO(3)$ symmetry it is enough to consider the north pole $\vec{\mathfrak{p}} = (0, 0, \mathfrak{p}^3)$ respectively

$$U^{-1} \mathcal{D}_{\mathfrak{p}} U = \sum_{a=1}^3 \sigma^a X^a - \sigma^3 |\vec{\mathfrak{p}}| \quad (5.4.9)$$

whose eigenvectors with minimal eigenvalues $\left(\sqrt{\frac{n-1}{n+1}} - |\vec{\mathfrak{p}}|\right)$ are given by $|\uparrow\rangle \otimes \left|\frac{n-1}{2}, \frac{n-1}{2}\right\rangle^6$. Thus the function f with respect to the Dirac operator $\mathcal{D}_{\mathfrak{p}}$ is given by

$$f(\vec{\mathfrak{p}}) = \left| \sqrt{\frac{n-1}{n+1}} - |\vec{\mathfrak{p}}| \right|. \quad (5.4.10)$$

Its minima (which at the same time are roots of f) are obviously given by $|\vec{\mathfrak{p}}_{\min}| = \sqrt{\frac{n-1}{n+1}}$ as in the Laplacian case, which means that we get the same result for the semi-classical limit \mathcal{M}

$$\mathcal{M} = \{x \in \mathbb{R}^3 : |x| = \sqrt{\frac{n-1}{n+1}} = 1 + \mathcal{O}\left(\frac{1}{n}\right)\}. \quad (5.4.11)$$

We have shown that the definition of the coherent states for the fuzzy sphere with respect to the Laplacian $\square_{\mathfrak{p}}$ is in some sense equivalent to the definition with respect to the Dirac operator $\mathcal{D}_{\mathfrak{p}}$. Nevertheless, in a numerical context the method using the Dirac operator has some advantages due to the fact that the minima of f are roots for all n . This fact ensures an existent good hierarchy even for very low n ; thus low-dimensional matrices can be used for the computation of coherent states. However, for the sake of comparability the 10×10 matrices in (5.4.6) are used.

Numerical test. For the Dirac case our numerical implementation finds a global minimum at

$$\vec{\mathfrak{p}}_{\min} \approx (0.0801524, -0.585913, 0.684444)$$

which corresponds to the function value

$$f(\vec{\mathfrak{p}}_{\min}) \approx 9.011 \times 10^{-10},$$

hence in good approximation $f(\vec{\mathfrak{p}}_{\min}) \approx 0$.

The eigenvalue moduli of the numerical Hesse matrix at point $\vec{\mathfrak{p}}_{\min}$ are given by $\approx (5.1, 7.7, 136.4)$. Note that one has to be very careful interpreting the values of these numbers because the function f is actually not differentiable at 0 and hence the values are strongly dependent on the arbitrary chosen step size of the finite differential quotient. However, the eigenvectors of the Hesse matrix should at least provide the correct directions for small enough steps $|\varepsilon|$.

It is of little surprise that the visual result is the same as in the Laplacian case and is not repeated here for this reason.

5.5. Fuzzy Torus revisited

Recall, the fuzzy torus T_n^2 is defined by the quantized embedding functions $X^a \sim x^a$ given by four $n \times n$ matrices

$$\begin{aligned} X^1 &= (U + U^\dagger)/2 \\ X^2 &= -i(U - U^\dagger)/2 \\ X^3 &= (V + V^\dagger)/2 \\ X^4 &= -i(V - V^\dagger)/2 \end{aligned} \quad (5.5.1)$$

⁶The vector $|\uparrow\rangle$ is defined in the usual way as eigenvector of σ^3 with the positive eigenvalue 1.

with U and V being the *shift* and *clock* matrix,

$$U = \begin{pmatrix} 0 & 1 & & & \\ & 0 & 1 & & \\ & & \ddots & \ddots & \\ & & & 0 & 1 \\ 1 & & & & 0 \end{pmatrix}, \quad V = \begin{pmatrix} 1 & & & & \\ & q & & & \\ & & q^2 & & \\ & & & \ddots & \\ & & & & q^{n-1} \end{pmatrix}, \quad (5.5.2)$$

and $q = e^{2\pi i/n}$.

5.5.1. The point probe Laplacian $\square_{\mathbf{p}}$. The Laplace operator $\square_{\mathbf{p}}$ is then defined as

$$\begin{aligned} \square_{\mathbf{p}} &= \sum_{a=1}^4 (X^a - \mathbf{p}^a)^2 = \mathbb{1} + |\vec{\mathbf{p}}|^2 - 2 \sum_{a=1}^4 X^a \mathbf{p}^a \\ &= \mathbb{1} + |\vec{\mathbf{p}}|^2 - U(\mathbf{p}^1 - i\mathbf{p}^2) - U^\dagger(\mathbf{p}^1 + i\mathbf{p}^2) - V(\mathbf{p}^3 - i\mathbf{p}^4) - V^\dagger(\mathbf{p}^3 + i\mathbf{p}^4). \end{aligned} \quad (5.5.3)$$

In this case we will skip an analytic treatment — although possible (see [16]) — and directly turn towards the numerical results.

To visualize the resulting point cloud which represents a two-dimensional manifold embedded in \mathbb{R}^4 , $\mathcal{M} \subset S^3 \subset \mathbb{R}^4$, one can use a generalized stereographic projection $\mathcal{P} : S^3 \rightarrow \bar{\mathbb{R}}^3$ defined by

$$\mathcal{P} : S^3 \subset \mathbb{R}^4 \rightarrow \bar{\mathbb{R}}^3 \quad (5.5.4)$$

$$\begin{pmatrix} p_1 \\ p_2 \\ p_3 \\ p_4 \end{pmatrix} \mapsto \frac{1}{1 - p_4} \begin{pmatrix} p_1 \\ p_2 \\ p_3 \end{pmatrix}.$$

The result $\mathcal{P}(\mathcal{M})$ is a two-dimensional manifold embedded in \mathbb{R}^3 which is shown in figure 5.5.1.

5.5.2. The point probe Dirac operator $\mathcal{D}_{\mathbf{p}}$. The Dirac operator $\mathcal{D}_{\mathbf{p}}$ is given by

$$\mathcal{D}_{\mathbf{p}} = \sum_{a=1}^4 \gamma^a (X^a - \mathbf{p}^a) \quad (5.5.5)$$

while the following matrices can be used as representation for the Clifford algebra $\mathcal{Cl}_4(\mathbb{R})$:

$$\begin{aligned} \gamma^1 &= \begin{pmatrix} 0 & 0 & 1 & 0 \\ 0 & 0 & 0 & 1 \\ 1 & 0 & 0 & 0 \\ 0 & 1 & 0 & 0 \end{pmatrix}, & \gamma^2 &= \begin{pmatrix} 0 & 0 & -i & 0 \\ 0 & 0 & 0 & -i \\ i & 0 & 0 & 0 \\ 0 & i & 0 & 0 \end{pmatrix}, \\ \gamma^3 &= \begin{pmatrix} 0 & 1 & 0 & 0 \\ 1 & 0 & 0 & 0 \\ 0 & 0 & 0 & -1 \\ 0 & 0 & -1 & 0 \end{pmatrix}, & \gamma^4 &= \begin{pmatrix} 0 & -i & 0 & 0 \\ i & 0 & 0 & 0 \\ 0 & 0 & 0 & i \\ 0 & 0 & -i & 0 \end{pmatrix}. \end{aligned} \quad (5.5.6)$$

The numerical procedure yields the same point cloud as in figure 5.5.1a. Remarkably, even for low dimensional matrices the hierarchy is clearly visible. Additionally, for 5×5 matrices the explicit numerical computation shows that for the torus T^2 we have

$$f(T^2) < 4.9 \times 10^{-7}$$

which suggests that the Dirac operator $\mathcal{D}_{\mathbf{p}}$ has exact zero modes at $T^2 \in \mathbb{R}^4$.

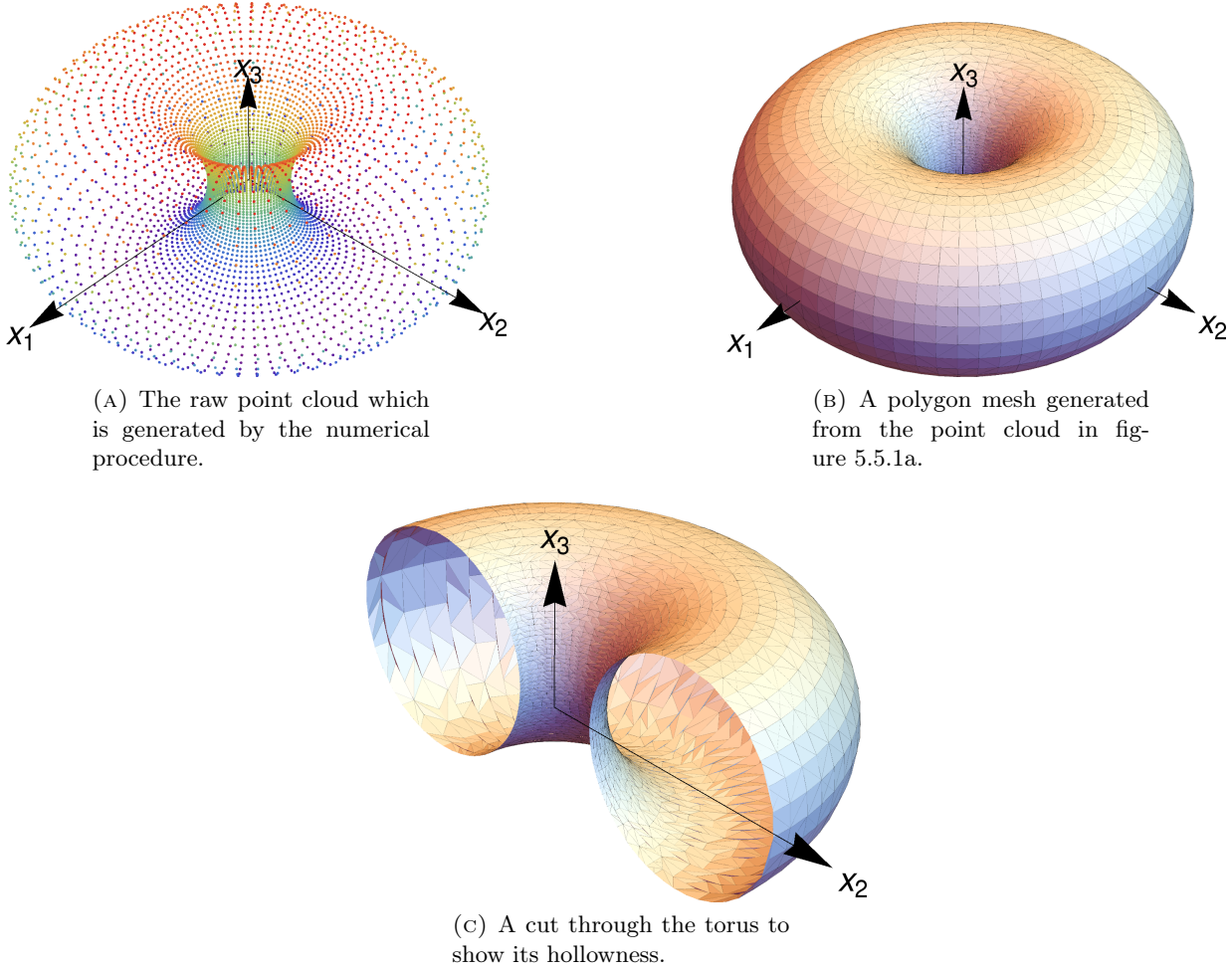


FIGURE 5.5.1. Visualization of the semi-classical limit of the fuzzy torus T_n^2 constructed from T_{20}^2 .

5.6. Squashed \mathbb{CP}_n^2 revisited

Now let us turn to squashed fuzzy \mathbb{CP}^2 given by six matrices $X^a \sim x^a$, $a \in \mathcal{I} = \{1, 2, 4, 5, 6, 7\}$ which obey the $\mathfrak{su}(3)$ commutation relations

$$[X^a, X^b] = i \frac{1}{\sqrt{n(1+n/3)}} c_{abc} X^c. \quad (5.6.1)$$

5.6.1. The point probe Laplacian $\square_{\mathbf{p}}$. The point probe Laplacian $\square_{\mathbf{p}}$ is naturally given by

$$\square_{\mathbf{p}} = \sum_{a \in \mathcal{I}} (X^a - \mathbf{p}^a)^2. \quad (5.6.2)$$

To be able to visualize the numerical result, one can restrict oneself to a 3-dimensional subspace of the target space \mathbb{R}^6 . An interesting choice is to consider the limit $x^2 = x^5 = x^7 \rightarrow 0^7$ which can be achieved by simply setting $\mathbf{p}^2 = \mathbf{p}^5 = \mathbf{p}^7 = 0$ in equation (5.6.2). This fits the limit in section §4.3.

Taking $n = 30$, i.e. the representation $(0, 30)$, one gets a global minimum at

$$\vec{\mathbf{p}}_{\min} \approx \{0.546391, -0.546396, 0.546392\}$$

⁷Again recall that the indices take values in $\mathcal{I} = \{1, 2, 4, 5, 6, 7\}$ for reasons discussed above.

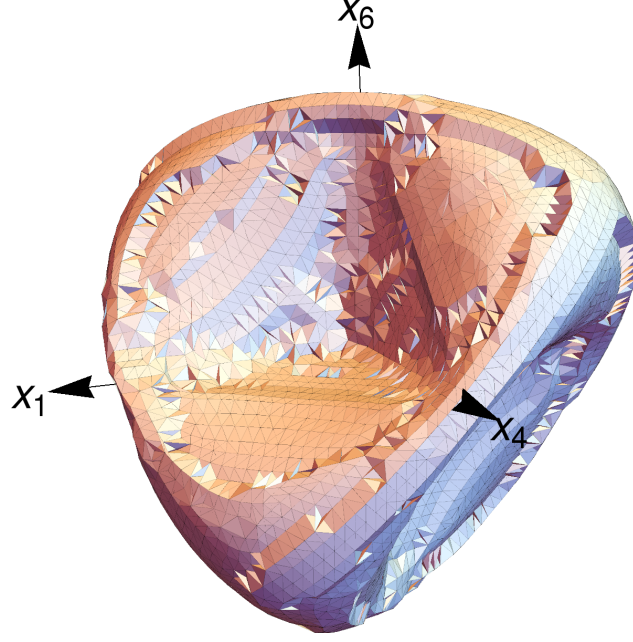


FIGURE 5.6.1. The numerically obtained expectation values $\vec{p}(\phi)$ of Laplace coherent states $\phi \in \mathcal{H}_{(0,30)}$ of \mathbb{CP}_{30}^2 .

with corresponding function value

$$f(\vec{\mathfrak{p}}_{\min}) \approx 0.052891.$$

The expectation values $\vec{p}(\phi)$ of the coherent state ϕ corresponding to this minimum agree with $\vec{\mathfrak{p}}_{\min}$ for at least 6 decimal digits. Hence $f(\vec{\mathfrak{p}}_{\min}) \approx \delta(\phi)$ to a very good approximation.⁸

In section §4.3 the theoretical considerations for Perelomov states were done and led to a minimal function value

$$f_{\min}^{\text{th}} = \frac{2}{3+n} \stackrel{n=30}{\approx} 0.0606061$$

which implies a relative deviation of $\approx 15\%$ from the numerical value. The predicted norm of the expectation values $|\vec{p}(\phi)|$ is

$$|\vec{p}(\phi)| = \sqrt{3}c_n n \stackrel{n=30}{\approx} 0.953463$$

which deviates by 0.7% from the numerically obtained norm.

Thus the numerical evidence suggests that the Laplace coherent states for the squashed fuzzy \mathbb{CP}^2 are not exactly the Perelomov coherent states but even better ones if one takes the dispersion $\delta(\phi)$ as a measure for quality. Nevertheless, the deviation of the expectation values are small, therefore the Perelomov states should suffice as a suitable approximation. This can also be seen in figure 5.6.1 which approximately looks like figure 4.3.1 in section §4.3.

5.6.2. The point probe Dirac operator $\not{D}_{\mathfrak{p}}$. It remains to examine the Dirac operator $\not{D}_{\mathfrak{p}}$ which in this case is defined as

$$\not{D}_{\mathfrak{p}} = \sum_{a \in \mathcal{I}} \gamma^a (X^a - \mathfrak{p}^a) \quad (5.6.3)$$

⁸See the general considerations above, especially equation (5.2.9).

with the six gamma matrices γ^a given by

$$\begin{aligned}
\gamma^1 &= \begin{pmatrix} 0 & 0 & 0 & 0 & 1 & 0 & 0 & 0 \\ 0 & 0 & 0 & 0 & 0 & 1 & 0 & 0 \\ 0 & 0 & 0 & 0 & 0 & 0 & 1 & 0 \\ 0 & 0 & 0 & 0 & 0 & 0 & 0 & 1 \\ 1 & 0 & 0 & 0 & 0 & 0 & 0 & 0 \\ 0 & 1 & 0 & 0 & 0 & 0 & 0 & 0 \\ 0 & 0 & 1 & 0 & 0 & 0 & 0 & 0 \\ 0 & 0 & 0 & 1 & 0 & 0 & 0 & 0 \end{pmatrix}, & \gamma^2 &= \begin{pmatrix} 0 & 0 & 0 & 0 & -i & 0 & 0 & 0 \\ 0 & 0 & 0 & 0 & 0 & -i & 0 & 0 \\ 0 & 0 & 0 & 0 & 0 & 0 & -i & 0 \\ 0 & 0 & 0 & 0 & 0 & 0 & 0 & -i \\ i & 0 & 0 & 0 & 0 & 0 & 0 & 0 \\ 0 & i & 0 & 0 & 0 & 0 & 0 & 0 \\ 0 & 0 & i & 0 & 0 & 0 & 0 & 0 \\ 0 & 0 & 0 & i & 0 & 0 & 0 & 0 \end{pmatrix}, \\
\gamma^4 &= \begin{pmatrix} 0 & 0 & 1 & 0 & 0 & 0 & 0 & 0 \\ 0 & 0 & 0 & 1 & 0 & 0 & 0 & 0 \\ 1 & 0 & 0 & 0 & 0 & 0 & 0 & 0 \\ 0 & 1 & 0 & 0 & 0 & 0 & 0 & 0 \\ 0 & 0 & 0 & 0 & 0 & 0 & -1 & 0 \\ 0 & 0 & 0 & 0 & 0 & 0 & 0 & -1 \\ 0 & 0 & 0 & 0 & -1 & 0 & 0 & 0 \\ 0 & 0 & 0 & 0 & 0 & -1 & 0 & 0 \end{pmatrix}, & \gamma^5 &= \begin{pmatrix} 0 & 0 & -i & 0 & 0 & 0 & 0 & 0 \\ 0 & 0 & 0 & -i & 0 & 0 & 0 & 0 \\ i & 0 & 0 & 0 & 0 & 0 & 0 & 0 \\ 0 & i & 0 & 0 & 0 & 0 & 0 & 0 \\ 0 & 0 & 0 & 0 & 0 & 0 & i & 0 \\ 0 & 0 & 0 & 0 & 0 & 0 & 0 & i \\ 0 & 0 & 0 & 0 & -i & 0 & 0 & 0 \\ 0 & 0 & 0 & 0 & 0 & -i & 0 & 0 \end{pmatrix}, \\
\gamma^6 &= \begin{pmatrix} 0 & 1 & 0 & 0 & 0 & 0 & 0 & 0 \\ 1 & 0 & 0 & 0 & 0 & 0 & 0 & 0 \\ 0 & 0 & 0 & -1 & 0 & 0 & 0 & 0 \\ 0 & 0 & -1 & 0 & 0 & 0 & 0 & 0 \\ 0 & 0 & 0 & 0 & 0 & -1 & 0 & 0 \\ 0 & 0 & 0 & 0 & -1 & 0 & 0 & 0 \\ 0 & 0 & 0 & 0 & 0 & 0 & 0 & 1 \\ 0 & 0 & 0 & 0 & 0 & 0 & 1 & 0 \end{pmatrix}, & \gamma^7 &= \begin{pmatrix} 0 & -i & 0 & 0 & 0 & 0 & 0 & 0 \\ i & 0 & 0 & 0 & 0 & 0 & 0 & 0 \\ 0 & 0 & 0 & i & 0 & 0 & 0 & 0 \\ 0 & 0 & -i & 0 & 0 & 0 & 0 & 0 \\ 0 & 0 & 0 & 0 & 0 & i & 0 & 0 \\ 0 & 0 & 0 & 0 & -i & 0 & 0 & 0 \\ 0 & 0 & 0 & 0 & 0 & 0 & 0 & -i \\ 0 & 0 & 0 & 0 & 0 & 0 & i & 0 \end{pmatrix}. \tag{5.6.4}
\end{aligned}$$

In this case we carry out the computations taking $n = 3$. As it turns out this value for n is high enough since a hierarchy is visible even for low n . The explicit matrices are given in appendix A.3.1.

Searching for a global minimum yields

$$\vec{\mathbf{p}}_{\min} \approx \{-0.0608956, -0.582712, -0.291495\}$$

with function value

$$f(\vec{\mathbf{p}}_{\min}) \approx 4.32 \times 10^{-9}.$$

A visualization of the computation result for Dirac coherent states can be seen in figure 5.6.2.

This is the first example where the Dirac coherent states do not agree with the Laplace coherent states, although some similarity can be recognized. Remarkably, the calculated states \mathcal{CS} satisfy

$$f(\vec{p}(\mathcal{CS})) < 1.3 \times 10^{-8}$$

which again suggests that these states could be exact zero modes of the Dirac operator $\mathcal{D}_{\mathbf{p}}$ and indeed we will see in the following section that this is the case.

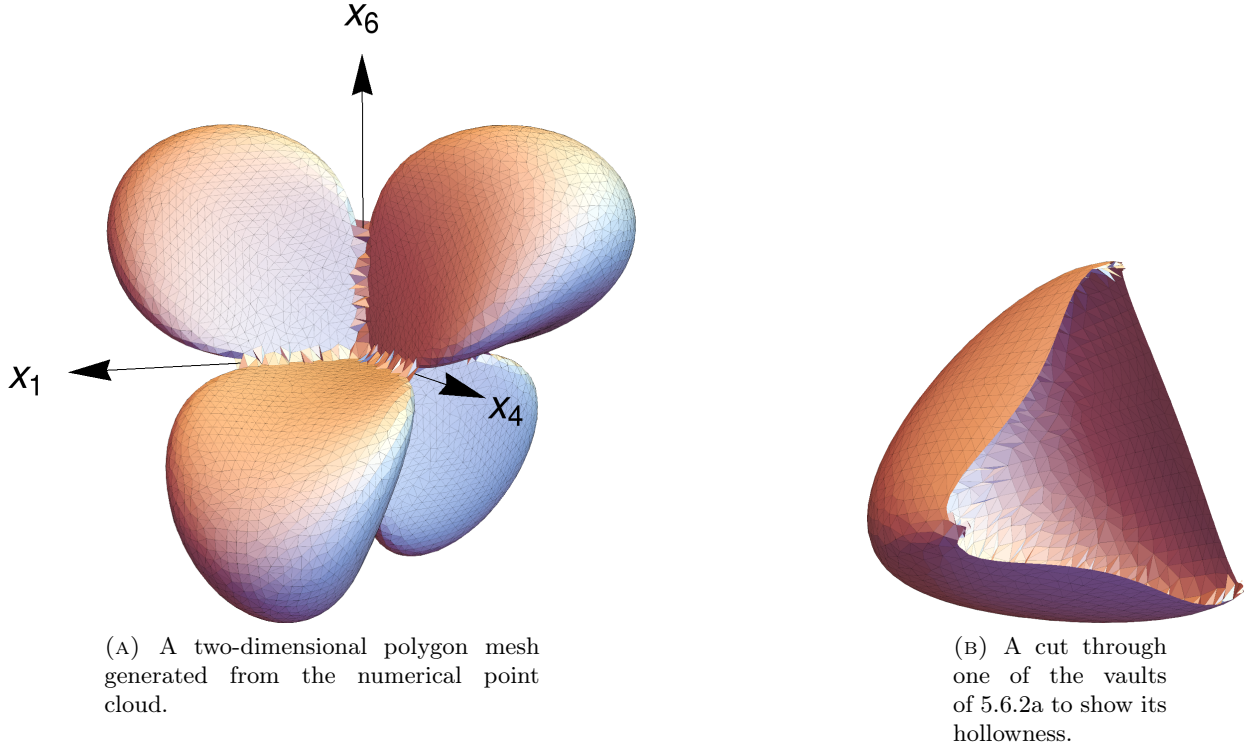
Zero modes of $\mathcal{D}_{(\mathbf{p}_1, 0, \mathbf{p}_4, 0, \mathbf{p}_6, 0)}$ on $\mathbb{C}^8 \otimes (0, 1)$. We claim that for the Dirac operator $\mathcal{D}_{(\mathbf{p}_1, \mathbf{p}_4, \mathbf{p}_6)} := \mathcal{D}_{(\mathbf{p}_1, 0, \mathbf{p}_4, 0, \mathbf{p}_6, 0)}$ acting on $\mathbb{C}^8 \otimes (0, 1)$ there exists at least a connected set $\mathcal{Z} \subset \mathbb{R}^3$, so that $\mathcal{D}_{\mathcal{Z}} = 0$ on an at least one-dimensional subspace of $\mathbb{C}^8 \otimes (0, 1)$.

To this end let us consider a smooth curve $\gamma : \mathbb{R} \rightarrow \mathbb{R}^3$ and the corresponding smooth curve of Dirac operators

$$t \mapsto \mathcal{D}_{\gamma(t)} \tag{5.6.5}$$

on the curve γ .

Then we can make use of the following theorem by Alekseevsky et al. [1]:

FIGURE 5.6.2. Visualization of Dirac coherent states of $\mathbb{CP}_{(0,3)}^2$.

THEOREM (Alekseevsky et al. [1]). *Let $A(t) = (A_{ij}(t))$ be a smooth curve of complex hermitian $(n \times n)$ -matrices, depending on a real parameter $t \in \mathbb{R}$, acting on a hermitian space $V = \mathbb{C}^n$, such that no two of the continuous eigenvalues meet of infinite order at any $t \in \mathbb{R}$ if they are not equal for all t . Then all the eigenvalues and all the eigenvectors can be chosen smoothly in t , on the whole parameter domain \mathbb{R} .*

Choosing a curve γ so that the conditions of the above theorem are fulfilled, we are able to numerically track eigenvalues due to the continuity of its eigenvectors. Note that the continuity of the eigenvalues is not enough to track them, because crossing of two different eigenvalues may occur, while the eigenvectors are always orthogonal to each other, and therefore the choice is always unique (at least if considering only one-dimensional eigenspaces).

With this knowledge we are able to numerically generate a smooth function $t \mapsto \lambda(t)$, where $\lambda(t)$ is an eigenvalue of $\mathcal{D}_{\gamma(t)}$, to arbitrary high resolution ΔT . Further, we can scan this function for sign changes, i.e. for a $T \in \mathbb{R}$, so that $\text{sign}(\lambda(T)) \neq \text{sign}(\lambda(T + \Delta T))$. Then, because of the *Intermediate Value Theorem*, we know, that there exists a root of $\lambda(t)$ between T and $T + \Delta T$.

Hence we found a method to numerically prove the existence of zero modes on a one parameter curve γ .

Let us now choose a concrete curve Γ , practically a straight line through 0 and $(1, 1, -1)$,

$$\Gamma(t) = \frac{1}{\sqrt{3}} \begin{pmatrix} 1 \\ 1 \\ -1 \end{pmatrix} t + \begin{pmatrix} 0 \\ \kappa \\ 0 \end{pmatrix} e^{-(t-1/10)^2} \quad (5.6.6)$$

setting κ very small. The reason for the (small) second term is, that the eigenvalues on $\bar{\Gamma}(t) = (1, 1, -1)t$ seem to be degenerate, which we want to avoid for the sake of simplicity.

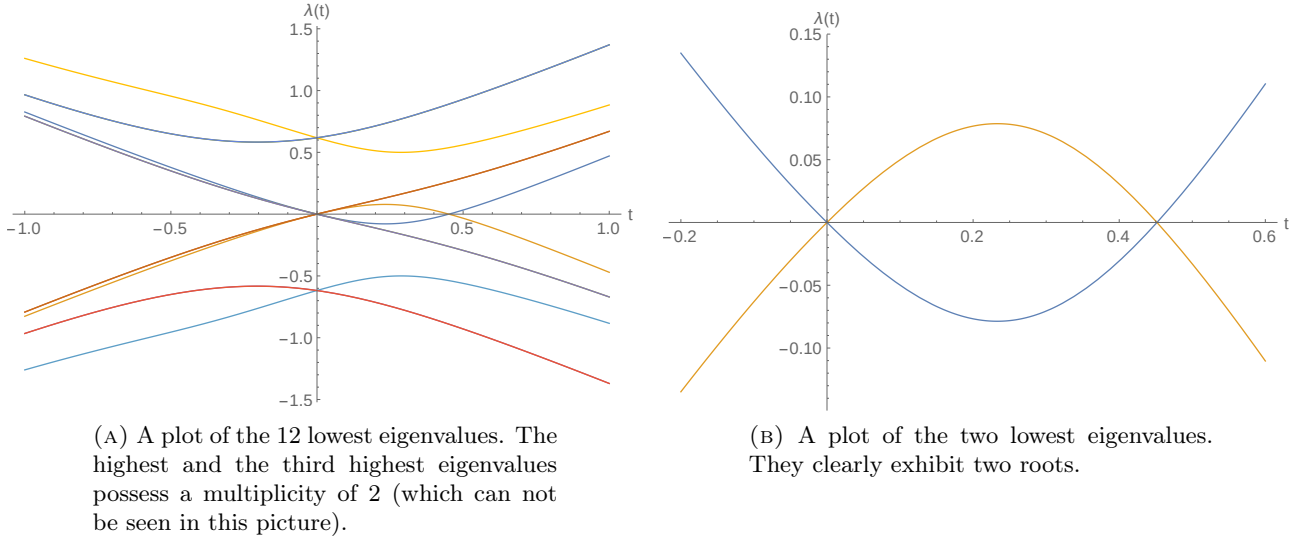


FIGURE 5.6.3. Visualization of tracked eigenvalues of $\mathcal{D}_{\Gamma(t)}$, indicated by differing colors, $\Gamma(\mathbb{R})$ practically being a straight line through the origin and the point $(1, 1, -1)$.

To get an idea of the behavior of the eigenvalues of $\mathcal{D}_{\Gamma(t)}$ we track the 12 lowest eigenvalues at point $\Gamma(t = 1/10)$.⁹ They are visualized in figure 5.6.3a. Further, only the lowest two eigenvalues are plotted in figure 5.6.3b.

One clearly observes the two sign changes; one at the origin and one near $\Gamma(t \approx 0.45)$. Having a zero mode at $\Gamma(t = 0)$ is not surprising, this can even be seen without numerical aid. However, the second root is not self-evident and could only be asserted by numerical means.

Now, considering not only a one-parameter curve of Dirac operators, but Dirac operators depending on three variables

$$(\mathbf{p}_1, \mathbf{p}_4, \mathbf{p}_6) \mapsto \mathcal{D}_{(\mathbf{p}_1, \mathbf{p}_4, \mathbf{p}_6)}, \quad (5.6.7)$$

the eigenvalues $(\mathbf{p}_1, \mathbf{p}_4, \mathbf{p}_6) \mapsto \lambda(\mathbf{p}_1, \mathbf{p}_4, \mathbf{p}_6)$ are continuous too (see e.g. [26]). Also observe the two points $x_1 = \Gamma(0.3)$ and $x_2 = \Gamma(0.5)$. We saw above that there exists a corresponding continuous eigenvalue function $\lambda(t)$ so that $\lambda(0.3) > 0$ and $\lambda(0.5) < 0$. Since the eigenvalues are continuous on \mathbb{R}^3 , on every curve

$$\gamma : [0, 1] \rightarrow \mathbb{R}^3 \quad (5.6.8)$$

with

$$\gamma(0) = x_1, \quad \gamma(1) = x_2,$$

there must exist an eigenvalue which changes sign on the curve γ , otherwise $\lambda(t)$ would not be able to exist. Therefore, on every such curve γ from x_1 to x_2 there must exist at least one zero mode. Thus, the set $\mathcal{Z} \subset \mathbb{R}^3$ where $\mathcal{D}_{\mathbf{p}}$ has zero modes has to enclose x_1 respectively x_2 and is connected.

⁹This is of course a completely arbitrary decision.

CHAPTER 6

Conclusion

This work shows, that in the unexplored realm of non-commutative geometry coherent states form a powerful instrument to enhance the understanding of novel non-commutative geometries arising from Yang-Mills theories, such as squashed fuzzy \mathbb{CP}^2 , and their special features. As we have seen with the help of coherent states, one is fully capable of extracting an approximation to the semi-classical limit which is not only vital for an intuitive perception of non-commutative geometries but also lays the foundation for grasping features going beyond the semi-classical limit.

While the numerical procedure to collect coherent states developed in this thesis is mainly used to visualize the corresponding classical manifolds, their applications do not end here, since the numerical data constitute more than just the position expectation values of coherent states. For example, expectation values of various observables with respect to coherent states might be of interest and could be calculated numerically with ease.

Although this work strongly focuses on squashed fuzzy \mathbb{CP}^2 , this algorithm is not restricted to this example, but applicable to the whole zoo of matrix geometries one can think of. Thus it provides a viable tool to assist further studies in this field.

One may have noticed that only the basic principles of the used algorithm are presented in this thesis. Since the print format chosen for this work is not appropriate to publish implementation details, the author hopes to publish the full implementation of the package (i.e. a *Wolfram Mathematica* package) including documentation in the future.

Despite the fact that this work concentrates on states which live in a finite dimensional Hilbert space, their application is, of course, not bound to this setup. However, at first sight it is not evident, how the established numerical procedure should be expanded to support infinite dimensional Hilbert spaces. The investigation of this is left to future research.

Bibliography

- [1] ALEKSEEVSKY, D., KRIEGL, A., MICHOR, P. W., AND LOSIK, M. Choosing roots of polynomials smoothly. *Israel Journal of Mathematics* 105, 1 (1998), 203.
- [2] ALEX, A., KALUS, M., HUCKLEBERRY, A., AND VON DELFT, J. A numerical algorithm for the explicit calculation of $SU(N)$ and $SL(N, \mathbb{C})$ Clebsch-Gordan coefficients. *J. Math. Phys.* 52 (Mar. 2011), 023507.
- [3] ALEXANIAN, G., BALACHANDRAN, A., IMMIRZI, G., AND YDRI, B. Fuzzy CP^2 . *Journal of Geometry and Physics* 42, 1 (2002), 28–53.
- [4] ASCHIERI, P., STEINACKER, H., MADORE, J., MANOUSSELIS, P., AND ZOUPANOS, G. Fuzzy extra dimensions: Dimensional reduction, dynamical generation and renormalizability. [SFINA1,25(2007)].
- [5] BARUT, A., AND GIRARDELLO, L. New 'coherent' states associated with noncompact groups. *Commun.Math.Phys.* 21 (1971), 41–55.
- [6] BERENSTEIN, D., AND DZIENKOWSKI, E. Matrix embeddings on flat R^3 and the geometry of membranes. *Phys. Rev. D* 86 (2012), 086001.
- [7] CHATZISTAVRAKIDIS, A., STEINACKER, H., AND ZOUPANOS, G. Intersecting branes and a standard model realization in matrix models. *Journal of High Energy Physics* 9 (Sept. 2011), 115.
- [8] CHU, C.-S., MADORE, J., AND STEINACKER, H. Scaling Limits of the Fuzzy Sphere at one Loop. *JHEP* 0108 (Aug. 2001), 038.
- [9] DOPLICHER, S., FREDENHAGEN, K., AND ROBERTS, J. E. The quantum structure of spacetime at the Planck scale and quantum fields. *Communications in Mathematical Physics* 172, 1 (1995), 187–220.
- [10] GEORGI, H. *Lie algebras in particle physics*. Westview Press, 1999.
- [11] GROSSE, H., AND PREŠNAJDER, P. The construction of noncommutative manifolds using coherent states. *Letters in Mathematical Physics* 28, 3 (1993), 239.
- [12] GROSSE, H., AND STEINACKER, H. Finite gauge theory on fuzzy CP^2 . *Nuclear Physics B* 707, 1 (2005), 145–198.
- [13] HEISENBERG, W. Über die in der Theorie der Elementarteilchen auftretende universelle Länge. In *Original Scientific Papers/Wissenschaftliche Originalarbeiten*. Springer, 1989, pp. 301–314.
- [14] HOPPE, J. R. *Quantum Theory of a Massless Relativistic Surface and a Two-Dimensional Bound State Problem*. PhD thesis, MASSACHUSETTS INSTITUTE OF TECHNOLOGY., 1982.
- [15] I.M. GEL'FAND, R. A .MINLOS, Z. YA. SHAPIRO, . *Representations of the Rotation and Lorentz Groups and Their Applications*. Macmillan Co, Pergamon.
- [16] ISHIKI, G. Matrix Geometry and Coherent States. *arXiv preprint arXiv:1503.01230* (2015).
- [17] KRAGH, H. *Dirac: a scientific biography*. Cambridge University Press, 1990.
- [18] MADORE, J. The Fuzzy sphere. *Class.Quant.Grav.* 9 (1992), 69–88.
- [19] MALKIN, I., AND MANKO, V. Dynamic symmetry and coherent states of quantum systems. *Moscow Izdatel Nauka* 1 (1979).
- [20] PERELOMOV, A. *Generalized Coherent States and their Applications*. Springer-Verlag, Berlin, 1986.
- [21] RADCLIFFE, J. Some properties of coherent spin states. *Journal of Physics A: General Physics* 4, 3 (1971), 313.
- [22] SCHREIVOGEL, P., STEINACKER, H., ET AL. Generalized Fuzzy Torus and its Modular Properties. *SIGMA. Symmetry, Integrability and Geometry: Methods and Applications* 9 (2013), 060.
- [23] STEINACKER, H. Non-commutative geometry and matrix models. *PoS QGGS2011* (2011), 004.
- [24] STEINACKER, H. C., AND ZAHN, J. Self-intersecting fuzzy extra dimensions from squashed coadjoint orbits in $\mathcal{N} = 4$ SYM and matrix models. *Journal of High Energy Physics* 1502, 2 (2015), 027.
- [25] STUDY, E. Kürzeste Wege im komplexen Gebiet. *Mathematische Annalen* 60, 3 (1905), 321.
- [26] TOSIO KATO. *Perturbation Theory for Linear Operators*. Classics in Mathematics. Springer.
- [27] WALDMANN, S. *Poisson-Geometrie*. Springer, 2007.
- [28] WATT, D. A., AND FINDLAY, W. *Programming language design concepts*. Wiley, 2004.
- [29] WEYL, H. *Gruppentheorie und Quantenmechanik*. Hirzel, Leipzig, 1928.
- [30] ZEZULA, P., AMATO, G., DOHNAL, V., AND BATKO, M. *Similarity Search - The Metric Space Approach*, vol. 32 of *Advances in Database Systems*. Kluwer, 2006.

APPENDIX A

The Lie group $SU(3)$

A.1. Definition

The set $SU(3)$ is defined as a set of all unitary 3×3 matrices with unit determinant:

$$SU(3) := \{U \in Mat_3(\mathbb{C}) \mid U^{-1} = U^\dagger, \det U = 1\}. \quad (\text{A.1.1})$$

The set forms a group with respect to usual matrix multiplication.

Every group element U can be written in the form

$$U = e^{iT} \quad (\text{A.1.2})$$

where T is an element of the so called Lie algebra $\mathfrak{su}(3)$ which is defined as the set of tracefree hermitian matrices

$$\mathfrak{su}(3) := \{T \in Mat_3(\mathbb{C}) \mid T^\dagger = T, \text{tr}(T) = 0\}.$$

They form an algebra with respect to the commutator $[\cdot, \cdot]$. A well known basis of $\mathfrak{su}(3)$ is the set of Gell-Mann matrices[10]:

$$\begin{aligned} \lambda_1 &= \begin{pmatrix} 0 & 1 & 0 \\ 1 & 0 & 0 \\ 0 & 0 & 0 \end{pmatrix}, & \lambda_2 &= \begin{pmatrix} 0 & -i & 0 \\ i & 0 & 0 \\ 0 & 0 & 0 \end{pmatrix}, & \lambda_3 &= \begin{pmatrix} 1 & 0 & 0 \\ 0 & -1 & 0 \\ 0 & 0 & 0 \end{pmatrix}, \\ \lambda_4 &= \begin{pmatrix} 0 & 0 & 1 \\ 0 & 0 & 0 \\ 1 & 0 & 0 \end{pmatrix}, & \lambda_5 &= \begin{pmatrix} 0 & 0 & -i \\ 0 & 0 & 0 \\ i & 0 & 0 \end{pmatrix}, & \lambda_6 &= \begin{pmatrix} 0 & 0 & 0 \\ 0 & 0 & 1 \\ 0 & 1 & 0 \end{pmatrix}, \\ \lambda_7 &= \begin{pmatrix} 0 & 0 & 0 \\ 0 & 0 & -i \\ 0 & i & 0 \end{pmatrix}, & \lambda_8 &= \frac{1}{\sqrt{3}} \begin{pmatrix} 1 & 0 & 0 \\ 0 & 1 & 0 \\ 0 & 0 & -2 \end{pmatrix} \end{aligned}$$

and accordingly their scaled version $t_a := \lambda_a/2$.

They satisfy the commutation relations

$$[t_a, t_b] = i c_{abc} t_c \quad (\text{A.1.3})$$

where c_{abc} are the so called *antisymmetric structure constants* of $\mathfrak{su}(3)$ given by

$$\begin{aligned} c_{123} &= 1 \\ c_{147} = c_{165} = c_{246} = c_{257} = c_{345} = c_{376} &= 1/2 \\ c_{458} = c_{678} &= \sqrt{3}/2, \end{aligned} \quad (\text{A.1.4})$$

while all the others are 0. They completely determine the structure of the Lie algebra respectively Lie group. Furthermore, they obey the relations

$$\sum_{a,b=1}^8 c_{abi} c_{abj} = 3 \delta_{ij}$$

which can be checked by hand.

On the other hand, we can define the *symmetric structure constants* d_{abc} of $\mathfrak{su}(3)$ by the relation

$$[t_a, t_b]_+ = \frac{1}{3}\delta_{ab} + d_{abc}t_c \quad (\text{A.1.5})$$

where $[a, b]_+ := a \cdot b + b \cdot a$ represents the anti-commutator. They are given by

$$\begin{aligned} d_{118} = d_{228} = d_{338} = -d_{888} &= 1/\sqrt{3} \\ d_{448} = d_{558} = d_{668} = d_{778} &= -1/(2\sqrt{3}) \\ d_{146} = d_{157} = -d_{247} = d_{256} = d_{344} = d_{355} = -d_{366} = -d_{377} &= 1/2. \end{aligned} \quad (\text{A.1.6})$$

Root generators. Often needed are so-called root generators (or also termed ladder operators) $t_1^\pm, t_2^\pm, t_3^\pm$ defined by

$$\begin{aligned} t_1^\pm &:= t_4 \pm it_5, \\ t_2^\pm &:= t_6 \pm it_7, \\ t_3^\pm &:= t_1 \pm it_2 = \pm[t_1^\pm, t_2^\mp]. \end{aligned} \quad (\text{A.1.7})$$

Together with the Cartan generators t_3 and t_8 they form a basis of the adjoint representation (see subsection A.2.3).

A.2. Representations

Formally, a representation of an abstract group is a realization of the group as linear maps on a vector space or more accurately a *representation* of a Lie group G is a Lie group homomorphism¹

$$\Pi : G \rightarrow \text{End}(\mathcal{H}) \quad (\text{A.2.1})$$

for some vector space \mathcal{H} which is often called *carrier space*. In our case \mathcal{H} is always a vector space over the field of complex number \mathbb{C} .

It turns out one can fully classify representations of compact Lie groups G via the representations π of their corresponding Lie algebra \mathfrak{g}

$$\pi : \mathfrak{g} \rightarrow \text{End}(\mathcal{H}), \quad (\text{A.2.2})$$

in particular $SU(3)$. We are only interested in finite dimensional representations which can always be made unitary. For $SU(3)$ finite dimensional irreducible representations are completely determined by a tuple of integers (n, m) (in contrast to $SU(2)$ where a representation is fully determined by one integer, usually called spin j).

In particular the dimension of the vector space $\mathcal{H}_{(n,m)}$ can be calculated as

$$\dim(\mathcal{H}_{(n,m)}) = \frac{1}{2}(n+1)(m+1)(n+m+2). \quad (\text{A.2.3})$$

We can always choose the basis of $\mathcal{H}_{(n,m)}$ in such a way that $\pi(t_3)$ and $\pi(t_8)$ are diagonal in that basis. Plotting the eigenvalues of these two matrices on a two-dimensional sheet (often called *weight space*) provides an overview of the Hilbert space in question. It turns out for $SU(3)$ the weight space has a special structure, see figure A.2.1a.

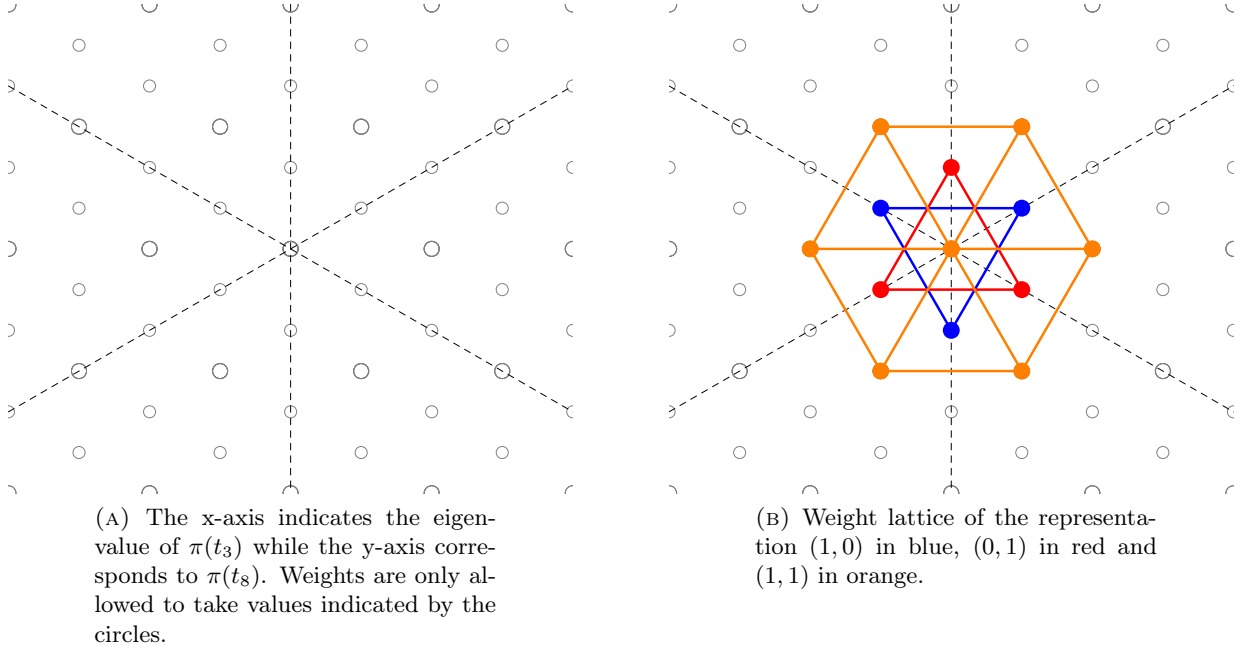
A.2.1. Example: The representation $(1, 0)$. As we can see from equation (A.2.3) the dimension of the carrier space is $\dim(\mathcal{H}_{(1,0)}) = 3$. The three blue dots in figure A.2.1b correspond to the three basis vectors with different weights.

The action of $SU(3)$ on $\mathcal{H}_{(1,0)}$ is given by simple matrix multiplication of $SU(3)$ matrices

$$g \triangleright |\psi\rangle = g \cdot |\psi\rangle, \quad (\text{A.2.4})$$

hence it is in some sense the most obvious non-trivial representation.

¹A Lie group homomorphism is a smooth group homomorphism.

FIGURE A.2.1. Weight lattice of $SU(3)$.

A.2.2. Example: The representation $(0, 1)$. Using again equation (A.2.3) we see that this representation also acts on a 3-dimensional space. This shows that representations with equal dimensions do not necessarily have to be equivalent. Again a graphical representation is given in figure A.2.1b in red color.

The action on $\mathcal{H}_{(0,1)}$ is given by

$$g \triangleright |\psi\rangle = \bar{g} \cdot |\psi\rangle, \quad (\text{A.2.5})$$

where \bar{g} denotes complex conjugation of g .

A.2.3. Example: The representation $(1, 1)$. This 8-dimensional representation is usually defined on the Lie algebra $\mathfrak{su}(3) \cong \mathbb{R}^8$ itself, that is by conjugation:

$$g \triangleright T = g \cdot T \cdot g^{-1}. \quad (\text{A.2.6})$$

As one can see the weight lattice in figure A.2.1b (orange) only has 7 dots. That means that there must be a degenerate weight. In fact it is the weight $(0, 0)$ which belongs to two eigenvectors, that is t_3 and t_8 , which is easy to check since $e^{it_{8,3}} \triangleright t_{8,3} = t_{8,3}$.

A.3. Constructing matrices for arbitrary representations (n, m)

Gelfand and Tsetlin provided the theory to construct arbitrary $\mathfrak{su}(N)$ representations, cf. [15, 2]. The key here is to consider the so called *Gelfand-Tsetlin* patterns. These are triangular arrangements of integers which are in 1–1 correspondence to basis vectors of an irreducible $\mathfrak{su}(N)$ representation. The crucial point is that this is in contrast to labeling the basis vectors by their weight, where degeneracies can arise (i.e. two linear independent vectors can have the same weight).

A general Gelfand-Tsetlin pattern M looks like

$$M = \begin{pmatrix} m_{1,N} & m_{2,N} & & \cdots & & m_{N-1,N} & m_{N,N} \\ & m_{1,N-1} & & & & m_{N-1,N-1} & \\ & & \ddots & & & & \\ & & & m_{1,2} & m_{2,2} & & \\ & & & & m_{1,1} & & \end{pmatrix} \quad (\text{A.3.1})$$

where the entries in the top row specify the irreducible representation, while the others are subject to the so-called *betweenness condition*

$$m_{k,l} \geq m_{k,l-1} \geq m_{k+1,l} \quad 1 \leq k < l \leq N \quad (\text{A.3.2})$$

and label a basis vector for each allowed combination.

For $SU(3)$ the representation (n, m) in our convention corresponds to the set of patterns where the top line is given by $(n + m, n, 0)$:

$$(n, m) \leftrightarrow (n + m, n, 0). \quad (\text{A.3.3})$$

A closed form has been found by Gelfand and Tsetlin for the matrix elements of the raising and lowering operators which acts on the particular representations:

$$-\langle M - M^{k,l} | J_-^{(l)} | M \rangle^2 = \frac{\prod_{k'=1}^l (m_{k',l+1} - m_{k,l} + k - k' + 1) \prod_{k'=1}^{l-1} (m_{k',l-1} - m_{k,l} + k - k')}{\prod_{\substack{k'=1 \\ k' \neq k}}^l (m_{k',l} - m_{k,l} + k - k' + 1) (m_{k',l} - m_{k,l} + k - k')} \quad (\text{A.3.4})$$

where $M^{k,l}$ is a pattern with $m_{k,l} = 1$ and zero elsewhere.

Equipped with this knowledge one can easily generate all possible patterns (i.e. all patterns that satisfy the betweenness condition (A.3.2)) for a irreducible representation and then calculate the raising and lowering operators with equation (A.3.4).

In the special case $SU(3)$ this procedure gives two raising respectively lowering operators $T_2^\pm = \pi(t_2^\pm)$ and $T_3^\pm = \pi(t_3^\pm)$.² Defining $T_1^\pm := \pm[T_2^\pm, T_3^\pm]$ the generators $T^a = \pi(t^a)$ can then be found by the relations

$$\begin{aligned} T^1 &= \frac{1}{2} (T_3^+ + T_3^-) & T^5 &= \frac{1}{2i} (T_1^+ - T_1^-) \\ T^2 &= \frac{1}{2i} (T_3^+ - T_3^-) & T^6 &= \frac{1}{2} (T_2^+ + T_2^-) \\ T^3 &= \frac{1}{2} [T_1^+, T_1^-] & T^7 &= \frac{1}{2i} (T_2^+ - T_2^-) \\ T^4 &= \frac{1}{2} (T_1^+ + T_1^-) & T^8 &= \frac{1}{2\sqrt{3}} ([T_2^+, T_2^-] + [T_3^+, T_3^-]). \end{aligned} \quad (\text{A.3.5})$$

The matrices T^a then satisfy the commutation relations

$$[T^a, T^b] = i c_{abc} T^c \quad (\text{A.3.6})$$

with c_{abc} being the structure constants defined in (A.1.4).

²This specific choice of numbering is due to the convention used in this paper.

A.3.1. Example: The representation $(0, 3)$. Since this representation is used for numerical calculations in section §5.6 the explicit matrices are provided here.

$$\begin{aligned}
T^1 &= \begin{pmatrix} 0 & 0 & 0 & 0 & 0 & 0 & 0 & 0 & 0 & 0 \\ 0 & 0 & \frac{1}{2} & 0 & 0 & 0 & 0 & 0 & 0 & 0 \\ 0 & \frac{1}{2} & 0 & 0 & 0 & 0 & 0 & 0 & 0 & 0 \\ 0 & 0 & 0 & 0 & \frac{1}{\sqrt{2}} & 0 & 0 & 0 & 0 & 0 \\ 0 & 0 & 0 & \frac{1}{\sqrt{2}} & 0 & \frac{1}{\sqrt{2}} & 0 & 0 & 0 & 0 \\ 0 & 0 & 0 & 0 & \frac{1}{\sqrt{2}} & 0 & 0 & 0 & 0 & 0 \\ 0 & 0 & 0 & 0 & 0 & 0 & \frac{\sqrt{3}}{2} & 0 & 0 & 0 \\ 0 & 0 & 0 & 0 & 0 & 0 & \frac{\sqrt{3}}{2} & 0 & 1 & 0 \\ 0 & 0 & 0 & 0 & 0 & 0 & 0 & 1 & 0 & \frac{\sqrt{3}}{2} \\ 0 & 0 & 0 & 0 & 0 & 0 & 0 & 0 & \frac{\sqrt{3}}{2} & 0 \end{pmatrix}, \\
T^2 &= \begin{pmatrix} 0 & 0 & 0 & 0 & 0 & 0 & 0 & 0 & 0 & 0 & 0 \\ 0 & 0 & -\frac{i}{2} & 0 & 0 & 0 & 0 & 0 & 0 & 0 & 0 \\ 0 & \frac{i}{2} & 0 & 0 & 0 & 0 & 0 & 0 & 0 & 0 & 0 \\ 0 & 0 & 0 & 0 & -\frac{i}{\sqrt{2}} & 0 & 0 & 0 & 0 & 0 & 0 \\ 0 & 0 & 0 & \frac{i}{\sqrt{2}} & 0 & -\frac{i}{\sqrt{2}} & 0 & 0 & 0 & 0 & 0 \\ 0 & 0 & 0 & 0 & \frac{i}{\sqrt{2}} & 0 & 0 & 0 & 0 & 0 & 0 \\ 0 & 0 & 0 & 0 & 0 & 0 & -\frac{1}{2}(i\sqrt{3}) & 0 & 0 & 0 & 0 \\ 0 & 0 & 0 & 0 & 0 & 0 & \frac{i\sqrt{3}}{2} & 0 & -i & 0 & 0 \\ 0 & 0 & 0 & 0 & 0 & 0 & 0 & i & 0 & -\frac{1}{2}(i\sqrt{3}) & 0 \\ 0 & 0 & 0 & 0 & 0 & 0 & 0 & 0 & \frac{i\sqrt{3}}{2} & 0 & 0 \end{pmatrix}, \\
T^3 &= \begin{pmatrix} 0 & 0 & 0 & 0 & 0 & 0 & 0 & 0 & 0 & 0 \\ 0 & \frac{1}{2} & 0 & 0 & 0 & 0 & 0 & 0 & 0 & 0 \\ 0 & 0 & -\frac{1}{2} & 0 & 0 & 0 & 0 & 0 & 0 & 0 \\ 0 & 0 & 0 & 1 & 0 & 0 & 0 & 0 & 0 & 0 \\ 0 & 0 & 0 & 0 & 0 & 0 & 0 & 0 & 0 & 0 \\ 0 & 0 & 0 & 0 & 0 & -1 & 0 & 0 & 0 & 0 \\ 0 & 0 & 0 & 0 & 0 & 0 & \frac{3}{2} & 0 & 0 & 0 \\ 0 & 0 & 0 & 0 & 0 & 0 & 0 & \frac{1}{2} & 0 & 0 \\ 0 & 0 & 0 & 0 & 0 & 0 & 0 & 0 & -\frac{1}{2} & 0 \\ 0 & 0 & 0 & 0 & 0 & 0 & 0 & 0 & 0 & -\frac{3}{2} \end{pmatrix}, \\
T^4 &= \begin{pmatrix} 0 & 0 & -\frac{\sqrt{3}}{2} & 0 & 0 & 0 & 0 & 0 & 0 & 0 & 0 \\ 0 & 0 & 0 & 0 & -\frac{1}{\sqrt{2}} & 0 & 0 & 0 & 0 & 0 & 0 \\ -\frac{\sqrt{3}}{2} & 0 & 0 & 0 & 0 & -1 & 0 & 0 & 0 & 0 & 0 \\ 0 & 0 & 0 & 0 & 0 & 0 & 0 & -\frac{1}{2} & 0 & 0 & 0 \\ 0 & -\frac{1}{\sqrt{2}} & 0 & 0 & 0 & 0 & 0 & 0 & -\frac{1}{\sqrt{2}} & 0 & 0 \\ 0 & 0 & -1 & 0 & 0 & 0 & 0 & 0 & 0 & -\frac{\sqrt{3}}{2} & 0 \\ 0 & 0 & 0 & 0 & 0 & 0 & 0 & 0 & 0 & 0 & 0 \\ 0 & 0 & 0 & -\frac{1}{2} & 0 & 0 & 0 & 0 & 0 & 0 & 0 \\ 0 & 0 & 0 & 0 & -\frac{1}{\sqrt{2}} & 0 & 0 & 0 & 0 & 0 & 0 \\ 0 & 0 & 0 & 0 & 0 & -\frac{\sqrt{3}}{2} & 0 & 0 & 0 & 0 & 0 \end{pmatrix},
\end{aligned}$$

$$\begin{aligned}
T^5 &= \begin{pmatrix} 0 & 0 & \frac{i\sqrt{3}}{2} & 0 & 0 & 0 & 0 & 0 & 0 & 0 \\ 0 & 0 & 0 & 0 & \frac{i}{\sqrt{2}} & 0 & 0 & 0 & 0 & 0 \\ -\frac{1}{2}(i\sqrt{3}) & 0 & 0 & 0 & 0 & i & 0 & 0 & 0 & 0 \\ 0 & 0 & 0 & 0 & 0 & 0 & 0 & \frac{i}{2} & 0 & 0 \\ 0 & -\frac{i}{\sqrt{2}} & 0 & 0 & 0 & 0 & 0 & 0 & \frac{i}{\sqrt{2}} & 0 \\ 0 & 0 & -i & 0 & 0 & 0 & 0 & 0 & 0 & \frac{i\sqrt{3}}{2} \\ 0 & 0 & 0 & 0 & 0 & 0 & 0 & 0 & 0 & 0 \\ 0 & 0 & 0 & -\frac{i}{2} & 0 & 0 & 0 & 0 & 0 & 0 \\ 0 & 0 & 0 & 0 & -\frac{i}{\sqrt{2}} & 0 & 0 & 0 & 0 & 0 \\ 0 & 0 & 0 & 0 & 0 & -\frac{1}{2}(i\sqrt{3}) & 0 & 0 & 0 & 0 \end{pmatrix}, \\
T^6 &= \begin{pmatrix} 0 & \frac{\sqrt{3}}{2} & 0 & 0 & 0 & 0 & 0 & 0 & 0 & 0 \\ \frac{\sqrt{3}}{2} & 0 & 0 & 1 & 0 & 0 & 0 & 0 & 0 & 0 \\ 0 & 0 & 0 & 0 & \frac{1}{\sqrt{2}} & 0 & 0 & 0 & 0 & 0 \\ 0 & 1 & 0 & 0 & 0 & 0 & \frac{\sqrt{3}}{2} & 0 & 0 & 0 \\ 0 & 0 & \frac{1}{\sqrt{2}} & 0 & 0 & 0 & 0 & \frac{1}{\sqrt{2}} & 0 & 0 \\ 0 & 0 & 0 & 0 & 0 & 0 & 0 & 0 & \frac{1}{2} & 0 \\ 0 & 0 & 0 & \frac{\sqrt{3}}{2} & 0 & 0 & 0 & 0 & 0 & 0 \\ 0 & 0 & 0 & 0 & \frac{1}{\sqrt{2}} & 0 & 0 & 0 & 0 & 0 \\ 0 & 0 & 0 & 0 & 0 & \frac{1}{2} & 0 & 0 & 0 & 0 \\ 0 & 0 & 0 & 0 & 0 & 0 & 0 & 0 & 0 & 0 \end{pmatrix}, \\
T^7 &= \begin{pmatrix} 0 & -\frac{1}{2}(i\sqrt{3}) & 0 & 0 & 0 & 0 & 0 & 0 & 0 & 0 \\ \frac{i\sqrt{3}}{2} & 0 & 0 & -i & 0 & 0 & 0 & 0 & 0 & 0 \\ 0 & 0 & 0 & 0 & -\frac{i}{\sqrt{2}} & 0 & 0 & 0 & 0 & 0 \\ 0 & i & 0 & 0 & 0 & 0 & -\frac{1}{2}(i\sqrt{3}) & 0 & 0 & 0 \\ 0 & 0 & \frac{i}{\sqrt{2}} & 0 & 0 & 0 & 0 & -\frac{i}{\sqrt{2}} & 0 & 0 \\ 0 & 0 & 0 & 0 & 0 & 0 & 0 & 0 & -\frac{i}{2} & 0 \\ 0 & 0 & 0 & \frac{i\sqrt{3}}{2} & 0 & 0 & 0 & 0 & 0 & 0 \\ 0 & 0 & 0 & 0 & \frac{i}{\sqrt{2}} & 0 & 0 & 0 & 0 & 0 \\ 0 & 0 & 0 & 0 & 0 & \frac{i}{2} & 0 & 0 & 0 & 0 \\ 0 & 0 & 0 & 0 & 0 & 0 & 0 & 0 & 0 & 0 \end{pmatrix}, \\
T^8 &= \begin{pmatrix} \sqrt{3} & 0 & 0 & 0 & 0 & 0 & 0 & 0 & 0 & 0 \\ 0 & \frac{\sqrt{3}}{2} & 0 & 0 & 0 & 0 & 0 & 0 & 0 & 0 \\ 0 & 0 & \frac{\sqrt{3}}{2} & 0 & 0 & 0 & 0 & 0 & 0 & 0 \\ 0 & 0 & 0 & 0 & 0 & 0 & 0 & 0 & 0 & 0 \\ 0 & 0 & 0 & 0 & 0 & 0 & 0 & 0 & 0 & 0 \\ 0 & 0 & 0 & 0 & 0 & 0 & 0 & 0 & 0 & 0 \\ 0 & 0 & 0 & 0 & 0 & 0 & -\frac{\sqrt{3}}{2} & 0 & 0 & 0 \\ 0 & 0 & 0 & 0 & 0 & 0 & 0 & -\frac{\sqrt{3}}{2} & 0 & 0 \\ 0 & 0 & 0 & 0 & 0 & 0 & 0 & 0 & -\frac{\sqrt{3}}{2} & 0 \\ 0 & 0 & 0 & 0 & 0 & 0 & 0 & 0 & 0 & -\frac{\sqrt{3}}{2} \end{pmatrix}.
\end{aligned}$$

They obey the relations $[T^a, T^b] = i c_{abc} T^c$ with c_{abc} given by equation (A.1.4).

APPENDIX B

Calculations for coherent states of Squashed \mathbb{CP}^2

B.1. Expectation values

Let the rotation $U(\varphi)$ with $\varphi = (\varphi_1, \varphi_2, \varphi_3, \varphi_4)$ be defined as

$$U(\varphi) = e^{i\varphi_1 T^4 + i\varphi_2 T^5 + i\varphi_3 T^6 + i\varphi_4 T^7} \quad (\text{B.1.1})$$

with $T^a = \pi_{(0,n)}(t^a)$. Additionally, let us define the rotated vector $|\varphi\rangle$ as

$$|\varphi\rangle := U(\varphi) |\Psi_0\rangle, \quad (\text{B.1.2})$$

where $|\Psi_0\rangle$ is the highest weight vector of a $(0, n)$ representation. We want to calculate the quantity

$$\vec{p}(\varphi)_a = \langle \varphi | X^a | \varphi \rangle. \quad (\text{B.1.3})$$

To this end consider the adjoint action of $SU(3)$ on $Mat_m(\mathbb{C})$ given by $U^{-1}MU$ for some $M \in Mat_m(\mathbb{C})$ and $U = \Pi_{(0,n)}(g)$ belonging to the $(0, n)$ representation. Since $Mat_m(\mathbb{C}) \doteq \bigoplus_{p=0}^n \mathcal{H}_{(p,p)}$ where $T^a \in \mathcal{H}_{(1,1)}$, the $SU(3)$ action leaves $\mathcal{H}_{(1,1)}$ invariant and we can write

$$Ad(T^a) = U^{-1}T^aU = \sum_{b=1}^8 R_{ab}T^b \quad (\text{B.1.4})$$

for an orthogonal 8×8 matrix R . Since the representations $Ad(T^a)$ and $Ad(t^a)$ are equivalent there exists an isomorphism $f : \mathcal{H}_{(1,1)} \rightarrow \mathfrak{su}(3)$ such that $f(Ad(T^a)) = Ad(f(T^a))$. Applying f to equation (B.1.4) we get

$$Ad(t^a) = \sum_{b=1}^8 R_{ab}t^b. \quad (\text{B.1.5})$$

Using the natural scalar product on $\mathfrak{su}(3)$ given by $(A, B) := 2 \text{tr}(A \cdot B)$ chosen such that the set $\{t^a, a = 1, \dots, 8\}$ forms an orthonormal basis we can explicitly calculate the matrix coefficients of R via

$$R_{ab} = (t^a, Ad(t^b)) = 2 \text{tr}(t^a U^{-1} t^b U) \quad (\text{B.1.6})$$

which for $U = U(\varphi)$ can be carried out by computer algebra systems.

Expression (B.1.3) can now be written as

$$\vec{p}(\varphi)_a = \sum_{b=1}^8 R_{ab} \langle \Psi_0 | X^b | \Psi_0 \rangle = c_n \sum_{b=1}^8 R_{ab} \langle \Psi_0 | T^b | \Psi_0 \rangle$$

and since $\langle \Psi_0 | T^8 | \Psi_0 \rangle = \frac{n}{\sqrt{3}}$ is the only non-zero component we get

$$\vec{p}(\varphi)_a = c_n R_{a8} \frac{n}{\sqrt{3}}$$

and after plugging in the coefficients R_{a8} we recover equation (4.3.11):

$$\vec{p}(\varphi) = c_n \frac{n}{2} \frac{1}{|\varphi|} \begin{pmatrix} \frac{(\varphi_1\varphi_3+\varphi_2\varphi_4)}{|\varphi|} (\cos|\varphi| - 1) \\ 2 \frac{(\varphi_1\varphi_4-\varphi_2\varphi_3)}{|\varphi|} \sin^2 \frac{|\varphi|}{2} \\ \varphi_2 \sin|\varphi| \\ -\varphi_1 \sin|\varphi| \\ \varphi_4 \sin|\varphi| \\ -\varphi_3 \sin|\varphi| \end{pmatrix}. \quad (\text{B.1.7})$$

B.2. Dispersion

Next we want to evaluate the dispersion (4.3.1) which reads

$$\delta(\varphi) = 1 - \sum_{i=3,8} \langle \varphi | (X^i)^2 | \varphi \rangle - |\vec{p}(\varphi)|^2. \quad (\text{B.2.1})$$

Having calculated the third term already we are left with the second term $\sum_{i=3,8} \langle \varphi | (X^i)^2 | \varphi \rangle$ which can be written as

$$\sum_{i=3,8} \langle \varphi | (X^i)^2 | \varphi \rangle = \sum_{i=3,8} \sum_{a,b=1}^8 R_{ia} R_{ib} \langle \Psi_0 | X^a X^b | \Psi_0 \rangle. \quad (\text{B.2.2})$$

The expression $M_{ab} := \langle \Psi_0 | X^a X^b | \Psi_0 \rangle = c_n^2 \langle \Psi_0 | T^a T^b | \Psi_0 \rangle$ can be calculated explicitly and yields

$$M = c_n^2 \frac{n}{4} \begin{pmatrix} 0 & 0 & 0 & 0 & 0 & 0 & 0 & 0 \\ 0 & 0 & 0 & 0 & 0 & 0 & 0 & 0 \\ 0 & 0 & 0 & 0 & 0 & 0 & 0 & 0 \\ 0 & 0 & 0 & 1 & i & 0 & 0 & 0 \\ 0 & 0 & 0 & -i & 1 & 0 & 0 & 0 \\ 0 & 0 & 0 & 0 & 0 & 1 & i & 0 \\ 0 & 0 & 0 & 0 & 0 & -i & 1 & 0 \\ 0 & 0 & 0 & 0 & 0 & 0 & 0 & \frac{4n}{3} \end{pmatrix}. \quad (\text{B.2.3})$$

With this we can compute (B.2.2) and get a long expression for the second term

$$\begin{aligned} \sum_{i=3,8} \langle \varphi | (X^i)^2 | \varphi \rangle &= c_n^2 \frac{n}{48} \frac{1}{|\varphi|^4} e^{-2i|\varphi|} \times \\ &\times \left(12e^{i|\varphi|} (n-1) (\varphi_1^2 + \varphi_2^2) (\varphi_3^2 + \varphi_4^2) + 12e^{3i|\varphi|} (n-1) (\varphi_1^2 + \varphi_2^2) (\varphi_3^2 + \varphi_4^2) \right. \\ &+ 3(n-1) (\varphi_1^4 + \varphi_2^4 + \varphi_2^2 (\varphi_3^2 + \varphi_4^2) + (\varphi_3^2 + \varphi_4^2)^2 + \varphi_1^2 (2\varphi_2^2 + \varphi_3^2 + \varphi_4^2)) \\ &+ 3e^{4i|\varphi|} (n-1) (\varphi_1^4 + \varphi_2^4 + \varphi_2^2 (\varphi_3^2 + \varphi_4^2) + (\varphi_3^2 + \varphi_4^2)^2 + \varphi_1^2 (2\varphi_2^2 + \varphi_3^2 + \varphi_4^2)) \\ &+ 2e^{2i|\varphi|} ((3+5n)\varphi_1^4 + (3+5n)\varphi_2^4 + (15+n)\varphi_2^2 (\varphi_3^2 + \varphi_4^2) + (3+5m)(\varphi_3^2 + \varphi_4^2)^2 \\ &\left. + \varphi_1^2 (2(3+m)\varphi_2^2 + (15+m)(\varphi_3^2 + \varphi_4^2))) \right). \quad (\text{B.2.4}) \end{aligned}$$

Plugging (B.1.7) and (B.2.4) into equation (B.2.1) and simplifying thankfully yields a more compact relation for the dispersion

$$\begin{aligned} \delta(\varphi) &= \frac{3}{8(3+n)} \frac{1}{|\varphi|^4} \{ 4(\varphi_1^2 + \varphi_2^2) (\varphi_3^2 + \varphi_4^2) \cos|\varphi| \\ &+ (\varphi_1^4 + \varphi_2^4 + \varphi_1^2 (2\varphi_2^2 + \varphi_3^2 + \varphi_4^2) + \varphi_2^2 (\varphi_3^2 + \varphi_4^2) + (\varphi_3^2 + \varphi_4^2)^2) \cos 2|\varphi| \\ &+ (7(\varphi_1^4 + \varphi_2^4) + 7(\varphi_3^2 + \varphi_4^2)^2 + 11\varphi_2^2 (\varphi_3^2 + \varphi_4^2)) \} \end{aligned} \quad (\text{B.2.5})$$

which concludes the calculation.

Lukas Schneiderbauer

Curriculum Vitae

Education

- 2013–current **Master of Science in Theoretical Physics**, *Universität Wien*, Vienna, Austria.
2013–current **Bachelor of Science in Mathematics**, *Universität Wien*, Vienna, Austria.
2009–2012 **Bachelor of Science in Physics**, *Universität Wien*, Vienna, Austria.
2003–2008 **Matura, HTL (IT and Organization)**, 4710 Grieskirchen, Austria.
This school specializes in IT (software development, databases, network engineering) and Organization (accountancy, business studies). The degree includes a Matura graduation thesis.
1999–2003 **Secondary School**, *Gymnasium*, 4910 Ried im Innkreis, Austria.
1995–1999 **Elementary School**, *Volksschule*, 4751 Dorf an der Pram, Austria.

Master Thesis

- Title *Semi-classical and Numerical Aspects of Fuzzy Brane Solutions in Yang-Mills Theories*
Supervisor Privatdoz. Mag. Harold Steinacker, PhD
Description This thesis explores non-commutative geometries (or fuzzy branes) arising from supersymmetric Yang-Mills theories. Tools are developed to numerically extract the semi-classical limit of fuzzy branes, which can be applied to arbitrary brane configurations characterized by a set of matrices, while the focus of this work rests on a special example, so-called Fuzzy \mathbb{CP}^2 .

Bachelor Thesis

- Title *Entanglement Or Separability*
Supervisor ao. Univ.-Prof. i.R. Dr. Reinhold Bertlmann
Description This work provides an introduction to quantum entanglement on a theoretical level. Among others it covers questions like: How can one define entanglement? How can one identify an entangled quantum system? How can entanglement be measured?

Matura Graduation Project

- Title Student Administration Software
Supervisor Dipl.-Ing. Peter Anzenberger
Description Software project for a school in Austria to provide a platform helping teachers in their daily workflow, especially managing groups of students.

Attended seminars

- May 2015 **Workshop 'Quantum Physics and Information'**, *International Academy Traunkirchen*, 4801 Traunkirchen, Austria.
May 2012 **Workshop 'Quantum Physics and Information'**, *International Academy Traunkirchen*, 4801 Traunkirchen, Austria.

Work Experience

University

- 2015 **Teaching Assistant**, *Universität Wien*, Vienna, Austria.
physics course for physicists
2013 **Teaching Assistant**, *Universität Wien*, Vienna, Austria.
mathematics course for physicists

- 2012–2014 **Teaching Assistant**, *Universtität für Bodenkultur Wien*, Vienna, Austria.
mathematics course for ‘Natural Resources and Life Sciences’-students
- 2010–2013 **Teaching Assistant**, *Universtität Wien*, Vienna, Austria.
practical physics course for biologists
- Vocational Jobs - IT
- 2010–2012 **Tutor**, *Mobile Nachhilfe*, Vienna, Austria.
tutoring in mathematics and physics
- 2009 **Vacational employment**, *SGS Industrial Service*, 4751 Dorf an der Pram, Austria.
IT department
- 2005 **Practical Training**, *AKH*, 4910 Ried im Innkreis, Austria.
IT department
- 2004 **Practical Training**, *Fronius*, 4600 Wels, Austria.
technical support
- Miscellaneous
- 2008–2009 **Zivildienst**, *assista*, 4674 Altenhof am Hausruck, Austria.
Assistance for persons with special needs
- 2006 **Vacation employment as doctor’s receptionist**, *Ophthalmologist Dr. Helmut Schneiderbauer*, 4722 Peuerbach, Austria.

Computer skills

OS	Linux, Windows		
programming	Ruby, basic C, basic Python	scripting	Bash
office suites	KDE, Openoffice.org, MS Office	typography	L ^A T _E X
image proc.	GIMP		
scientific	Mathematica, Gnuplot		

Languages

German	Native
English	Fluent